Copy 186

NASA MEMO 12-14-58L

C, 186

LOAN COPY: RETU
AFWL (WLL—
KIRTLAND AFB, N

TECH LIBRARY KAFB, NM
0062967

NASA MEMO 12-14-58L

NASA MEMORANDUM

TRANSONIC WIND-TUNNEL INVESTIGATION OF STATIC LONGITUDINAL AND LATERAL STABILITY AND CONTROL CHARACTERISTICS AND DRAG RISE OF A REPRESENTATIVE FIGHTER AIRPLANE

By P. Kenneth Pierpont

Langley Research Center
Langley Field, Va.

NATIONAL AERONAUTICS AND SPACE ADMINISTRATION
WASHINGTON
March 1959

1186

Classification canceled ([redacted])

by authority of NASA Classification Chg. Notice #70 dtd. 7/20/66

Name and grade of officer authorizing change

Linda Beattie - HS 2 12 September 1966

Name & Grade of Officer making change

2 cols removed 21 Jan 64 fa

[redacted]

NATIONAL AERONAUTICS AND SPACE ADMINISTRATION

MEMORANDUM 12-14-58L

TECH LIBRARY KAFB, NM
0062967

TRANSONIC WIND-TUNNEL INVESTIGATION OF STATIC LONGITUDINAL AND LATERAL STABILITY AND CONTROL CHARACTERISTICS AND DRAG RISE OF A REPRESENTATIVE FIGHTER AIRPLANE* **

By P. Kenneth Pierpont

SUMMARY

An investigation was made in the Langley 8-foot transonic tunnel and the Langley 8-foot transonic pressure tunnel of the drag rise and the static longitudinal stability characteristics of a model, representative of current fighter design, at Mach numbers from 0.6 to 1.43. Effects of body shape, wing and tail thicknesses, wing camber, leading-edge flap deflection, and speed-brake location were studied. Some lateral stability and control data were obtained. The results showed that longitudinal stability would increase with both angle of attack and Mach number but that a considerable loss of horizontal-tail effectiveness near a Mach number of 1.0 would occur. Fuselage modifications reduced the drag rise by about 30 percent, improved the trimmed lift-drag ratio nearly 25 percent at 35,000 feet altitude at supersonic speeds, and substantially improved the longitudinal-control effectiveness. Fuselage modifications in conjunction with reductions in wing and tail thicknesses from about 5.5 percent to 4 percent reduced the drag rise 50 percent. Deflection of the wing leading-edge flap increased the lift-drag ratio at subcritical speeds. Use of conical camber resulted in improvements of lift-drag ratio up to 20 percent throughout the speed range and caused no trim or stability changes. The model was laterally stable throughout the test range, and the effective dihedral generally increased with both Mach number and angle of attack up to about 6°. Aileron effectiveness decreased above the critical Mach number by nearly 50 percent at a Mach number of 1.43. A differentially operated stabilizer provided adequate longitudinal-control effectiveness but inadequate lateral-control effectiveness. Both speed-brake installations tested resulted in significant longitudinal-trim changes throughout the Mach number range.

---

*The information presented herein was previously given limited distribution in NACA Research Memorandum SL56I19.

**Title, Unclassified.

[redacted]

[redacted]

INTRODUCTION

The design of high performance transonic and supersonic aircraft requires that the entire airplane be considered as an entity in order to achieve satisfactory drag and stability characteristics. In order to obtain information which will be useful in the design of new transonic and low supersonic aircraft, a model representative of current fighter design has been investigated in the Langley 8-foot transonic tunnel and the Langley 8-foot transonic pressure tunnel. Initial objectives of the program were to determine the transonic drag rise and the static longitudinal stability. Subsequently, the program included the investigation of means for reducing the transonic and supersonic drag levels and evaluation of some of the lateral characteristics of the model. In addition, tests were included utilizing several wing and tail modifications to improve further the potential performance capabilities of the design. Speed brakes were installed and their effectiveness was measured, and a differentially operated stabilizer was compared with a conventional stabilizer and aileron.

The range of Mach numbers for which data were obtained extended from 0.6 to 1.2, and a small amount of information was taken at $M = 1.43$. For some configurations, data were obtained at angles of attack or sideslip to a maximum of about 12°.

NOTATION AND SYMBOLS

All the data, measured with respect to body axes, have been reduced to standard coefficient form with moments and forces referred to the stability axes. In the stability system, the Z-axis lies in the plane of symmetry (fig. 1) and is normal to the relative wind; the Y-axis is normal to the plane of symmetry; and the X-axis is normal to the Y- and Z-axes. The moment reference was 28.7 percent of the mean aerodynamic chord.

C_L lift coefficient, $\frac{\text{Lift}}{qS}$

C_D drag coefficient, $\frac{\text{Drag}}{qS}$

C_Y side-force coefficient, $\frac{\text{Side force}}{qS}$

C_{X_s} longitudinal-force coefficient, $\frac{\text{Longitudinal force}}{qS}$

($C_D = -C_{X_s}$ when $\beta = 0^\circ$)

[redacted]

C_m pitching-moment coefficient, $\frac{\text{Pitching moment}}{qS\bar{c}}$

C_n yawing-moment coefficient, $\frac{\text{Yawing moment}}{qSb}$

C_l rolling-moment coefficient, $\frac{\text{Rolling moment}}{qSb}$

A cross-sectional area, normal to longitudinal axis

b wing span

c chord of wing parallel to free stream

$\bar{c}$ mean aerodynamic chord of wing, determined without chord-extensions, $\frac{2}{S}\int_0^{b/2} c^2 dy$

l_t model overall length

L/D lift-drag ratio

M Mach number

S wing area

R Reynolds number, based on mean aerodynamic chord

q dynamic pressure

V free-stream velocity

x distance rearward, either from model nose or reference origin

α angle of attack of fuselage reference line, deg

β angle of sideslip, deg

δ deflection of control surface, deg

ρ mass density of air

i_t incidence of horizontal tail relative to fuselage reference line in plane of symmetry, deg

i_w incidence of wing relative to fuselage reference line in plane of symmetry, deg

C_{n_β} rate of change of C_n with respect to β

C_{Y_β} rate of change of C_Y with respect to β

C_{l_β} rate of change of C_l with respect to β

$C_{m_{C_L}}$ rate of change of C_m with respect to C_L

C_{L_α} rate of change of C_L with respect to α

$C_{D_{C_L{}^2}}$ rate of change of C_D with respect to $C_L{}^2$

$C_{m_{i_t}}$ rate of change of C_m with respect to i_t

C_{l_δ} rate of change of roll with control-surface deflection

$C_{L_{(L/D)max}}$ lift coefficient corresponding to $(L/D)_{max}$

ΔC_D increment in drag coefficient

Subscripts:

min minimum

max maximum

i inboard

o outboard

a aileron

n leading-edge flap

b speed brake

APPARATUS AND MODELS

Wind-Tunnel Equipment

The investigation was conducted in both the Langley 8-foot transonic tunnel and the Langley 8-foot transonic pressure tunnel. Both tunnels incorporate the slotted-throat principle for continuous operation through the transonic speed range. The transonic tunnel has a dodecagonal test section and operates at approximately atmospheric total pressure. The transonic pressure tunnel has a square test section with slots on the top and bottom only and may be operated over a range of total pressures. A description of the transonic tunnel and its air-flow characteristics is presented in reference 1. Diagrammatic sketches of the model mounted in each of the tunnels are contained in figure 2. Representative Mach number distributions at the tunnel center line for the transonic pressure tunnel are shown in figure 3 for transonic speeds. When this tunnel is used to obtain data at $M = 1.4$, the slots are modified and closed as described in reference 2. For the slot configuration used in the present investigation, the average test section Mach number was 1.43.

Angle-of-attack changes were obtained in the transonic tunnel by rotating the model about a point 77.9 inches downstream of the center-of-gravity location. A coupling of 10° was inserted in the support system to maintain the model nearly in the tunnel center for the entire angle-of-attack range. At maximum or minimum angles of attack, the model center of gravity was 9.6 inches from the tunnel axis. In the transonic pressure tunnel the use of a coupling for this purpose was not required since the model rotated about a point only 27.9 inches downstream of the model center of gravity; hence, the maximum vertical displacement was only 5.8 inches.

Models

The model used for this investigation was designed to be representative of a current fighter airplane. The wing, located at the top of the fuselage to permit variable incidence, had a quarter-chord sweepback of 42°, and incorporated chord-extensions, a full-length leading-edge flap, and a combination flap and aileron located inboard. An all-movable horizontal tail and a conventional fin and rudder provided longitudinal and directional control, respectively. The quarter-chord sweepback of both empennage surfaces was 45°.

Basic model.- A three-view drawing of the basic model is shown in figure 4. For clarity, the model support sting has been shown only in the top view of the drawing. Inasmuch as the internal strain-gage balance interfered with the attainment of adequate internal air flow to simulate

the engine operation condition, the inlet was plugged and faired smooth for the entire investigation. The wing had no camber or twist and utilized an NACA 65A006 root section and an NACA 65A005 tip section. The tail surfaces were tapered in thickness from 6 percent at the root to 4 percent at the tip. Additional dimensions and details of the basic model which consisted of fuselage 1, wing 1, and tail 1 are given in table I. A photograph of the model as it was prepared for testing is shown in figure 5.

Fuselages.- At the outset of the investigation, it became apparent that fuselage modification would be required to provide acceptable transonic and supersonic drag characteristics. Figure 6(a) illustrates the body changes for which data are reported herein. Lengthening and slenderizing both the nose and tail portions of the fuselage constituted fuselage 2. The configuration designated 3 was obtained by the addition of bumps to fuselage 2 to improve the longitudinal distribution of cross-sectional area of the complete model. After the tests of fuselage 3, another fuselage configuration known as fuselage 4 was tested to determine whether a number of relatively local shape and area smoothing changes would significantly affect the transonic drag rise.

The design Mach number for the modifications was 1.2. The curve representing the average of five cuts through the model was used to determine the modifications in the manner of reference 3. Approximately half the area to be added was placed above the wing chord plane and half below (fig. 6(a)). The representative cross sections on the lower part of the figure show the basic fuselage to the left and comparisons of the modifications on the right half of each section. At station 19.32, fuselages 2, 3, and 4 were identical. Area distributions normal to the reference axis of the model are illustrated in figure 7 for the model equipped with the original wing and tail surfaces. The curves shown comprise the sum of the fuselage plus wing and tail and are presented nondimensionally based on the total model length for the four fuselage configurations previously described and illustrated in figure 6(a).

Tails.- Four tail configurations were tested; the first three differed only in the stabilizer, whereas tail 4 consisted of a revised vertical fin as well as horizontal stabilizer. The plan forms of the three different horizontal tails are shown in figure 6(b). Stabilizers 1 and 2 differed principally in the method or axis of rotation; the former was swept back 22.5°, whereas the latter was normal to the fuselage axis. Stabilizer 2 was approximately 15 percent smaller in exposed area than number 1. Stabilizer 3 was obtained by repositioning stabilizer 1 on top of the fuselage with the intent of improving the structural rigidity and thereby enable slenderizing of the rearward end of the fuselage. Stabilizer 4 corresponded in plan form and location to number 2 but had a uniform thickness of 4 percent throughout. Vertical fin 1 (fig. 4), used with stabilizers 1, 2, and 3, had root and tip thicknesses of 6 and 4 percent, respectively, whereas fin 2 which was used with stabilizer 4

had a constant thickness of 4 percent. Small, but generally negligible, physical differences in geometry of the two fin installations were noted in the long, narrow dorsal fin which were associated with the manner of fairing the body. The 4-percent-thick vertical fin 2 was used only in conjunction with the 4-percent-thick horizontal stabilizer 4.

Wings.- Two wings, in addition to the basic wing 1, which were tested on the model are shown in figure 6(c) and table I. Wing 2 had an identical plan form to that of wing 1, but had a thickness of 4 percent along the entire span. Relative thicknesses of the root sections are illustrated at the upper left of the figure. Wing 3 was not equipped with leading-edge extensions, but instead incorporated conical camber. The root section was uncambered and had a thickness of 4 percent, whereas the tip section had a camber illustrated in the figure. The forward part of the warped chord plane of the wing was formed by straight-line elements from the leading edge of the root section to the camber line at the tip section. The wing section was obtained by wrapping an NACA 65A004 thickness distribution around the warped chord plane. In order to avoid confusion the 5-percent-thick tip section of wing 1 has been omitted from the figure.

Speed brakes.- Two speed-brake arrangements were tested and are illustrated in figure 8. The first consisted of two symmetrically placed brakes located on the lower part of the fuselage sides near the leading edges of the wing root. The second configuration consisted of a single, large brake which had about the same total area as the two forward brakes combined. The single brake was located on the bottom of the fuselage rearward of the main landing-gear housing near the wing-root trailing edge. Both arrangements were tested at deflections of 30° and 60° relative to the local fuselage surface.

INSTRUMENTATION AND METHODS

The model was instrumented with an internally housed six-component strain-gage balance and pressure tubes to measure the base pressure. Normally the model was mounted upright in the wind tunnel; however, it was necessary to rotate it 90° to facilitate sideslip tests. For the upright position, the angle of attack was obtained by measuring the support sting angle and correcting this value according to calibrations of the sting and balance deflections. The sting angle was measured with an oil-damped pendulum type of strain-gage attitude indicator. Sideslip angles for the model upright were determined directly by visual measurement using a cathetometer. Methods to obtain angles of attack and sideslip were interchanged when the model was rotated 90°. Simultaneous angles of attack and sideslip were obtained by inserting a fixed coupling

in the support sting in a direction perpendicular to the plane of rotation of the wind-tunnel support sting. All force, pressure, and angle data were recorded electronically by means of a punched-card system.

TESTS

This investigation was conducted in both the Langley 8-foot transonic and the 8-foot transonic pressure tunnels. Longitudinal data were taken at constant Mach numbers at 0° sideslip through an angle-of-attack range limited at its upper end by balance loads. Some lateral tests were made at fixed nominal angle of attack while the sideslip angle was varied; other lateral tests were made at fixed nominal angles of sideslip while the angle of attack was varied. A summary of the configurations and tests reported herein is presented in table II. The range of test Reynolds number plotted as a function of Mach number is shown in figure 9.

Almost all the tests were made with the model in a smooth condition; however, some of the effects of fixing transition were obtained. Transition was fixed with a 1/8-inch-wide band of carborundum attached to the body 3 inches from the nose and to the upper and lower surfaces of the wing 1/2 inch from the leading edge. For most of these tests, grain density of 40 to 60 grains per linear inch of carborundum 0.0098-inch average size was employed; however, for one test, carborundum of 0.0049, average size, was employed. Transition was fixed on the tail surfaces by a thick band of the lacquer 1/8 inch wide without carborundum 1/2 inch from the leading edge.

REDUCTION OF DATA

Corrections

The force along the longitudinal body axis, measured by the strain gage, was adjusted so that the result corresponded to that for a pressure at the model base equal to the free-stream static pressure. No sting-interference corrections have been applied apart from the base-pressure adjustment described since corrections obtained from reference 4 indicated a correction less than the estimated accuracy. Buoyancy corrections were calculated for representative configurations and were considered negligible.

Wind-tunnel-wall interference effects at subsonic speeds for both the transonic tunnel and the transonic pressure tunnel were within the accuracy of the data according to references 5 and 6. At supersonic speeds between $M = 1.03$ and 1.12, effects of wall-reflected disturbances

were large; no data are therefore presented in this range. At other supersonic speeds, effects of wall-reflected disturbances were considered small. No corrections for wind-tunnel-wall interference have therefore been applied to any of the data.

Precision

The accuracy of the data from these tests estimated largely on the basis of the repeatibility of the results is presented below:

α, β, deg	±0.1
M	±0.005
C_L	±0.01
C_D, C_{X_s}	±0.001
C_m	±0.004
C_l	±0.0003
C_n	±0.0005
C_Y	±0.003

Some difference in turbulence levels exists between the transonic tunnel and the transonic pressure tunnel utilized for these tests. These differences are largely manifested as differences in viscous drag. For this reason, the basic data have been grouped so that data from both tunnels are not superimposed. For comparisons of wave drag, this difficulty has been largely removed.

RESULTS AND DISCUSSION

The results are presented in the form of basic and summary data curves. Basic longitudinal data (figs. 10-27) are presented as functions of lift coefficient and basic lateral data (figs. 28-34) as functions of angles of attack or sideslip. Most of the summary data (figs. 35-48) are presented as functions of Mach number. The longitudinal parameter C_{L_α} was measured for $-0.2 < C_L < 0.2$, $C_{M_{C_L}}$ for $C_L = \pm 0.05$, and $C_{D_{C_L{}^2}}$ for $\Delta C_L = 0.3$ above the minimum drag coefficient. The lateral-stability parameters were measured for $-2^\circ < \beta < 2^\circ$. An index of the basic data is provided in table II and the summary data in table III.

L-477

Drag-Reduction Methods

The subsonic drag level is shown in figure 35 for the basic model to be $C_{D_{min}} = 0.0170$ at $M = 0.90$. The critical Mach number, based on the slope of the curve of C_D plotted against M of 0.1, was 0.92. At supersonic speeds, a drag coefficient of 0.0450 was measured. Because of this high supersonic drag level, a number of modifications and configuration changes were investigated and are discussed in the following sections.

Fuselage modifications.- Effects of fuselage modifications on the minimum drag coefficient are shown in figures 36 and 37 for the wing and body and the complete model, respectively. Similarly, wave-drag comparisons based upon the subcritical value at $M = 0.90$ are shown in figures 38 and 39. For the wing and body alone, the minimum drag coefficient was reduced at $M = 1.15$ (fig. 36) by body modifications from 0.0375 for fuselage 1 to 0.0295 for fuselage 3. For the complete model (fig. 37) the reduction was from 0.0450 for fuselage 1 to 0.0360 for fuselage 3. The latter represents a 20-percent improvement in total drag and corresponds to a 30-percent wave-drag reduction. (See fig. 39.)

Although the design Mach number for fuselage 3 was 1.2, the range of small drag variation extended from approximately $M = 1.1$ to $M = 1.4$. From the shape of the curve in figure 39 for fuselage 2, it is doubtful whether the fuselage bumps (fuselages 3 or 4) would be useful above about $M = 1.5$. By comparing the curves of figures 38 and 39, it can be seen that caution must be exercised in the designing of the entire configuration; for example, the difference in tail-on and tail-off wave drag was reduced from 45 counts (0.0045) for fuselage 1 to nearly 25 counts for fuselage 3, a reduction of more than 40 percent.

Effects of fixing transition on the minimum drag and wave-drag coefficients are incomplete; however, figure 36 for the wing and body shows no sizable drag coefficient differences whether coarse (0.0098 diameter) or fine (0.0049 diameter) carborundum was used. This lack of change with grain size may have resulted from differences in distribution and band thickness. An average drag-coefficient increment due to transition fixed of about 30 drag counts is shown for the entire Mach number range. Figures 38 and 39 show that no important wave-drag changes resulted from fixing transition for either the wing and body or the complete model.

Wave-drag reductions which resulted from fuselage modifications were reflected in improvements in maximum values of L/D shown in figures 36 and 37. Compared with fuselage 1, the use of the bumped fuselage (fuselage 3) provided a gain in L/D at $M = 1.13$ of about 15 percent. Apparent gains at subsonic speeds are unrealistic because early transition

was probably induced at the inlet fairing plug of fuselage 1. Fixing transition is shown to have resulted in sizable decreases in L/D at all Mach numbers. Since the subsonic drag level is primarily dependent upon the wetted area and since the wave-drag variation has been shown to be essentially independent of fixing transition, it appears obvious that the improved fuselage shapes such as 3 or 4 can be expected to provide higher values of L/D at supersonic speeds than the basic fuselage, irrespective of surface conditions.

A more satisfactory comparison of the performance of L/D may be obtained by comparing L/D with natural transition for trimmed level-flight conditions. An assumed wing loading of 55.5 lb/sq ft was used for the calculations. Figure 41 provides a comparison for the basic model (fuselage 1) and fuselage 3. It is shown that the area-rule improvements are not as important at sea level or low altitudes as at the higher flight altitudes of 35,000 and 50,000 feet. At 35,000 feet and $M = 1.15$, the trimmed L/D has been increased from 2.5 to 3.1 or 24 percent; at 50,000 feet the corresponding increase was from 4.1 to 4.9.

It is also of interest to ascertain the changes in longitudinal stability which may have accompanied these fuselage modifications. The longitudinal stability of the basic model (figs. 10 and 35) increased with both Mach number and lift coefficient. A significant increase in longitudinal stability resulted however when fuselage 2 was installed. (See fig. 37.) This fuselage was longer, employed generally smoother fairing, and had more oval-shaped forward parts than its predecessor so that the basic loading probably changed. Except for $M = 0.98$ and $M = 1.00$, adding bumps (compare fuselage 2 with fuselage 3 in fig. 6(a)) did not alter the longitudinal stability whether transition was natural or fixed.

Because of the high transonic drag of the basic model, there was no interest in lateral data with fuselage 1. Figures 29 and 40 show that with fuselage 4 the model was laterally stable throughout the test range of angles of attack and sideslip. The effect of adding bumps to the fuselage is shown to be small for the two Mach numbers for which data are available, except possibly for the directional parameter at $M = 1.0$.

Leading-edge flap.- In order to permit high values of the low-speed lift coefficient and reasonable landing attitudes, full-span leading-edge flaps were incorporated. The data of figure 15 show effect of flaps on L/D at cruise conditions. These data together with figure 42 show that little change in longitudinal stability occurred but that a trim change which would require up to about 2° of stabilizer incidence resulted. The maximum untrimmed L/D at $M = 0.8$ was increased by means of the flaps from 10.5 to nearly 12.5. Estimates of the trim drag would reduce the increment from 2.0 to about 1.6. Increasing Mach number

resulted in decreases in L/D such that by M = 0.95 all gains had been nullified because of the rapid drag increase due both to early drag rise and to increased drag at lifting conditions.

Wing and tail thicknesses.- Improvements to the transonic drag which could be achieved by further modifications are shown in figures 42 and 43. Wing 1 had an effective thickness of about 5.5 percent and wings 2 and 3 both had 4 percent along the span. The combination of horizontal stabilizer 2 with vertical fin 1 (called tail 2) had an effective thickness of about 5.2 percent, whereas the combination of stabilizer 4 and fin 2 (called tail 4) had a uniform 4 percent. Reducing the tail thickness on fuselage 2 with the thick wing (wing 1) resulted in only small drag reductions. (See fig. 43.) However, thinning the tail surfaces (tail 4) on fuselage 4 with the thick wing (wing 1) produced substantial transonic-drag improvements shown in figure 43.

Decreasing only the wing thickness (fig. 44) to 4 percent reduced the wave drag at M = 1.15 by 22 percent and at 1.43 by 33 percent. The 4-percent-thick tails decreased the wave drag at the lower supersonic speeds, but at M = 1.43 the reduction is insignificant. The combined wing and tail modifications (wing 2 with tail 4) in conjunction with the fuselage modifications produced a maximum reduction in wave drag at M = 1.15 of more than 50 percent compared with that for the basic model. (Compare fig. 44 with fig. 39.) In fact, the wave drag was reduced to less than the subsonic or viscous drag; hence, the drag-rise ratio decreased from nearly 2.0 to less than 1.0. Figure 42 shows that gains in $(L/D)_{max}$ at M = 1.15 up to 12.5 percent were obtained and that no change in longitudinal stability resulted from thinning the surfaces.

Wing camber.- After the reduction of the wave drag by thinning the wing and tail surfaces, an attempt was made to improve the L/D at cruise conditions. A new 4-percent-thick wing incorporating conical camber but without the chord-extension was tested, data for which are shown in figures 14 and 42. The principal effect of the camber was to achieve higher values of L/D throughout the subsonic and low supersonic speed range. At M = 0.9 an L/D of 12.0 was obtained as compared with 11.4 or 10.2 for the flapped and unflapped wings, respectively. At M = 1.13, the conically cambered wing provided an increase of 20 percent in L/D above that for wing 1 with the same fuselage and nearly 33 percent above that for the basic model. (See fig. 35.) At M = 1.43, the increased minimum drag resulting from camber caused a small reduction in L/D as compared with the uncambered 4-percent-thick wing. (See fig. 42.) Only a slight trim change (fig. 14) was caused by installing the cambered wing and the static longitudinal stability was unchanged.

Speed Control

Drag increments resulting from speed-brake deflection are presented in figure 45. Grouping of the data for 30° and 60° deflection indicates that deflection is the most important parameter. Up to 30°, negligible variation with Mach number is shown for either tails on or tails off. For 60°, however, an increase in drag-coefficient increment of about 30 percent occurred from $M = 0.6$ to $M = 0.98$.

The twin speed brake mounted ahead of the wing (brake 1) is shown in figure 26 to have caused both a nose-down trim change and a longitudinal-stability decrease at subsonic speeds. At supersonic speeds, only a trim change is indicated. The magnitude of the trim change for a deflection of 60° can be estimated from figure 46 to vary from about 3° to 6° from $M = 0.60$ to $M = 0.98$. A similar but smaller variation at 30° is shown. Between $M = 0.98$ and $M = 1.03$, the required trim change decreased by about 50 percent. Speed brake 2, a single brake located behind the wing, is shown in figure 27 to have caused insignificant stability changes and nose-up trim changes only about two-thirds as large as the twin brakes at $M = 0.94$ or less. No trim change is indicated at $M = 0.98$.

Longitudinal Stability and Control

Installation of the three tails at 0° incidence on the wing and body resulted in stable but generally nonlinear pitching-moment characteristics. (See figs. 10 and 35.) In the range of Mach numbers from 0.9 to 1.0, the tail contribution to the longitudinal stability varied with Mach number and was generally less than at either lower or higher Mach numbers. Deflection of the all-movable horizontal tail up to 20° (figs. 11 to 13) resulted in pitching-moment characteristics of essentially similar shape.

A comparison of control effectiveness is illustrated in figure 46 for several configurations. An increase in the effectiveness of the tail of more than 20 percent accompanied the change from fuselage 1 to fuselage 4. Furthermore, the more than 35-percent loss of effectiveness near sonic speeds has been largely eliminated with fuselage 4 which incorporates the area rule. This may be attributed to the improved flow near the tail which resulted from decreased wing-body interference caused by improved fuselage shape. Included in figure 46 is the longitudinal effectiveness of the stabilizer when deflected differentially to obtain lateral control. At subsonic speeds, the effectiveness is nearly equal to that for the conventional control with fuselage 4; some decrease, however, is seen at supersonic speeds.

Lateral Stability and Control

The model was stable laterally for all test conditions as shown in figure 40. It can be seen in figure 28 that the effective dihedral generally increased with angle of attack and Mach number up to about 6°. The directional-stability parameter C_{n_β} was higher at supersonic speeds for fuselage 4 incorporating the area rule (fig. 40), but for fuselage 2, either the increase was delayed or did not exist. Figure 28 shows that only small changes occurred in C_{n_β} with angle of attack at subsonic speeds up to 10° or 12°.

The effects on lateral stability and control caused by deflecting the ailerons located inboard to obtain lateral control are shown in figures 30 to 33 and figure 47. Control effectiveness is presented in figure 48. Installing the tails on the model is shown to decrease the rolling effectiveness as much as 25 percent at $M = 1.13$. For either tails on or tails off, C_{l_δ} decreased with increasing Mach number above the drag-rise Mach number. Using the data of figure 33, for $\delta_a = 20°$ at an angle of attack of -5°, to obtain an indication of the effectiveness at $M = 1.43$ gives a value of $C_{l_\delta} = 0.0012$. This value represents a decrease of nearly 50 percent from that at subcritical Mach numbers. Although the effects on the dynamic stability are not known, figure 33 shows that there is a considerable longitudinal contribution caused by the ailerons at $M = 1.43$. No such variation was, however, suggested by the data in figure 28(g) in which there is no aileron deflection.

The rolling effectiveness of the horizontal stabilizer deflected differentially in a manner similar to that of reference 7 is included in figure 48. Only one deflection was tested, which corresponded to a nominal stabilizer setting of -5° with a superimposed differential deflection nominally equal to 5° ($i_t = -10°$ for right stabilizer, $i_t = 0°$ for left stabilizer). The data show that the subsonic rolling effectiveness would not be satisfactory compared with the ailerons. The value of C_{l_δ} at $M = 1.12$, however, is approximately the same as that for the ailerons on the rigid wing and nearly double that for subcritical speeds. Such a control was shown in figure 46 to provide adequate longitudinal effectiveness throughout the Mach number range of these tests.

CONCLUSIONS

A transonic investigation was made in the Langley 8-foot transonic tunnel and the Langley 8-foot transonic pressure tunnel of the drag rise

and the static longitudinal stability and control characteristics of a representative fighter-airplane model. Effects of body shape, wing thickness and camber, wing leading-edge flap deflection, tail-surface thickness, and speed-brake location were investigated. Limited data on the lateral stability characteristics and lateral-control effectiveness with ailerons and differentially operated stabilizer were obtained. The range of test Mach numbers extended from 0.60 to 1.43 and the Reynolds number was about 1.9×10^6 based upon the mean aerodynamic chord. The most important conclusions are summarized as follows:

1. The longitudinal stability increased with both lift coefficient and Mach number for the complete model.

2. The effective dihedral generally increased with Mach number and angle of attack up to about 6°. Only small changes in directional stability occurred with angle of attack at subsonic speeds up to 10° or 12°.

3. Area-rule modifications applied only to the fuselage provided reductions in the transonic drag rise up to 30 percent.

4. Reduction in wing thickness and tail thickness from about 5.5 to 4 percent in conjunction with area-rule modifications applied to the fuselage provided reductions in transonic drag rise up to 50 percent.

5. Fuselage modifications permitted increases at supersonic speeds of 24 percent in trimmed lift-drag ratio at 35,000 feet. Similar large improvements were indicated for 50,000 feet, but effects at sea level were insignificant.

6. A leading-edge flap increased the maximum lift-drag ratio from 10.5 to 12.5 at a Mach number of 0.80, but the effectiveness decreased rapidly at higher Mach numbers. Trim drag would be expected to reduce the gain from 2.0 to about 1.6.

7. Use of a conically cambered 4-percent-thick wing provided subsonic gains in lift-drag ratio from 10.2 to 12.0 at a Mach number of 0.9 and up to about 20 percent supersonically with no accompanying change in trim drag.

8. Both speed-brake configurations provided substantial drag increments but were accompanied by longitudinal trim changes throughout the Mach number range which would require 3° to 6° of stabilizer deflection.

9. Fuselage modifications were accountable for more than 20 percent increase in stabilizer effectiveness at both subsonic and supersonic speeds and removed a large decrease near a Mach number of 1.0.

10. Aileron effectiveness decreased above the critical Mach number so that at a Mach number of 1.43 the reduction amounted to nearly 50 percent.

11. Use of a differentially operated stabilizer provided adequate longitudinal control at all test Mach numbers, but insufficient lateral control at subsonic speeds. The rolling effectiveness at a Mach number of 1.12 was approximately equal to that for the ailerons.

Langley Research Center,
National Aeronautics and Space Administration,
Langley Field, Va., August 31, 1956.

REFERENCES

1. Wright, Ray H., Ritchie, Virgil S., and Pearson, Albin O.: Characteristics of the Langley 8-Foot Transonic Tunnel With Slotted Test Section. NACA Rep. 1389, 1958. (Supersedes NACA RM L51H10 by Wright and Ritchie and RM L51K14 by Ritchie and Pearson.)

2. Matthews, Clarence W.: An Investigation of the Adaptation of a Transonic Slotted Tunnel to Supersonic Operation by Enclosing the Slots With Fairings. NACA RM L55H15, 1955.

3. Whitcomb, Richard T.: Some Considerations Regarding the Application of the Supersonic Area Rule to the Design of Airplane Fuselages. NACA RM L56E23a, 1956.

4. Cahn, Maurice S.: An Experimental Investigation of Sting-Support Effects on Drag and a Comparison With Jet Effects at Transonic Speeds. NACA Rep. 1353, 1958. (Supersedes NACA RM L56F18a.)

5. Whitcomb, Charles F., and Osborne, Robert S.: An Experimental Investigation of Boundary Interference on Force and Moment Characteristics of Lifting Models in the Langley 16- and 8-Foot Transonic Tunnels. NACA RM L52L29, 1953.

6. Davis, Don D., Jr., and Moore, Dewey: Analytical Study of Blockage- and Lift-Interference Corrections for Slotted Tunnels Obtained by the Substitution of an Equivalent Homogeneous Boundary for the Discrete Slots. NACA RM L53E07b, 1953.

7. Critzos, Chris C.: Lateral-Control Investigation at Transonic Speeds of Differentially Deflected Horizontal-Tail Surfaces for a Configuration Having a 6-Percent-Thick 45° Sweptback Wing. NACA RM L55I26, 1955.

[redacted]

TABLE I.- MODEL DIMENSIONS

[All dimensions are in inches]

	Number 1	Number 2	Number 3	Number 4
Complete model:				
Overall length	28.58	29.09		
Frontal area	9.74	9.91		
Fineness ratio	7.18	7.86		
Frontal area to wing area	0.098	0.104		
Center-of-gravity location, percent $\bar{c}$	28.7	28.7		
Wings:				
Airfoil section, root	65A006	65A004	65A004	
Airfoil section, tip	65A005	65A004	[a]65A004	
Airfoil chord, root	8.48	8.48	8.48	
Airfoil chord, tip	2.12	2.10	2.10	
Span projected	17.91	17.97	17.97	
Area projected (excluding extensions)	95.0	95.1	95.1	
Aspect ratio	3.37	3.33	3.33	
Taper ratio	0.25	0.25	0.25	
Mean aerodynamic chord	5.94	5.95	5.95	
Mean-aerodynamic-chord location, spanwise	3.60	3.60	3.60	
Mean-aerodynamic-chord location, longitudinal, from fuselage reference station	17.49	17.49	17.49	
Sweepback, leading edge, deg	47.1	47.1	47.1	
Sweepback, c/4 chord, deg	42.0	42.0	42.0	
Dihedral, deg	-5	-5	-5	
Incidence at root chord, deg	-1	-1	-1	
Twist, deg	0	0	(a)	
Location of c/4 root chord, above ref.	1.12	1.12	1.12	
Location of c/4 root chord, longitudinal	15.74	15.74	15.74	
Horizontal tails:				
Airfoil section, root	65A006	65A006	65A006	65A004
Airfoil section, tip	65A004	65A004	65A004	65A004
Airfoil chord, root	4.81	4.56	4.40	4.56
Airfoil chord, tip	0.72	0.67	0.72	0.67
Span, projected	9.70	9.12	8.88	9.12
Area, projected, exposed	17.3	14.5	14.1	14.5
Aspect ratio, based on total area	2.53	1.97	1.80	1.97
Taper ratio	0.15	0.15	0.16	0.15
Dihedral, deg	5.2	5.2	5.0	5.0
Sweepback, leading edge, deg	50	50	50	50
Sweepback, c/4 chord, deg	45	45	45	45
Location of root chord, longitudinal	24.85	24.75	24.75	24.75
Location of root chord, above or below ref. axis	-0.34	-0.34	0.85	-0.34
Vertical tail:				
Airfoil section, root	65A006	65A004		
Airfoil section, tip	65A004	65A004		
Chord, root	5.59	5.59		
Chord, tip	1.72	1.72		
Span, total	6.09	6.11		
Area, total	25.25	25.35		
Area, exposed	17.65	17.71		
Aspect ratio	1.47	1.47		
Taper ratio	0.26	0.26		
Sweepback, leading edge, deg	50	50		
Sweepback, c/4 chord, deg	45	45		
Location of root chord, longitudinal	22.26	22.26		
Location of root chord, above axis	1.26	1.26		
Fuselage:				
Length	[b]25.30	27.88		
Frontal area	6.72	6.81		
Fineness ratio	8.63	9.45		

[a]Conical camber.

[b]No plug.

[redacted]

TABLE II.- INDEX OF BASIC DATA

Figure	Description	Configurations		
		Body	Wing	Tail[1]
	Longitudinal data			
10	Horizontal tail modifications	1	1	Off, 1, 2, 3
11	Stabilizer effect	1	1	2
12	Stabilizer effect	4	1	2
13	Stabilizer effect (differential)	3	1	2
14	Wing modifications	4	1, 2, 3	2, 4
15	Wing leading-edge flaps	4	1	2
16	[2]Tail thickness	2	1	Off, 2, 4
17	Wing and tail thicknesses	2	1	2
		2	2	4
18	Wing and tail thicknesses	4	1	2
		4	2	2
		4	2	4
19	Fuselage modifications - wing and body	1, 3	1	Off
20	Fuselage modifications - complete model	1, 2, 3	1	2
21	Fixed transition	3	1	Off
22	Fixed transition	2	1	2
23	Fixed transition	3	1	2
24	Fixed transition	2	2	4
25	Fixed transition	4	1	2
26	Speed brake 1	1	1	Off, 2
27	Speed brake 2	1	1	Off, 2
	Lateral data			
28	Sideslip in pitch	4	1	2
29	Pitch in sideslip	2, 4	1	2
30	Ailerons, longitudinal	4	1	2
31	Ailerons, lateral	4	1	2
32	Effect of tail in pitch, ailerons deflected	3	1	Off, 2
33	[2]Effect of ailerons in sideslip, M = 1.43	2	1	2
34	Differential stabilizer	3	1	2

[1]Tail denotes complete tail, that is, both horizontal and vertical. The numerical designation is as follows:

Tail	Horizontal	Vertical
1	1	1
2	2	1
3	3	1
4	4	2

[2]Data from Langley 8-foot transonic pressure tunnel.

[redacted]

TABLE III.- INDEX OF SUMMARY FIGURES

Figure	Description
35	Effect of tail modifications
36	Effects of fuselage modifications and fixed transition, tails off
37	Effects of fuselage modification and fixed transition, complete model
38	Effects of fuselage modifications and fixed transition on wave drag, tails off
39	Effects of fuselage modifications and fixed transition on wave drag, tail 2
40	Effect of fuselage modifications on lateral-stability derivatives
41	Effect of fuselage modifications on trimmed lift-drag ratio
42	Effect of wing modifications
43	Effect of tail thickness modifications
44	Effects of wing and tail modifications on wave drag
45	Speed-brake drag increments
46	Stabilizer effectiveness
47	Effect of ailerons on lateral-stability derivatives
48	Comparison of rolling effectiveness

[redacted]

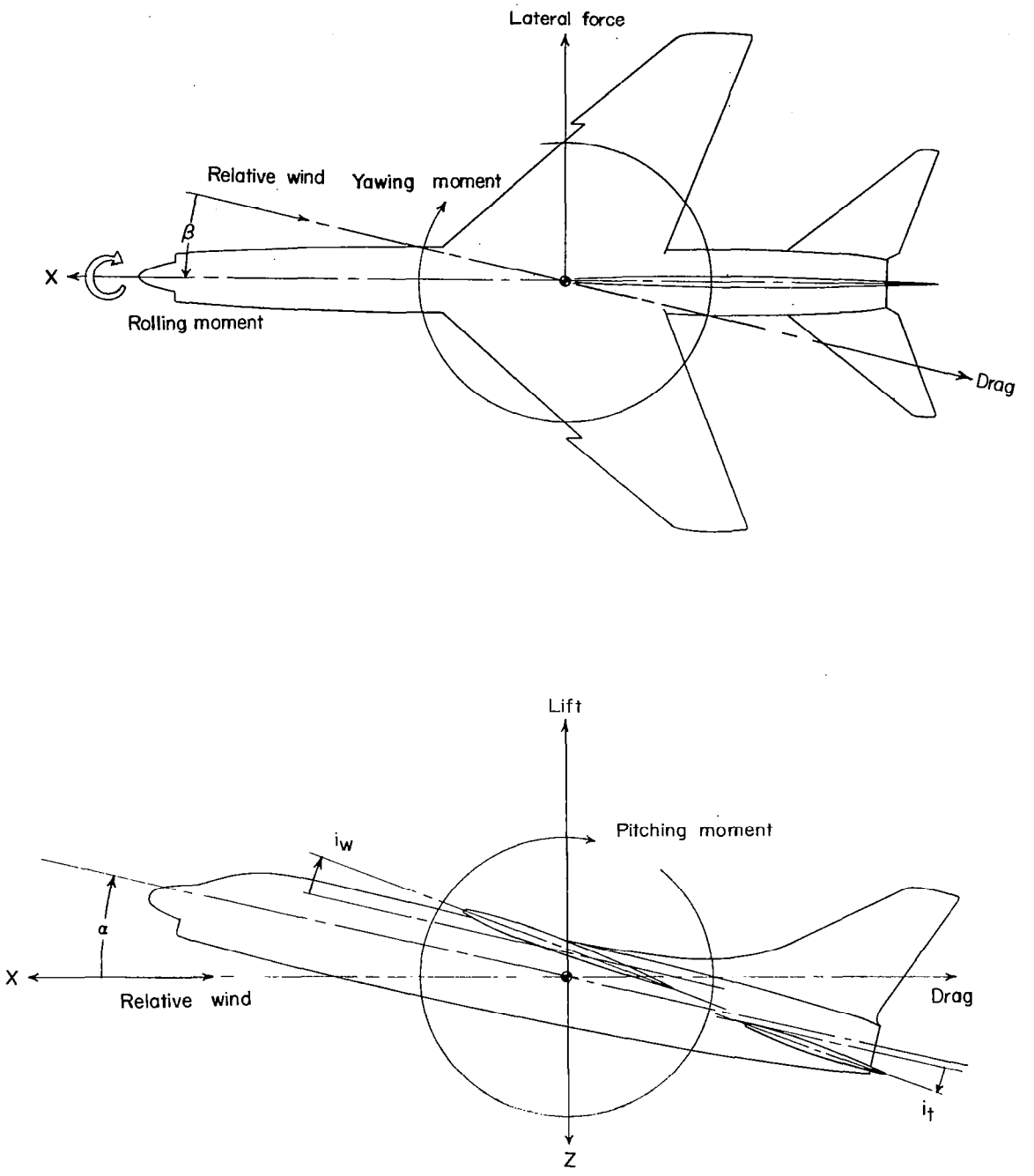

Figure 1.- Coordinate system of stability axes used.

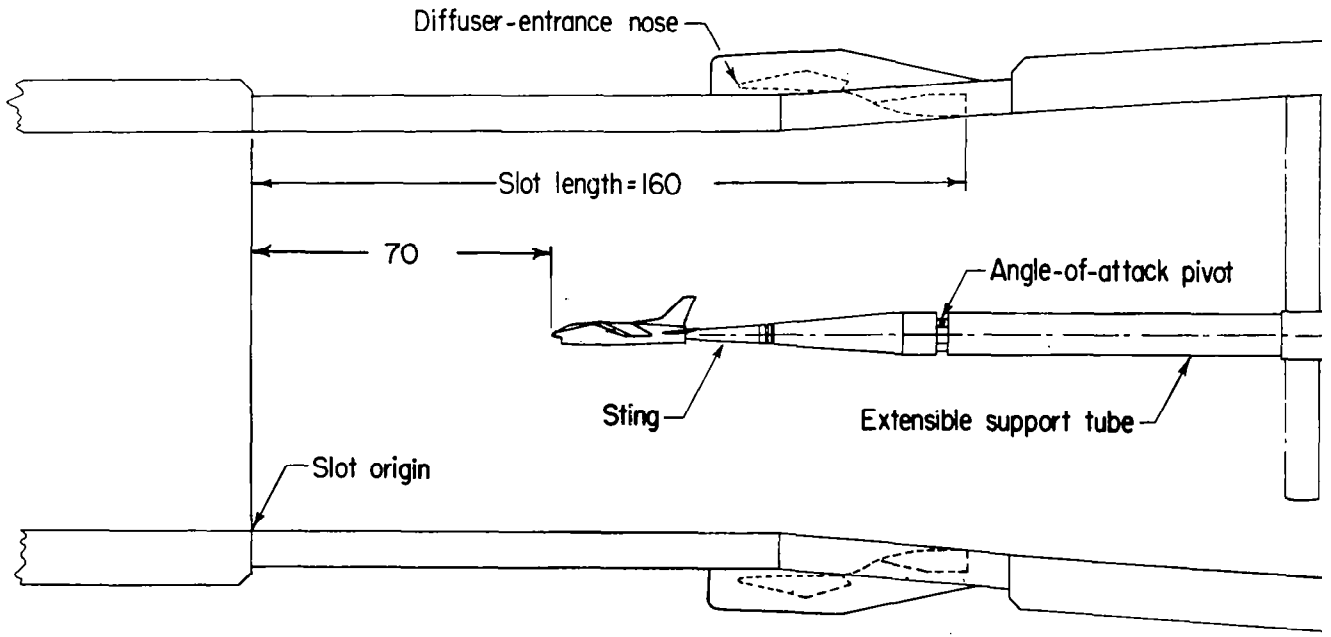

(a) 8-foot transonic tunnel.

Figure 2.- Sketches of model mounted in wind tunnels. (All dimensions are in inches.)

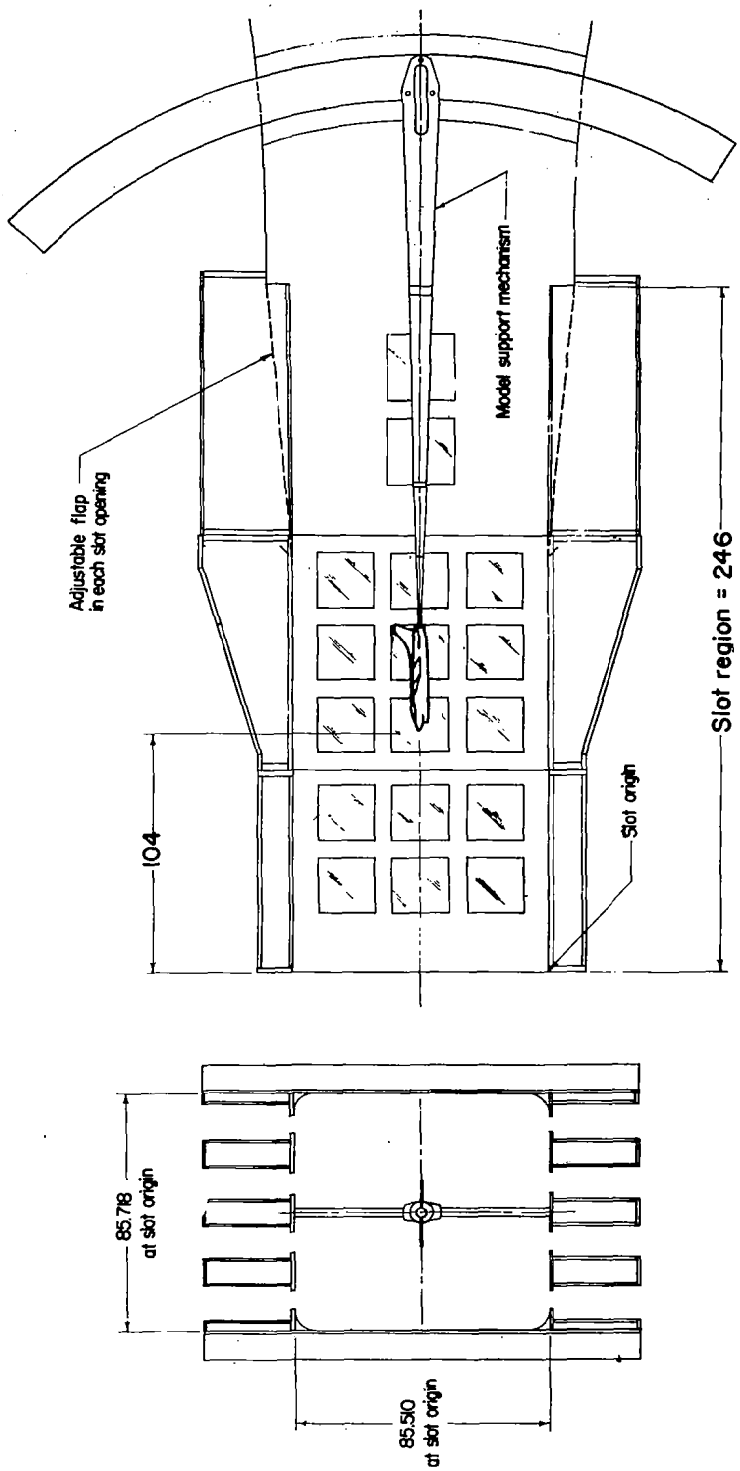

(b) 8-foot transonic pressure tunnel.

Figure 2.- Concluded.

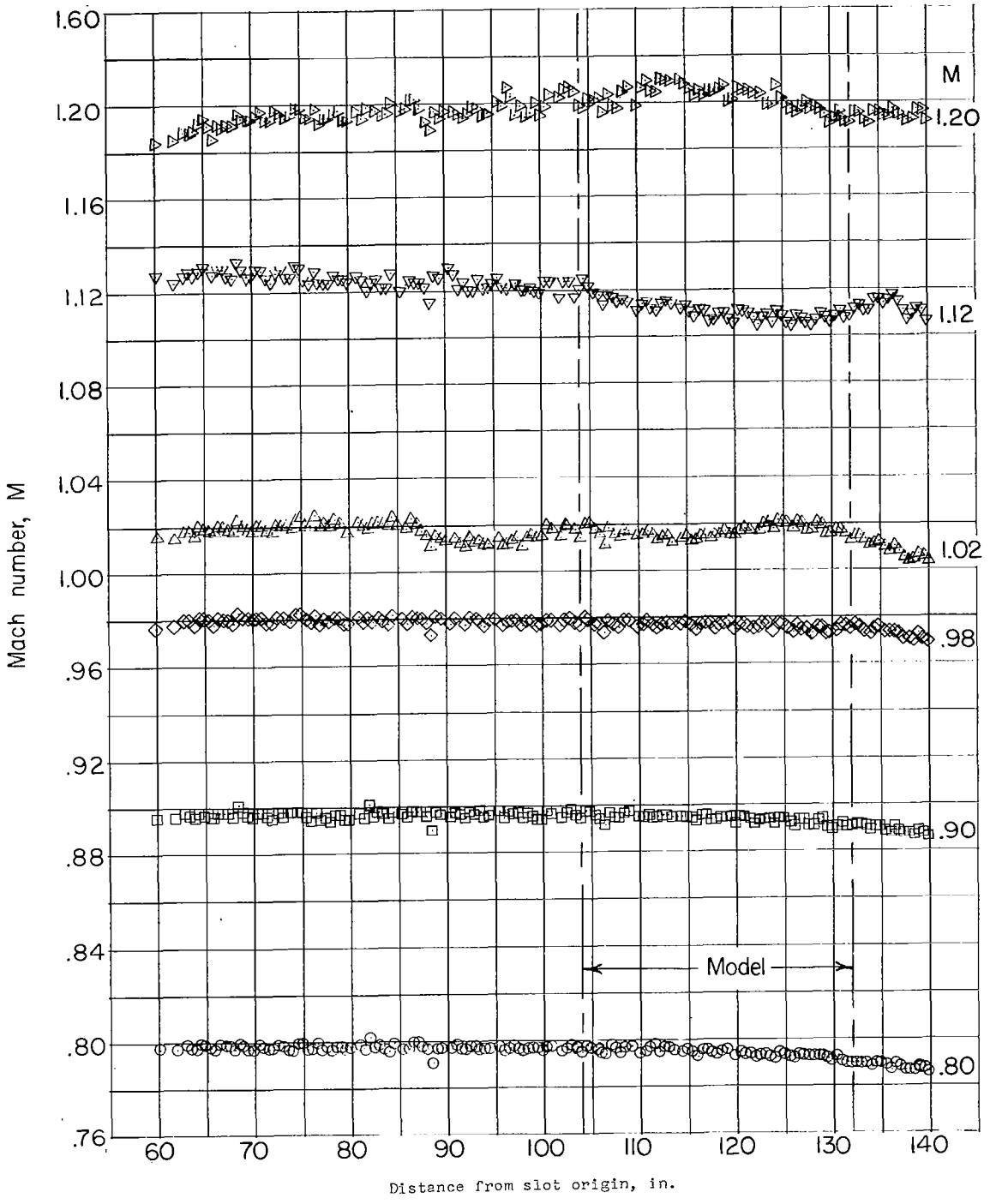

Figure 3.- Representative Mach number distribution in test section of Langley 8-foot transonic pressure tunnel.

Wing geometry (not including chord extension)	
Aspect ratio	3.37
Taper ratio	0.25
Sweep angle (c/4), deg	42.00
Dihedral, deg	-5.00
M.A.C.	5.94
Airfoil:	
Root	65A006
Tip	65A005
Center of gravity (distance from L.E. of $\bar{c}$)	0.287$\bar{c}$

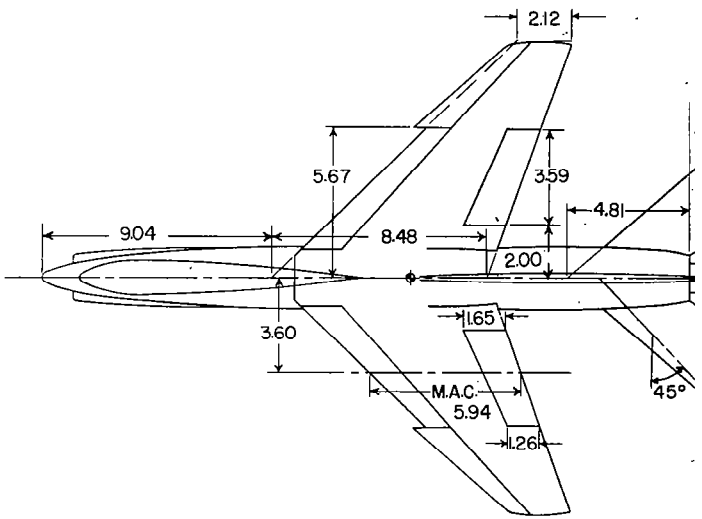

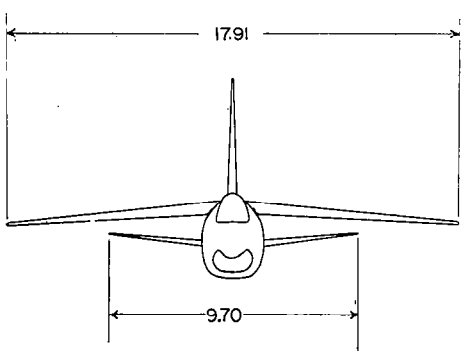

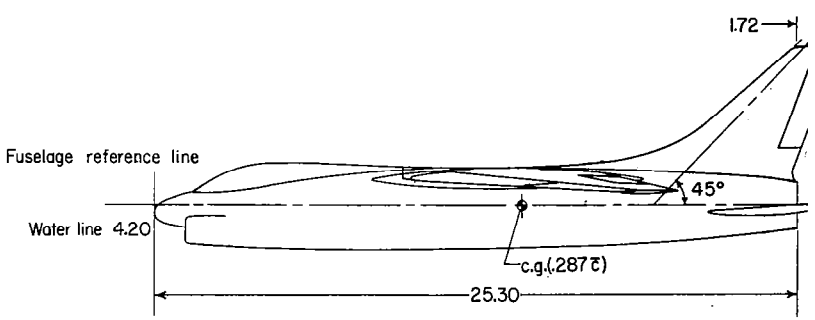

Figure 4.- Three-view drawing showing principal dimensions of airplane model. (All dim
are in inches.)

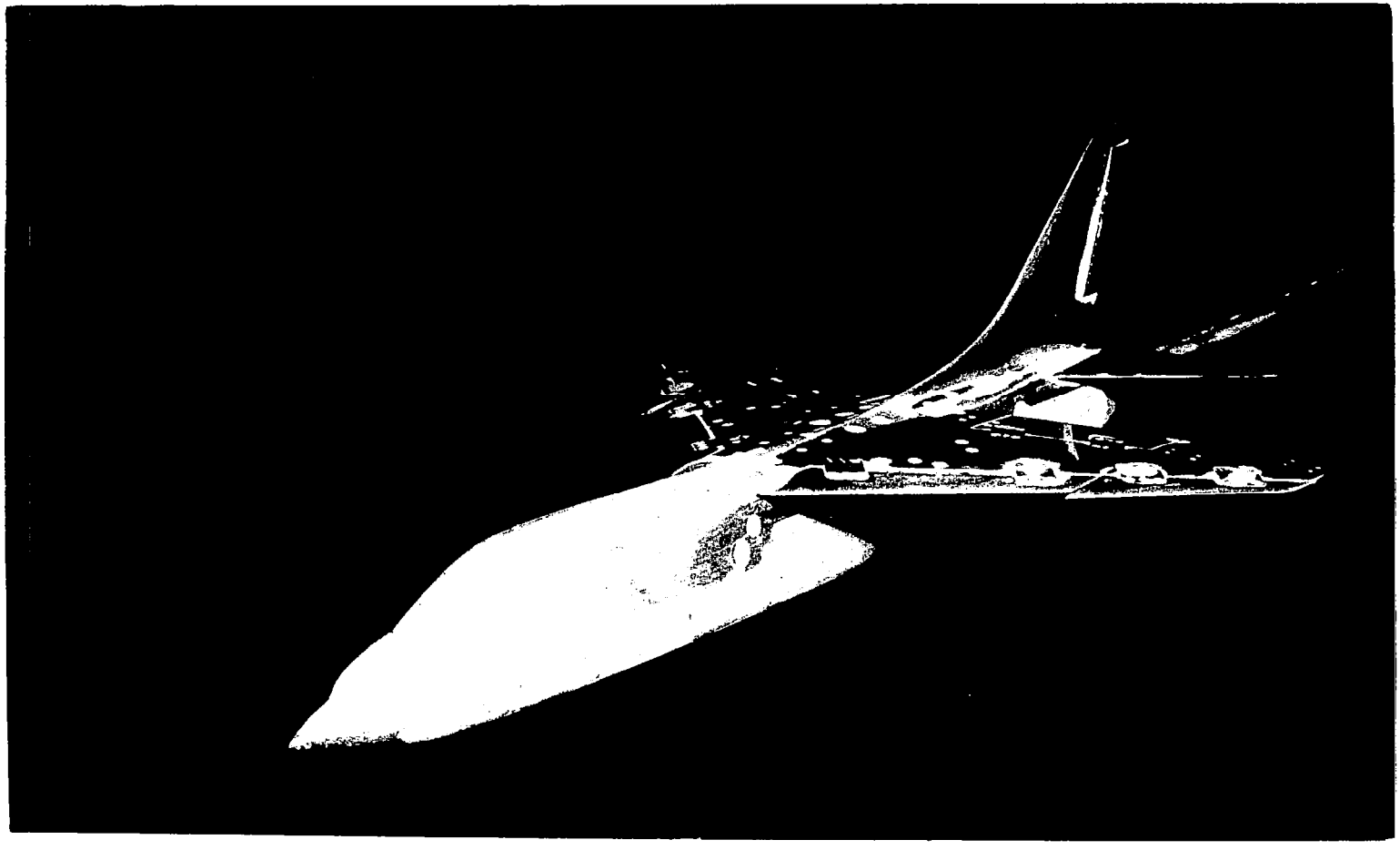

L-82454

Figure 5.- View of complete model with basic fuselage and raised horizontal tail.

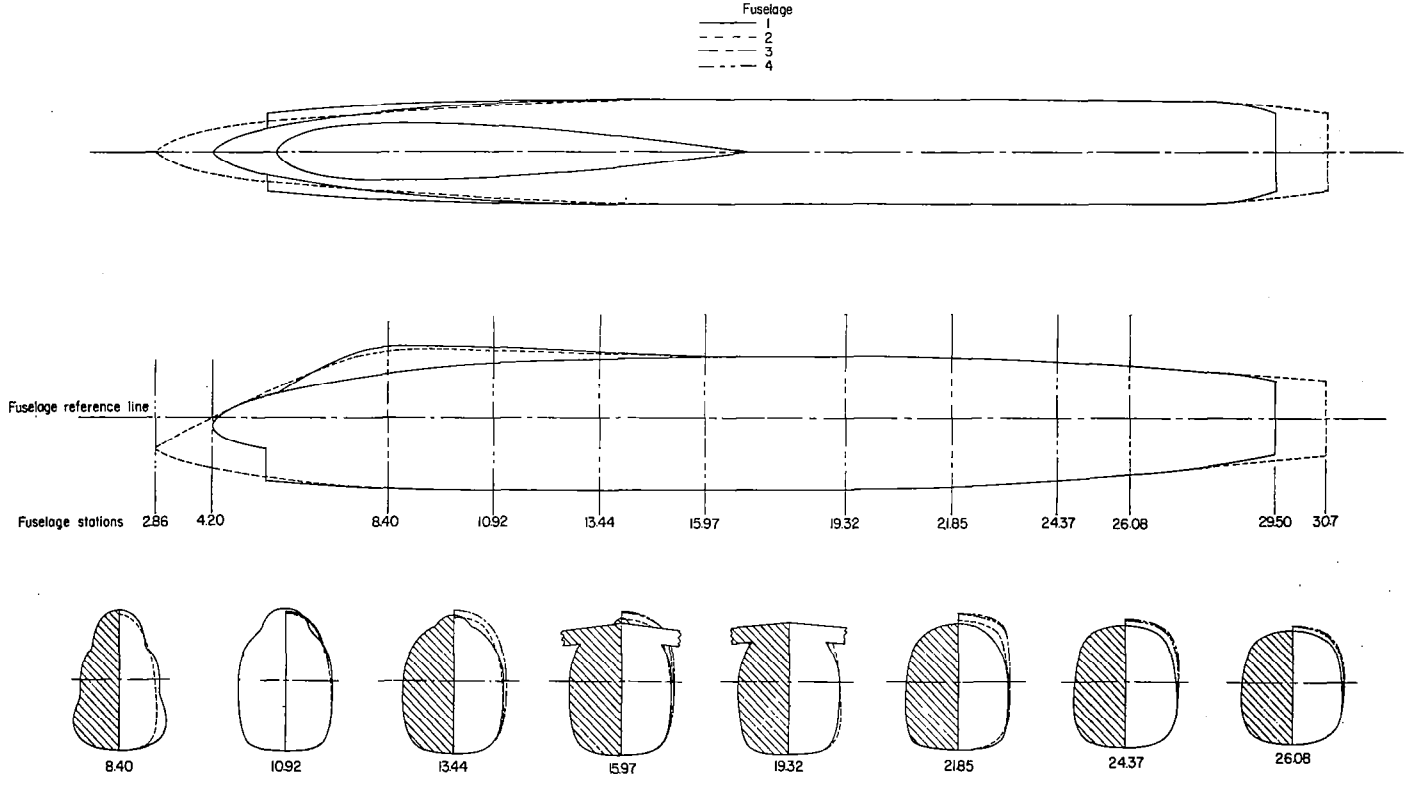

(a) Fuselage modifications.

Figure 6.- Modifications tested on model of airplane. (All dimensions are in inches.)

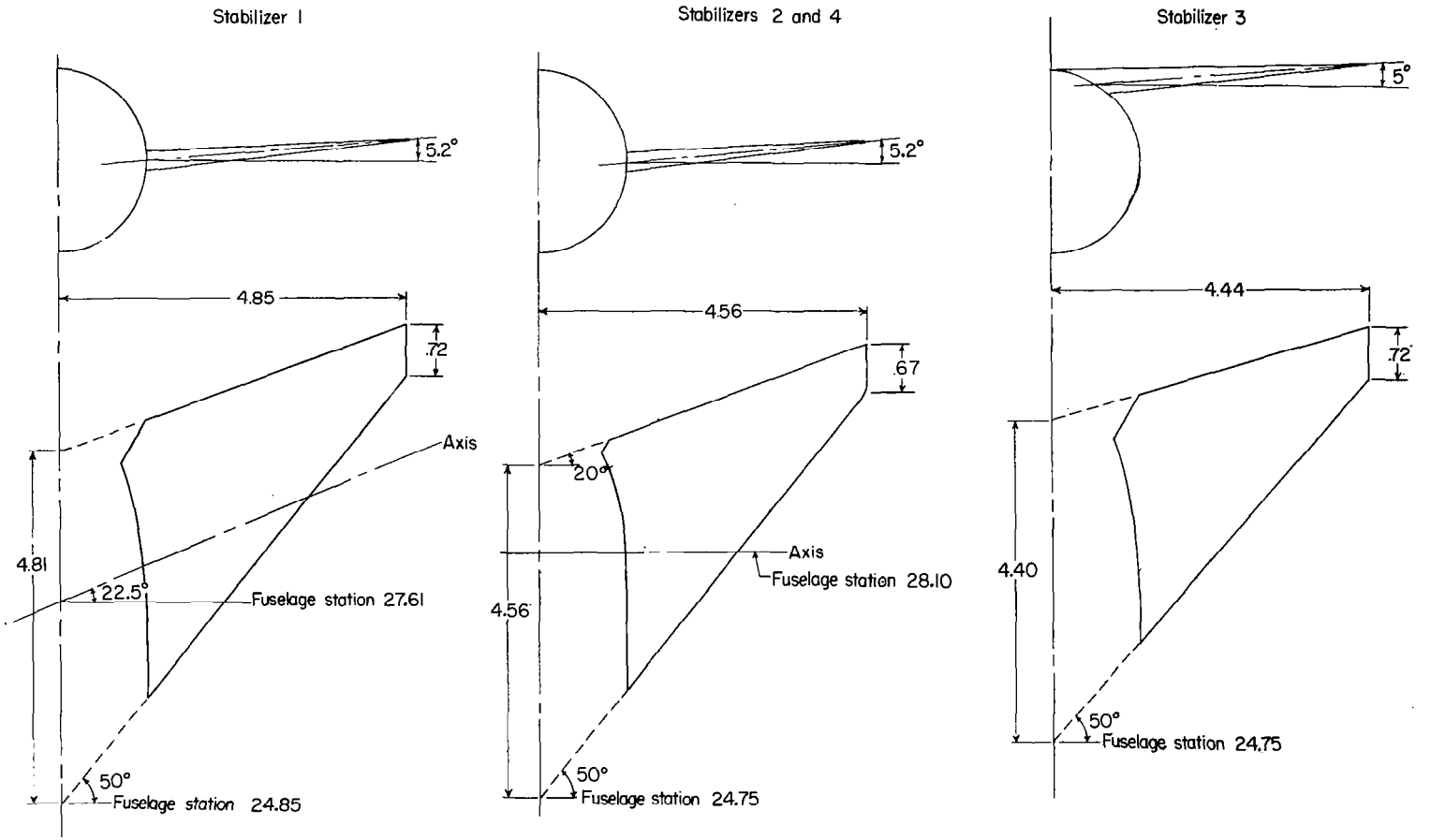

(b) Stabilizer modifications.

Figure 6.- Continued.

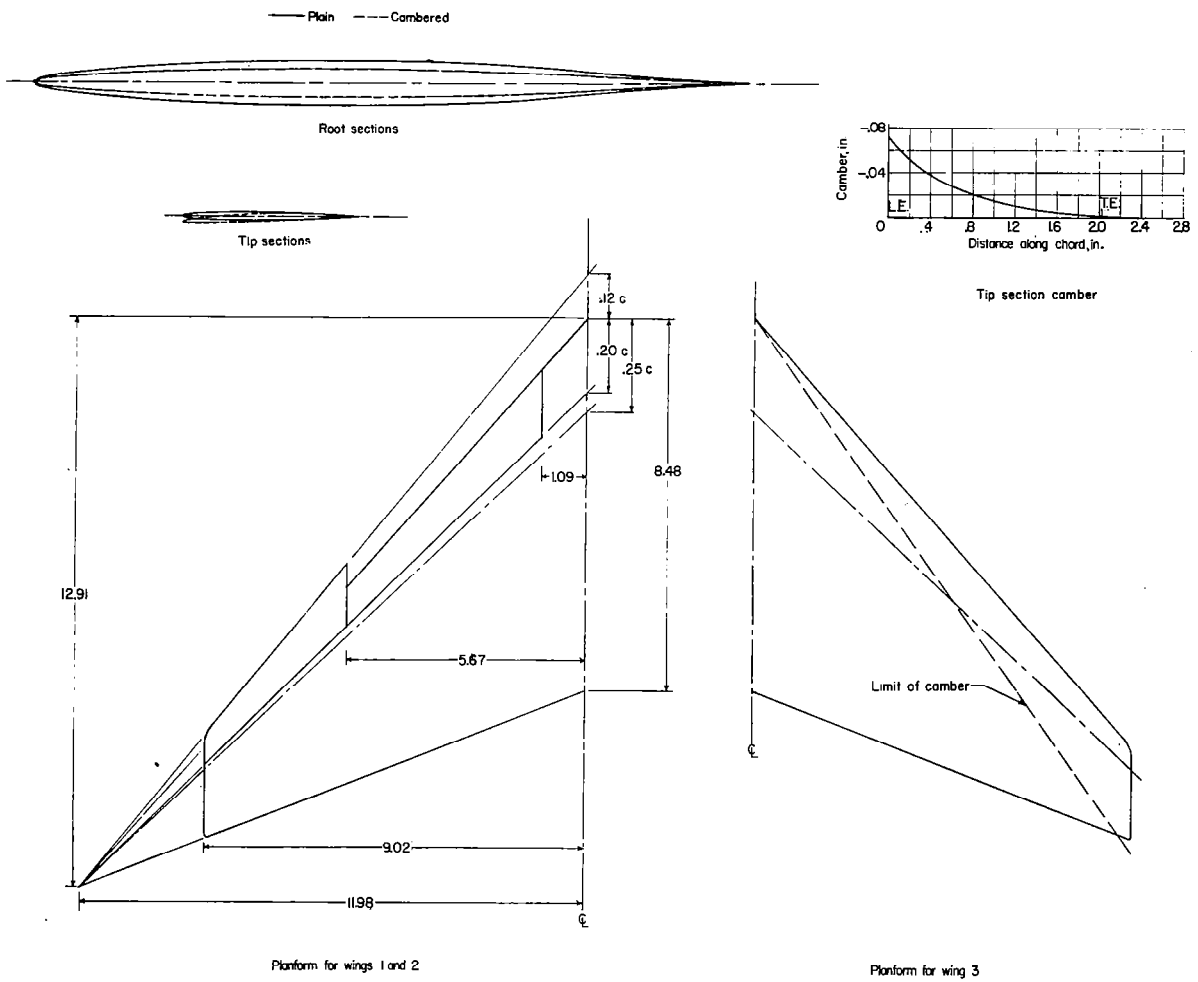

(c) Wing modifications.

Figure 6.- Concluded.

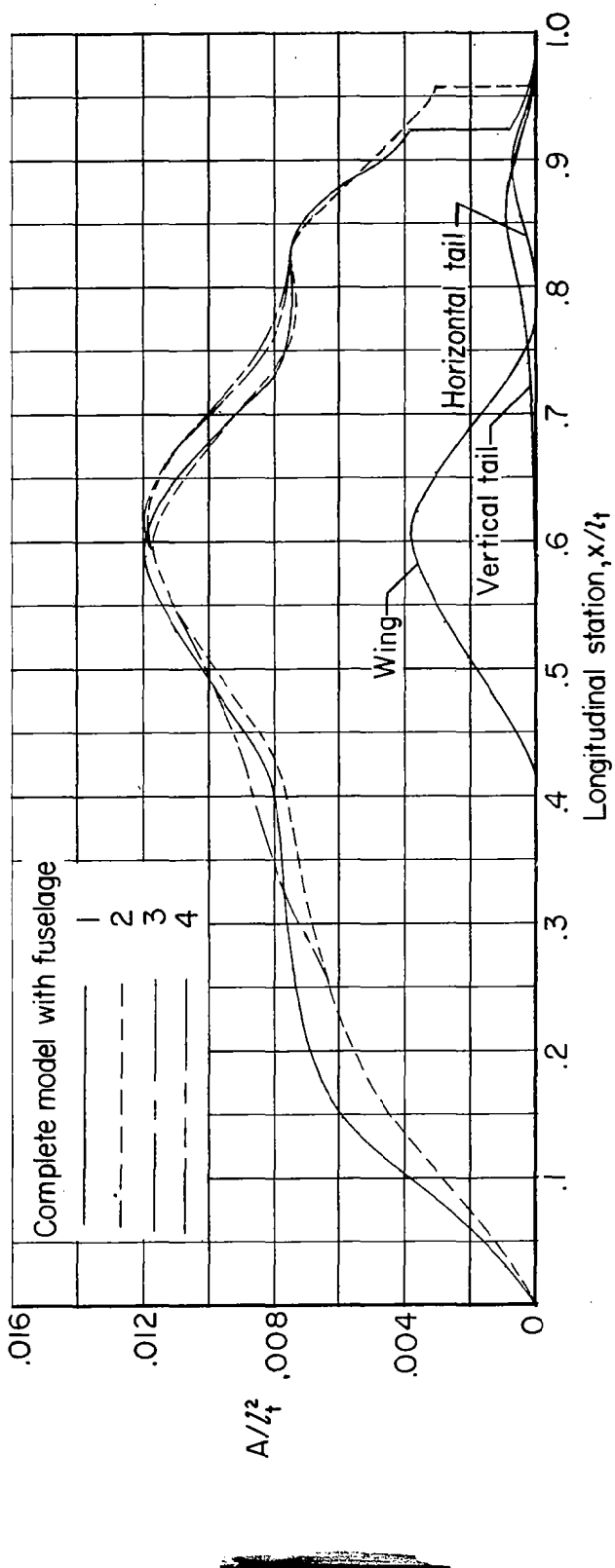

Figure 7.- Area distributions normal to fuselage reference axis of model with wing 1 and tail 1.

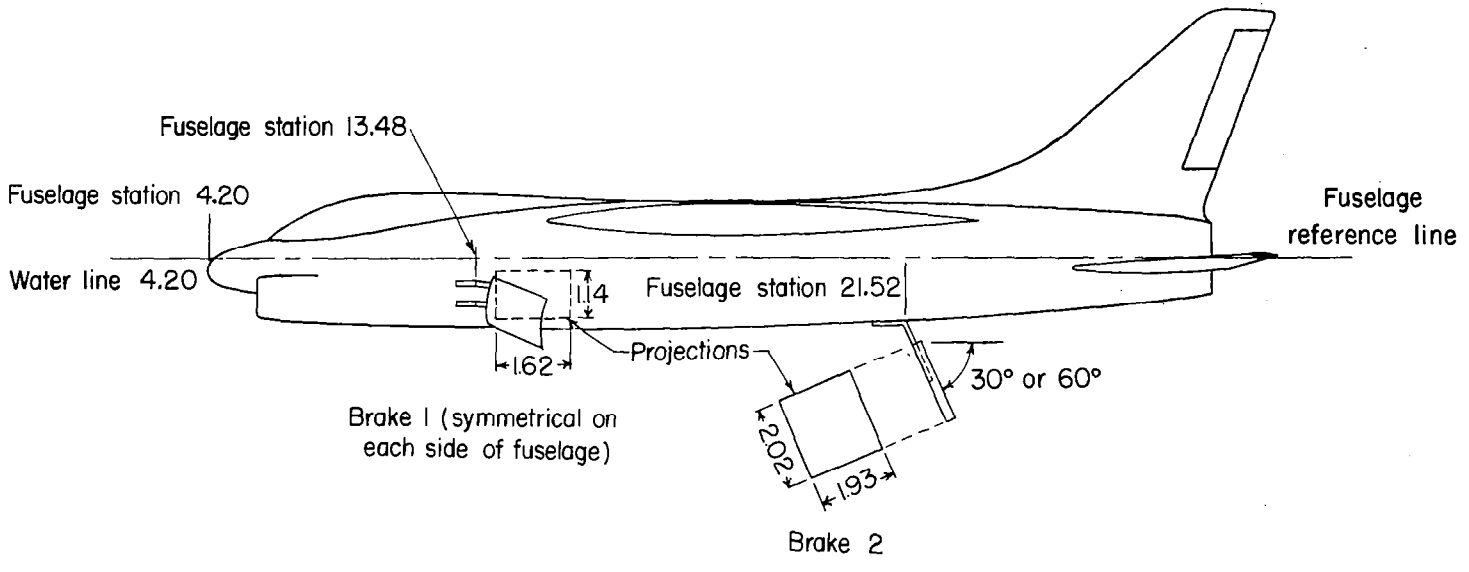

Figure 8.- Speed-brake configurations tested on model.

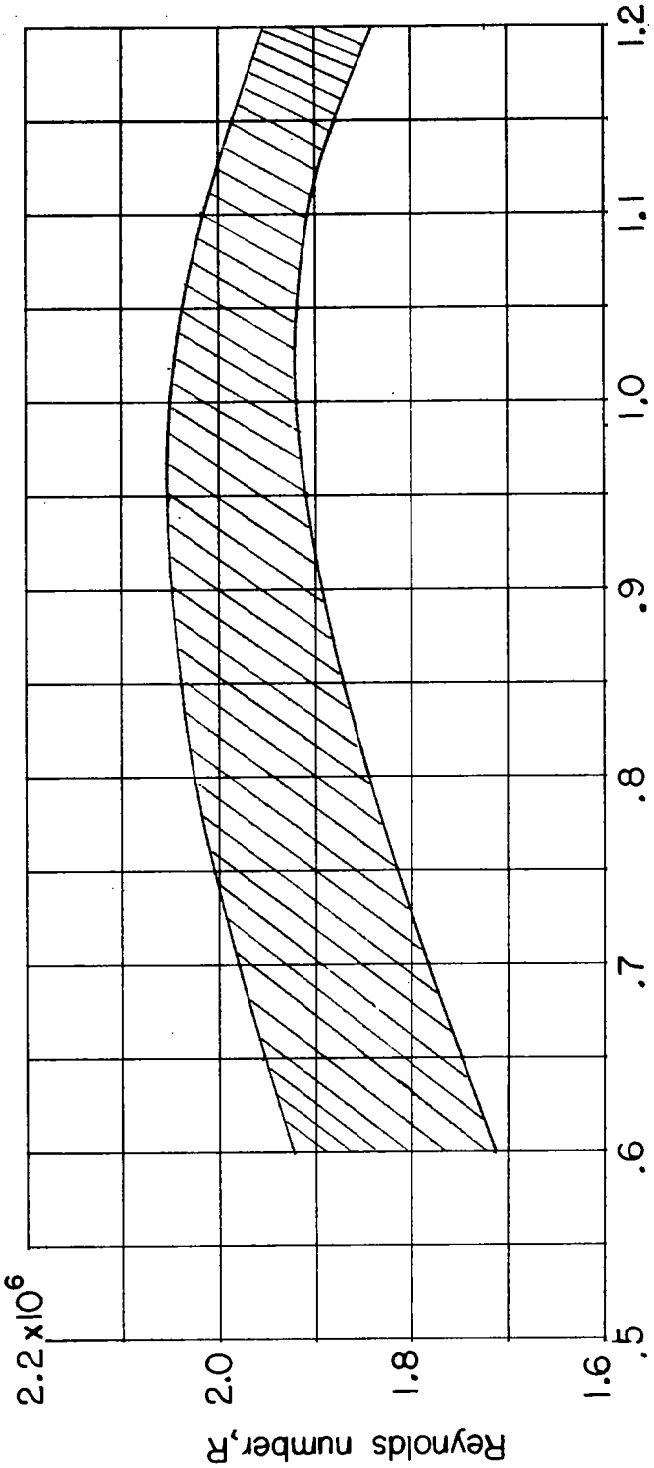

Figure 9.- Range of test Reynolds numbers as a function of test Mach numbers, based on wing mean aerodynamic chord.

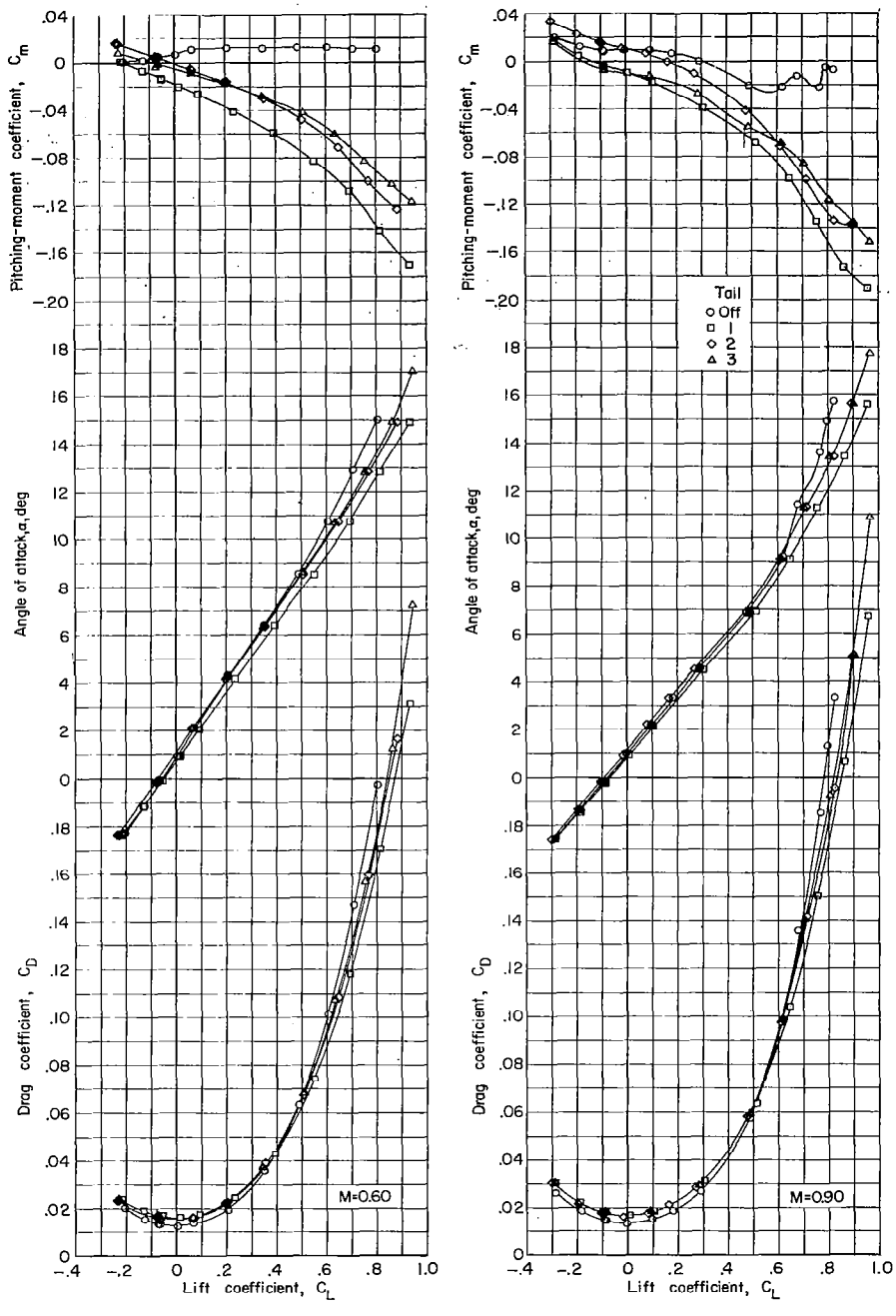

(a) M = 0.60 and 0.90.

Figure 10.- Effect of horizontal-stabilizer modifications on basic longitudinal aerodynamic characteristics; fuselage 1, wing 1, $i_t = 0^o$.

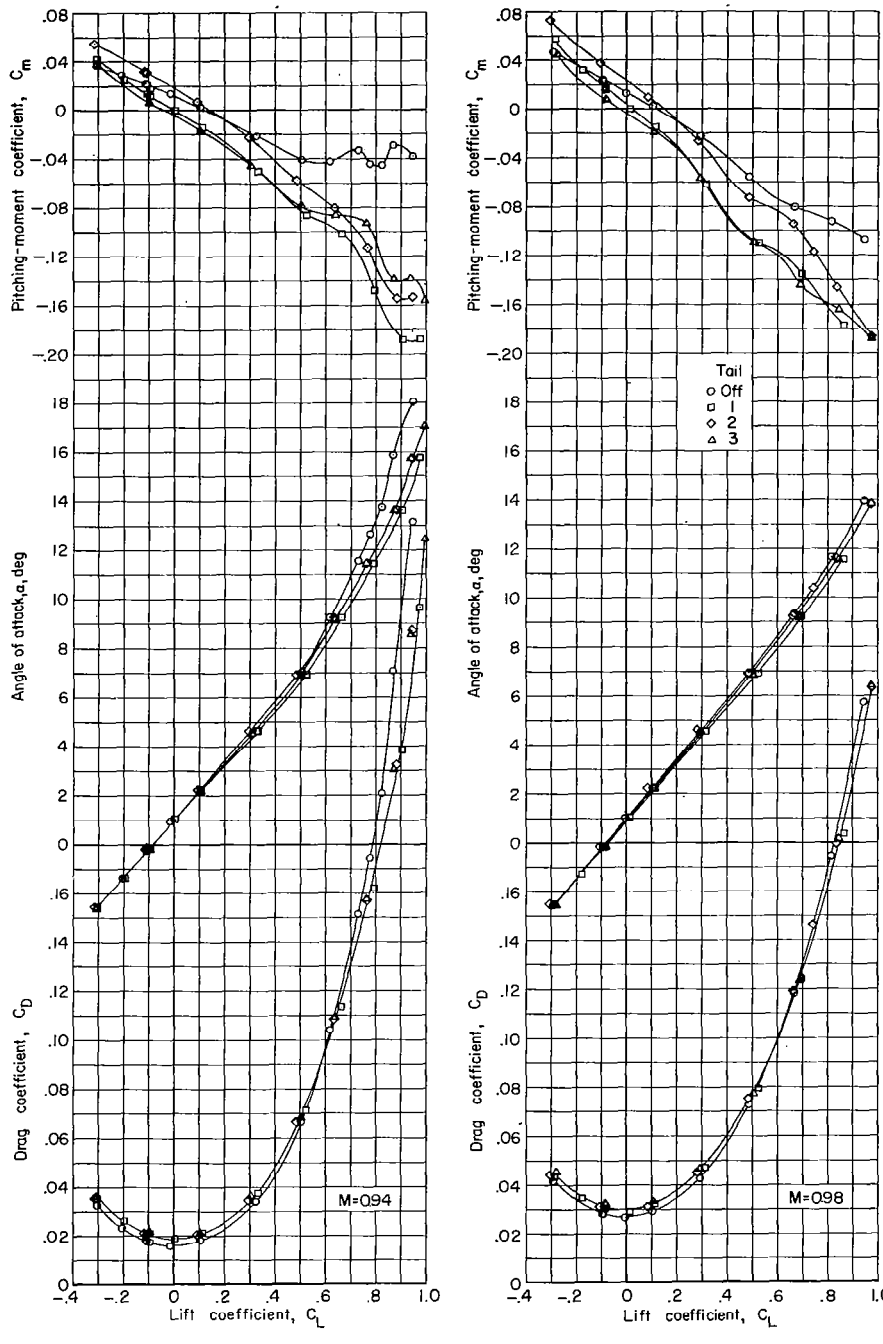

(b) M = 0.94 and 0.98.

Figure 10.- Continued.

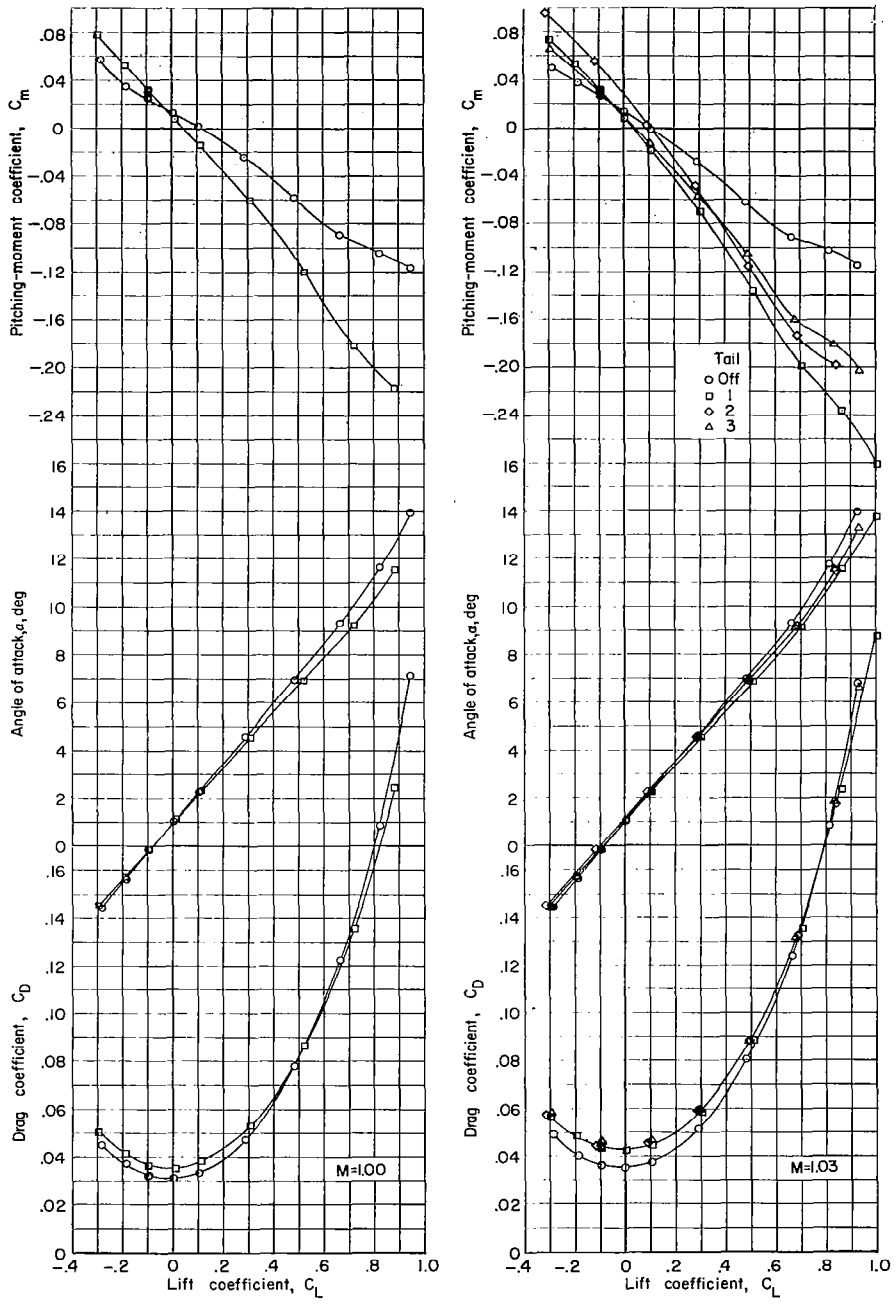

(c) M = 1.00 and 1.03.

Figure 10.- Continued.

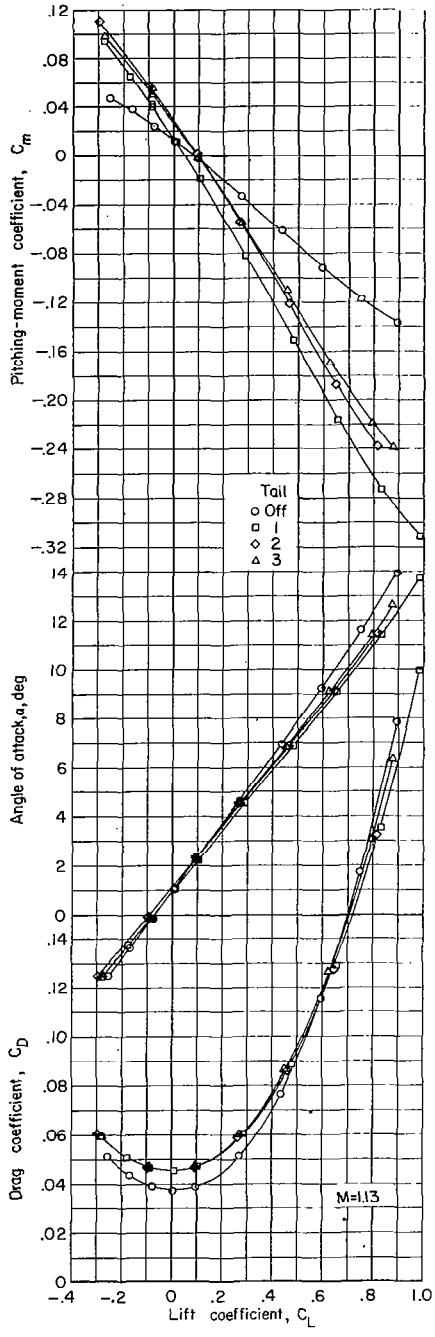

(d) M = 1.13.

Figure 10.- Concluded.

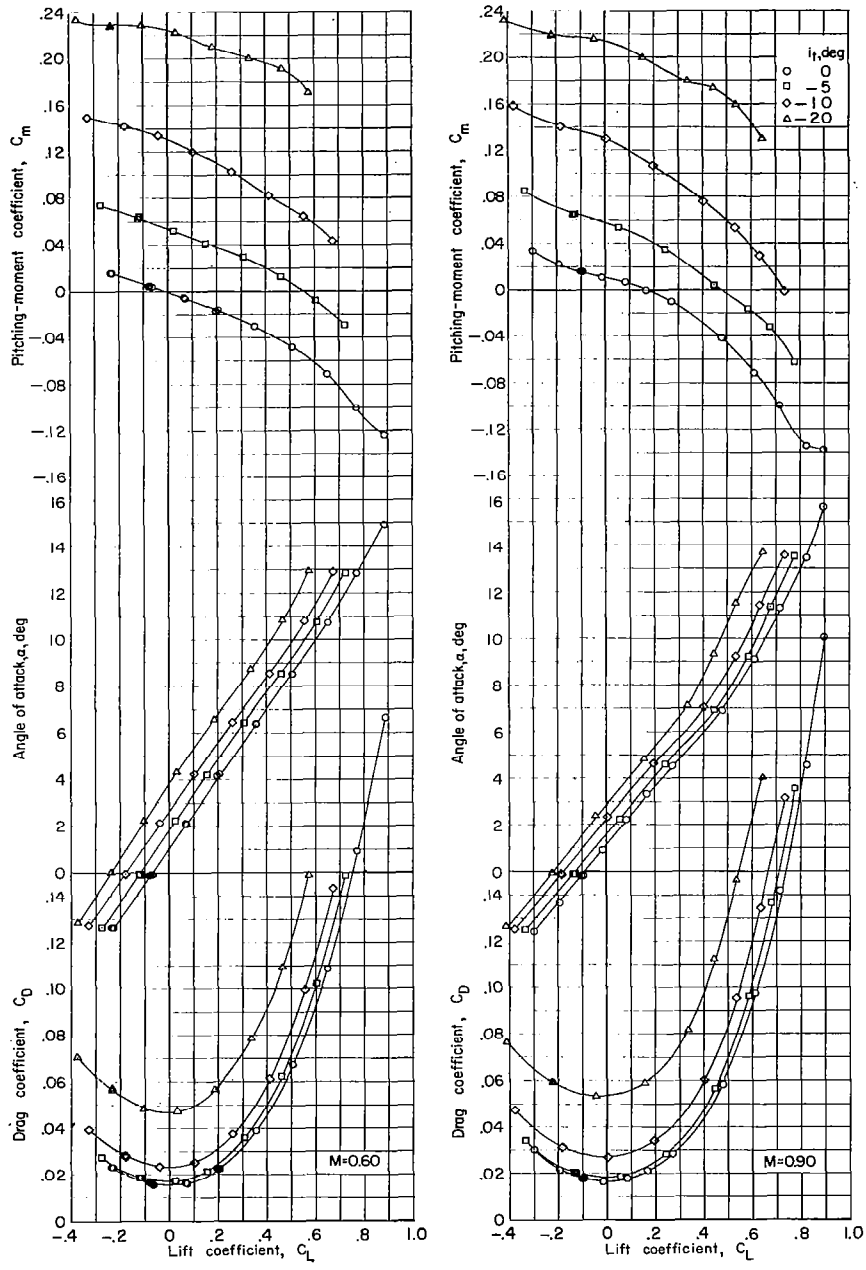

(a) M = 0.60 and 0.90.

Figure 11.- Effect of stabilizer incidence on the longitudinal characteristics; fuselage 1, wing 1, tail 2.

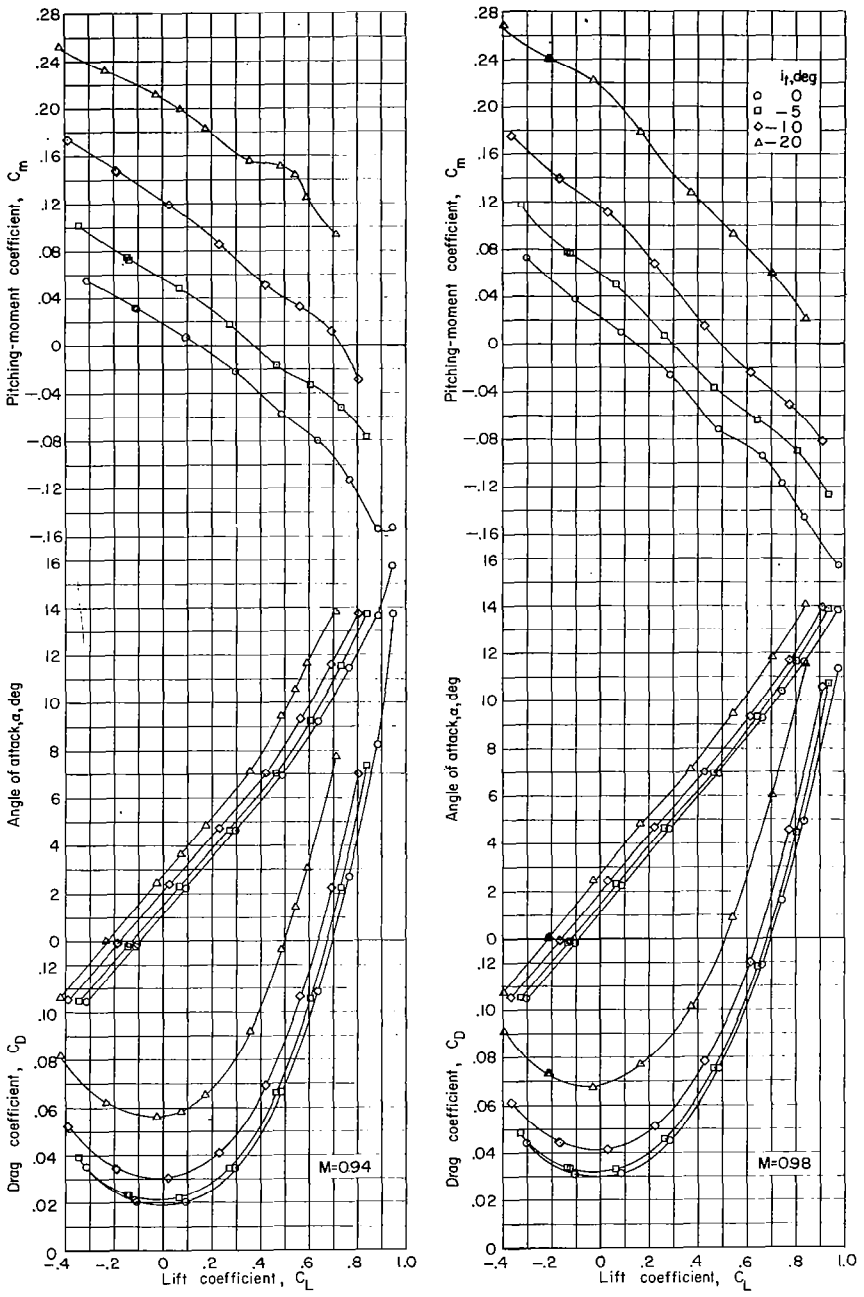

(b) M = 0.94 and 0.98.

Figure 11.- Continued.

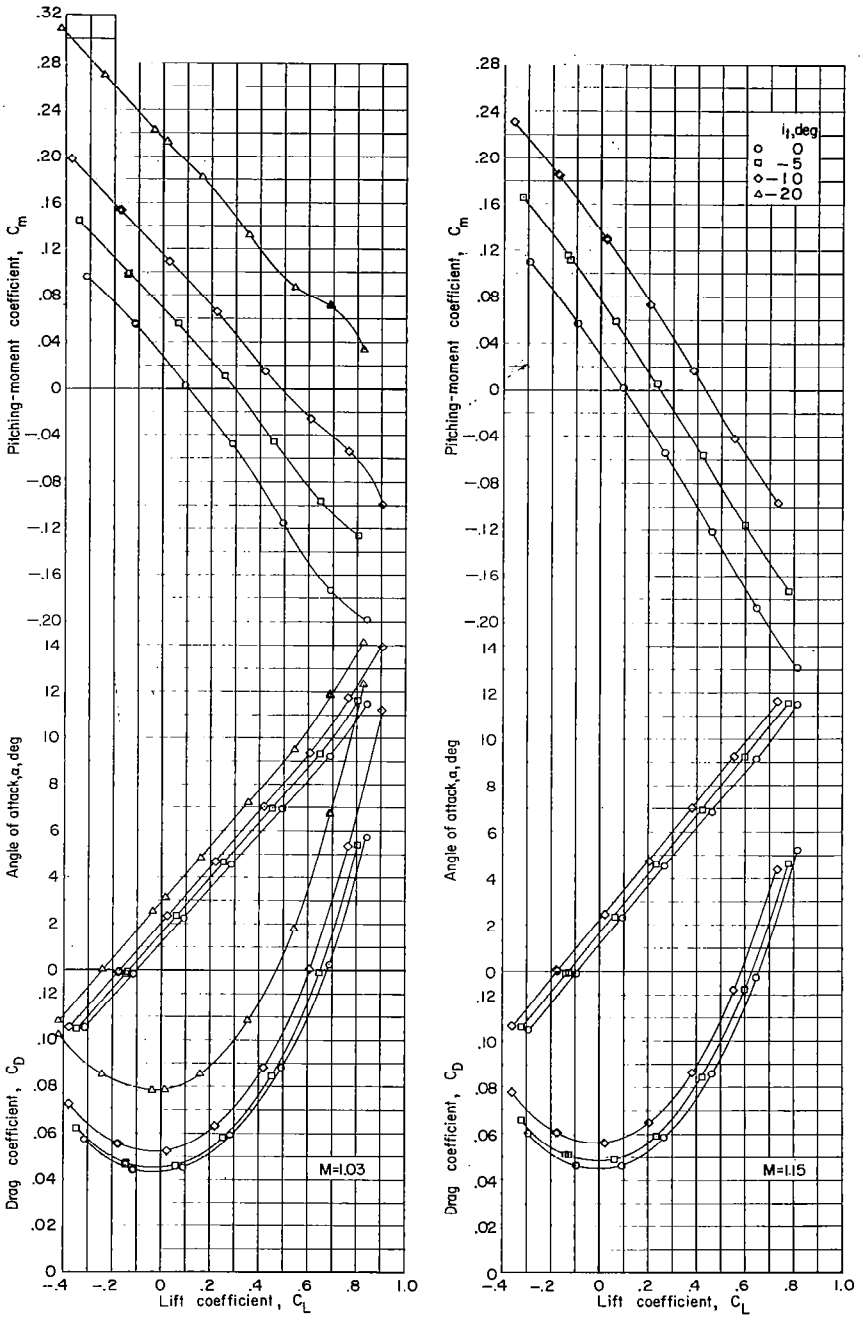

(c) M = 1.03 and 1.15.

Figure 11.- Concluded.

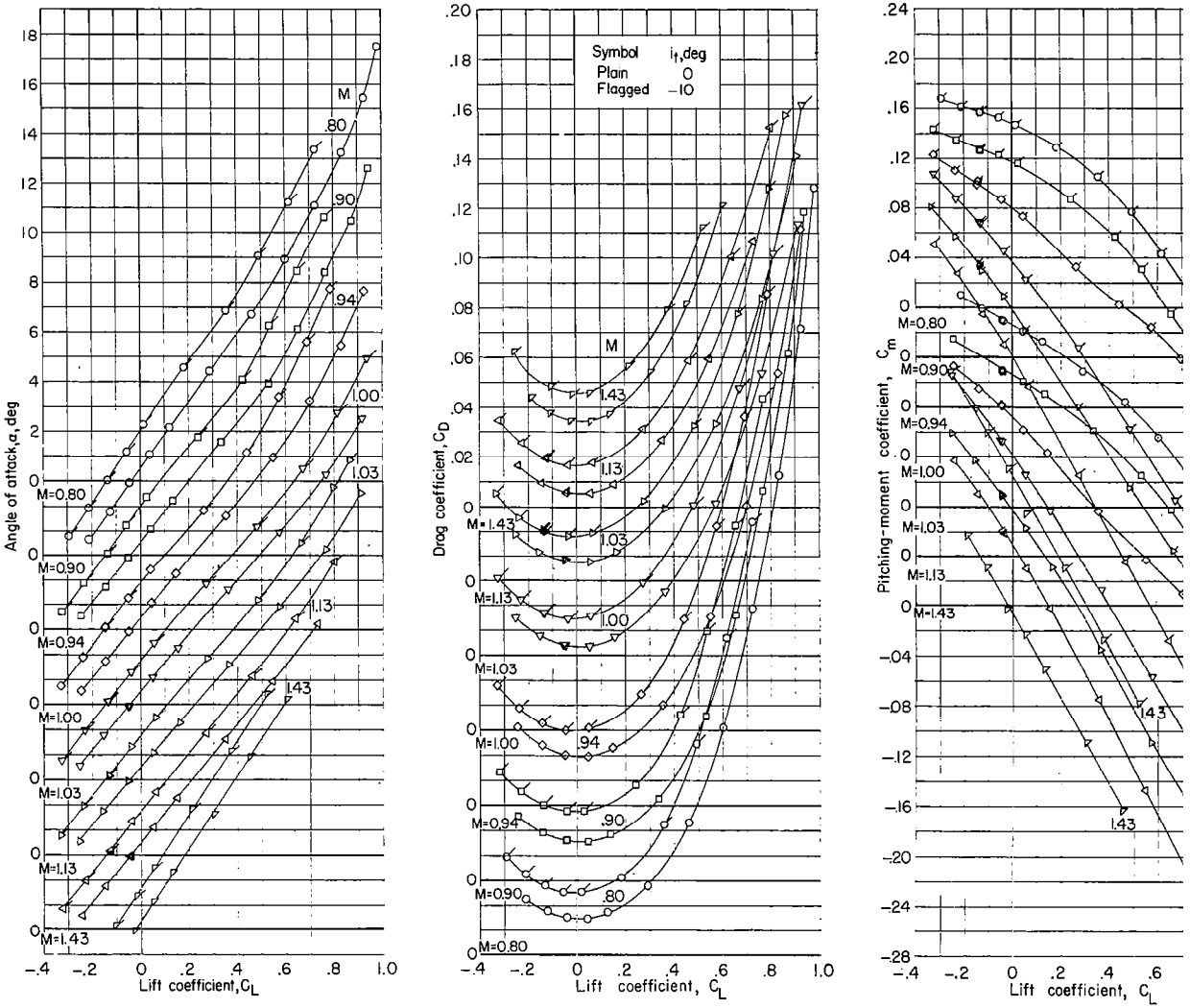

Figure 12.- Effect of stabilizer incidence on longitudinal aerodynamic characteristics; fuselage 4, wing 1, tail 2.

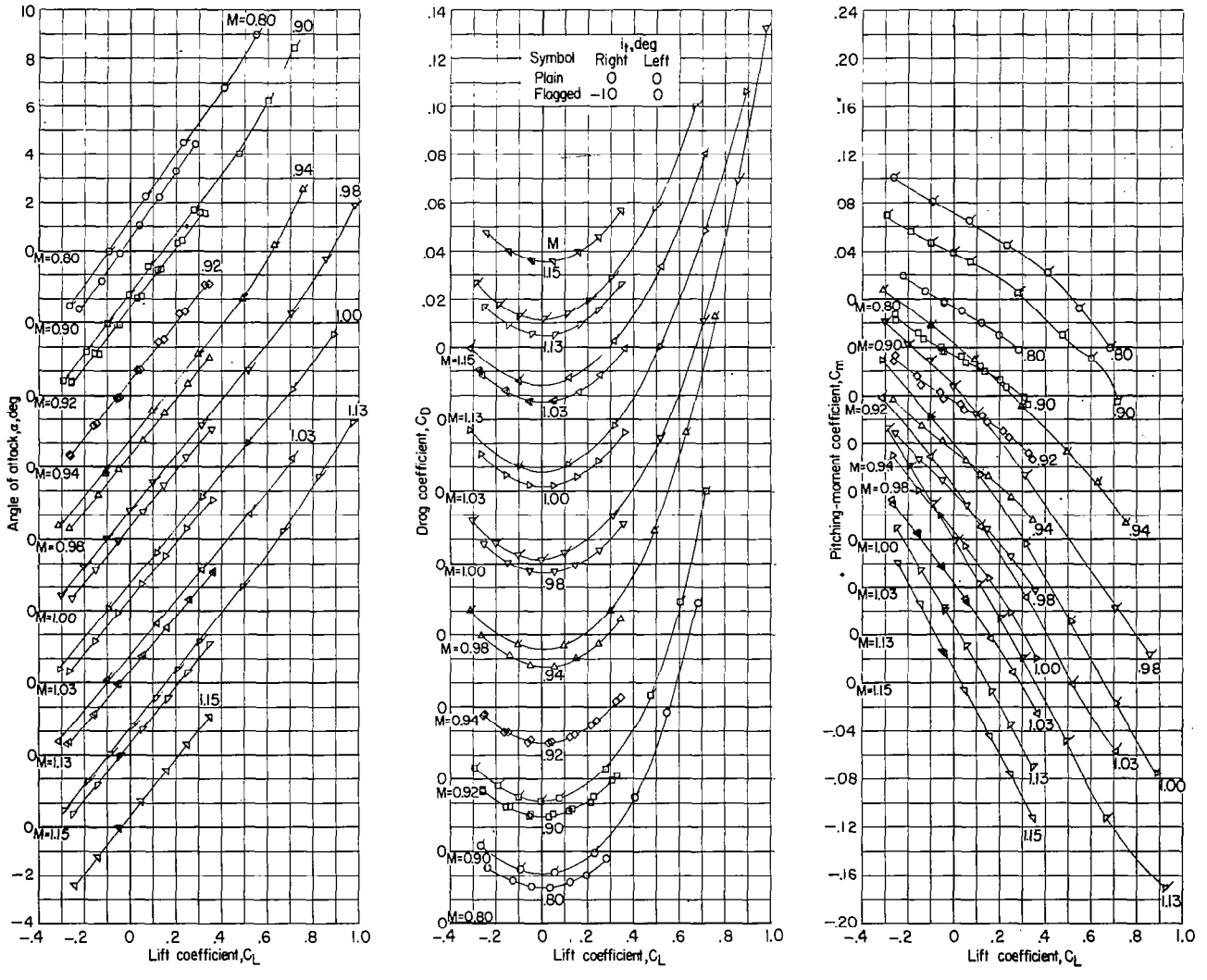

Figure 13.- Effect of stabilizer incidence, operated differentially, on longitudinal aerodynamic characteristics; fuselage 3, wing 1, tail 2.

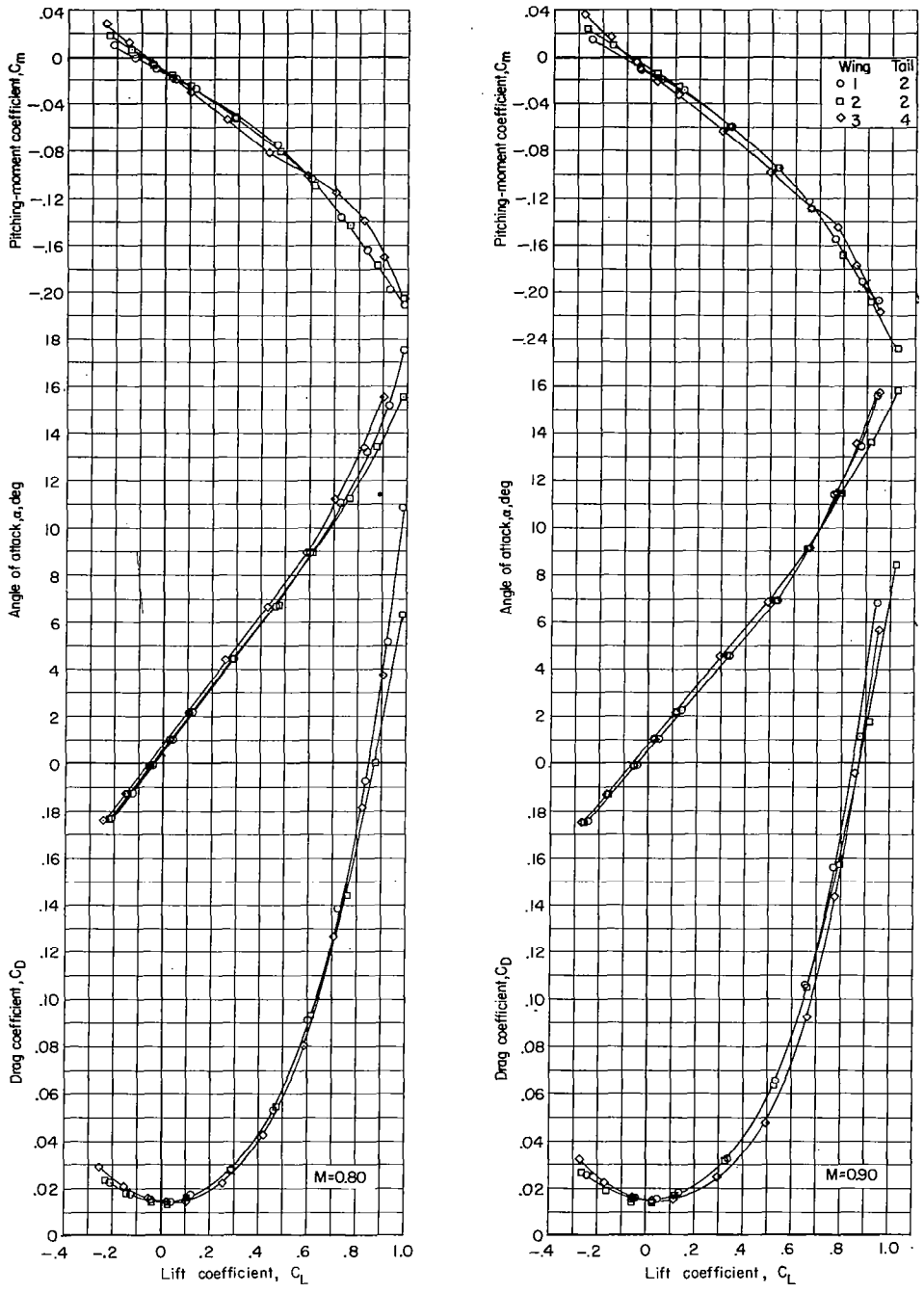

(a) M = 0.80 and 0.90.

Figure 14.- Effects of wing thickness and camber on longitudinal characteristics; fuselage 4, $i_t = 0^o$.

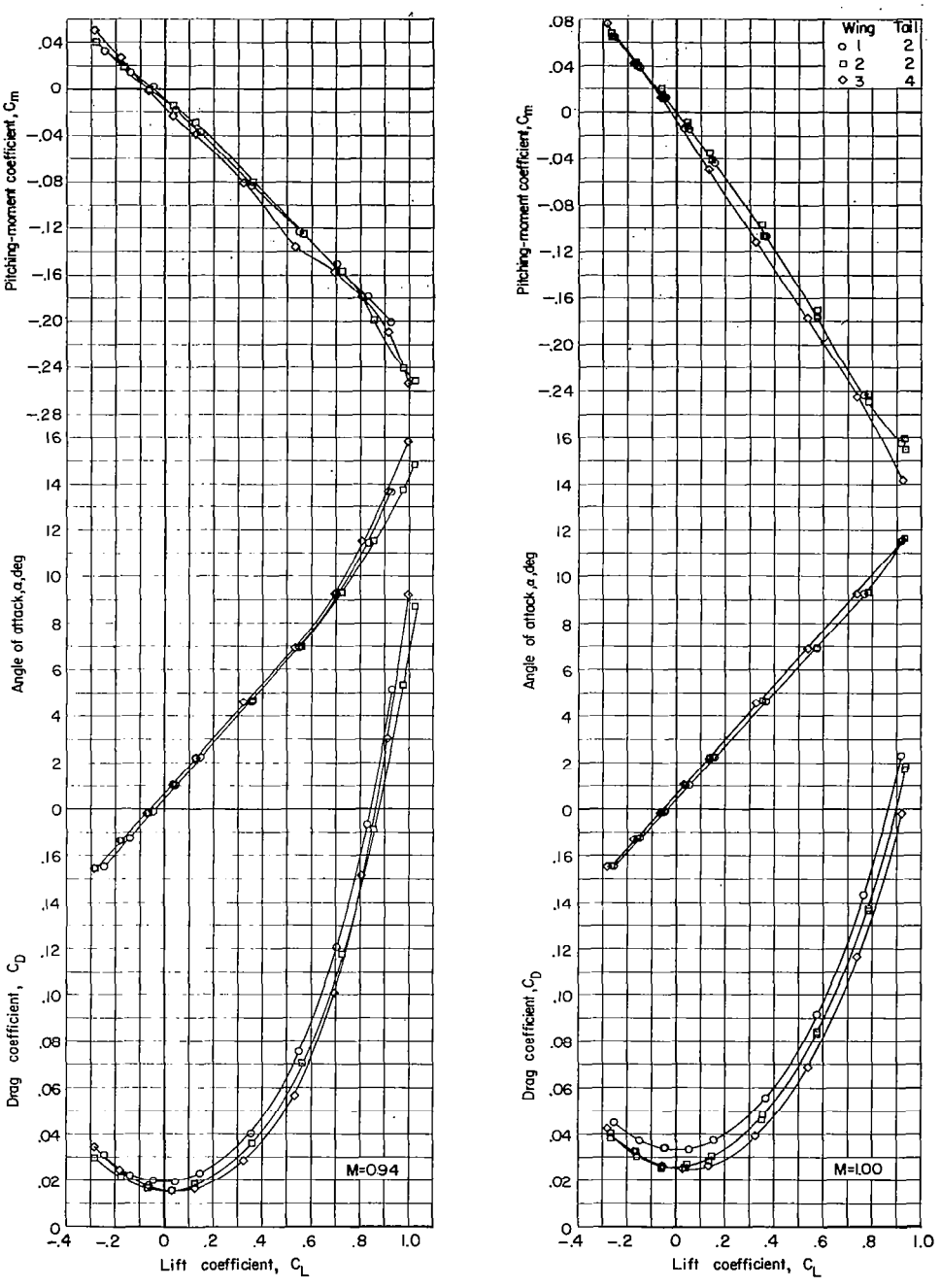

(b) M = 0.94 and 1.00.

Figure 14.- Continued.

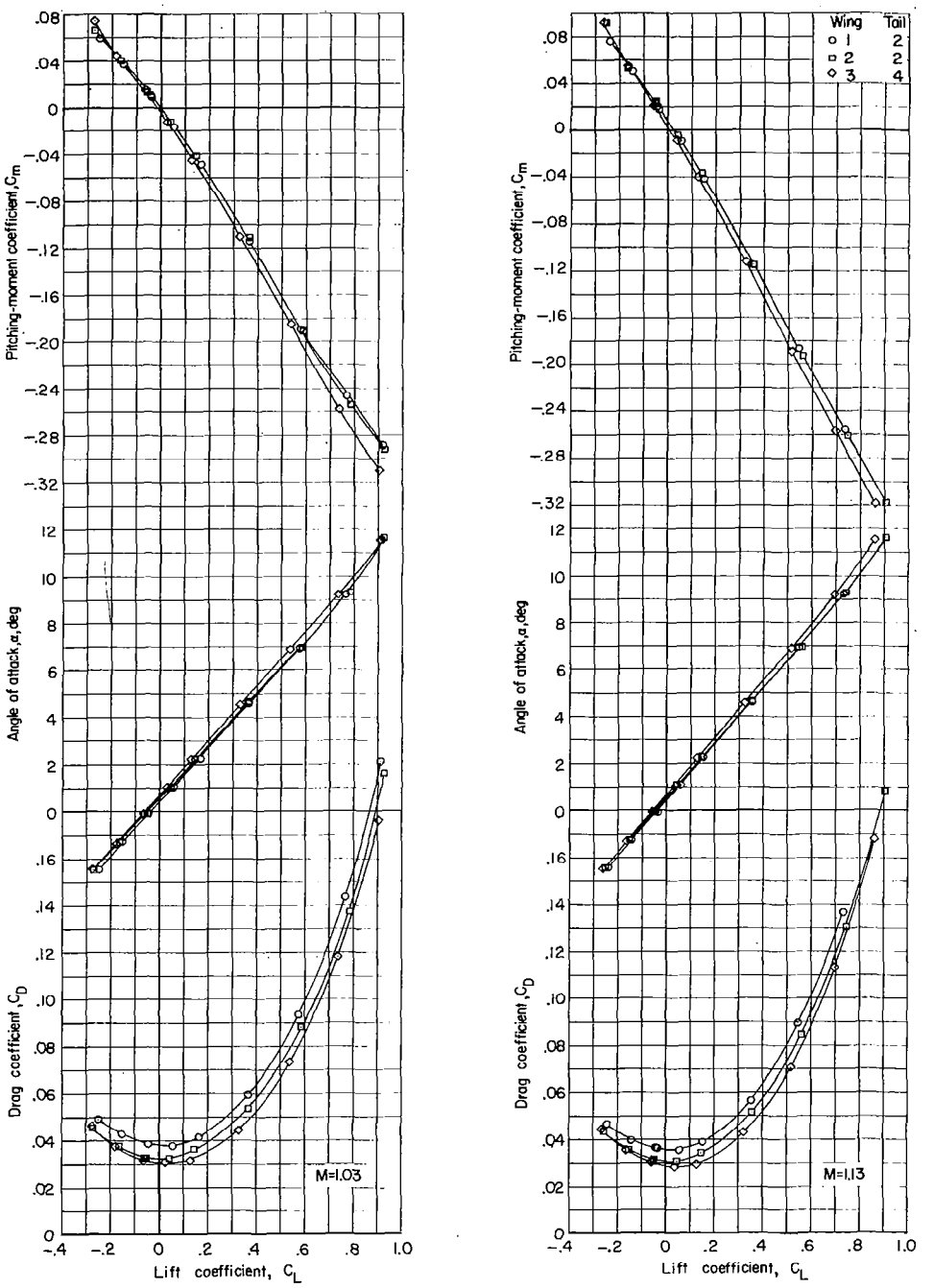

(c) M = 1.03 and 1.13.

Figure 14.- Continued.

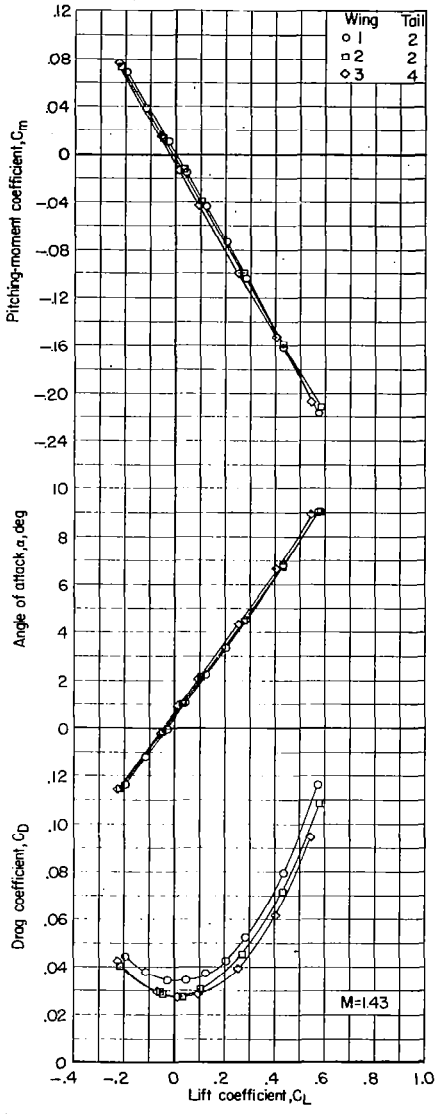

(d) M = 1.43.

Figure 14.- Concluded.

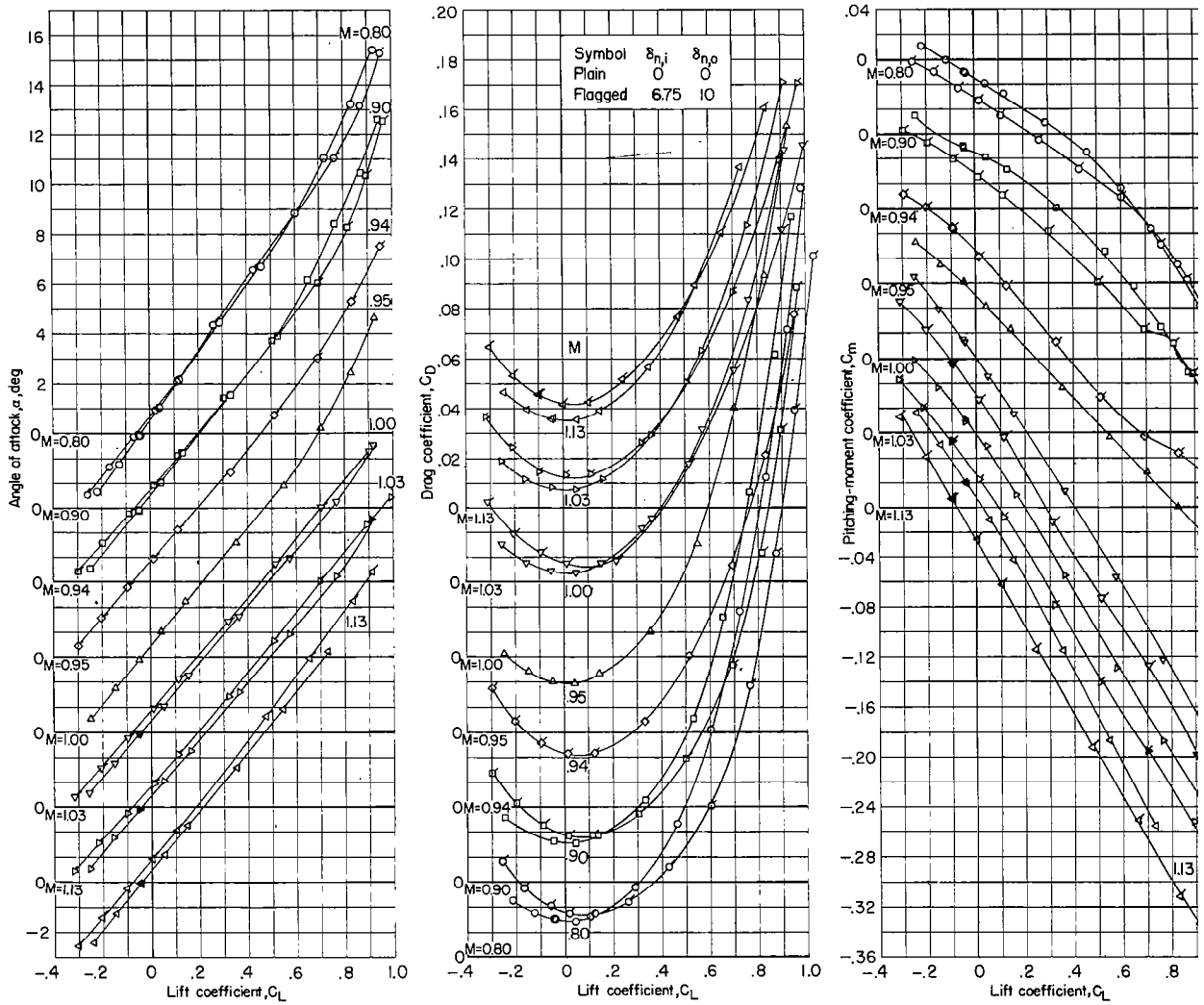

Figure 15.- Effect of leading-edge flap on longitudinal characteristics; fuselage 4, wing 1, tail 2, $i_t = 0^\circ$.

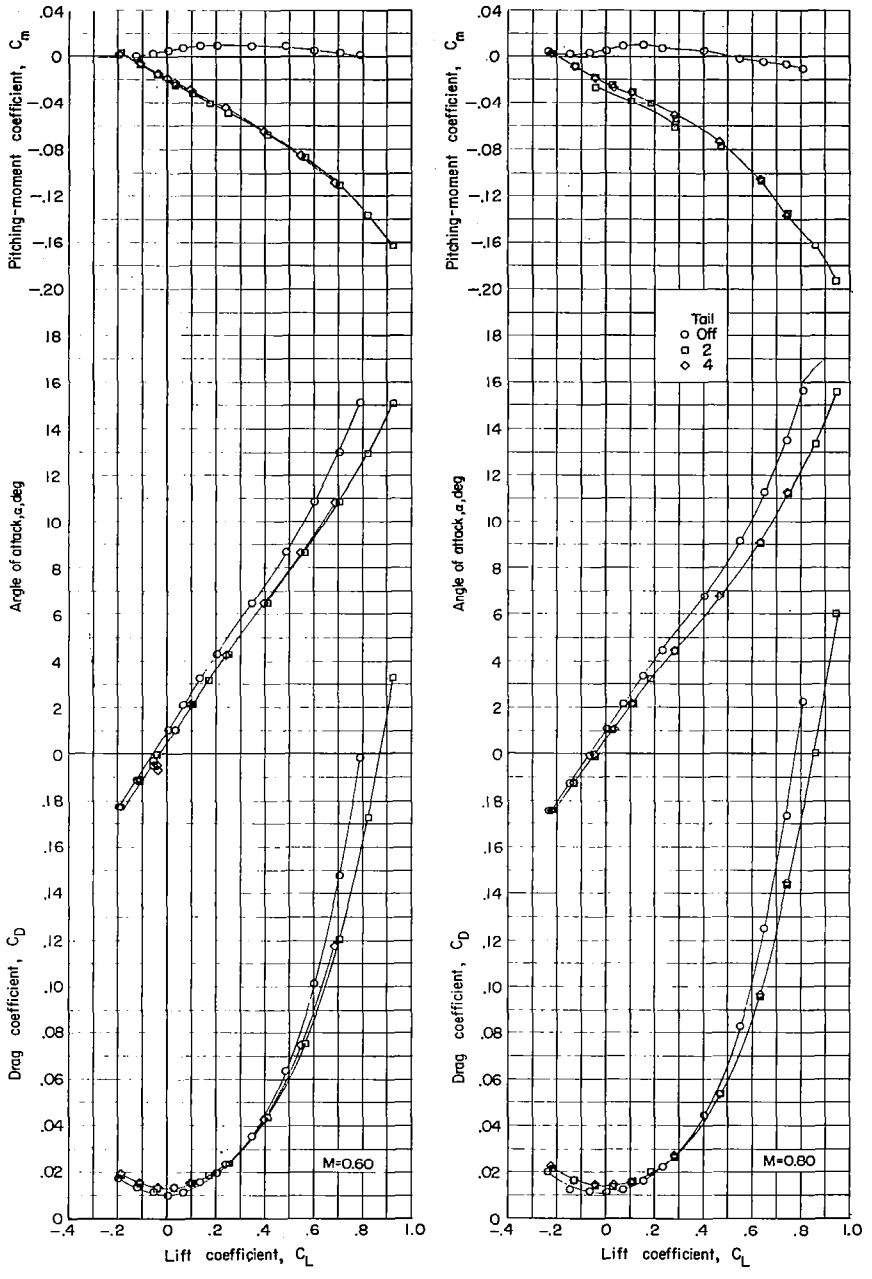

(a) M = 0.60 and 0.80.

Figure 16.- Effects of tail and tail thickness on longitudinal characteristics in Langley 8-foot transonic pressure tunnel; fuselage 2, wing 1, $i_t = 0^\circ$.

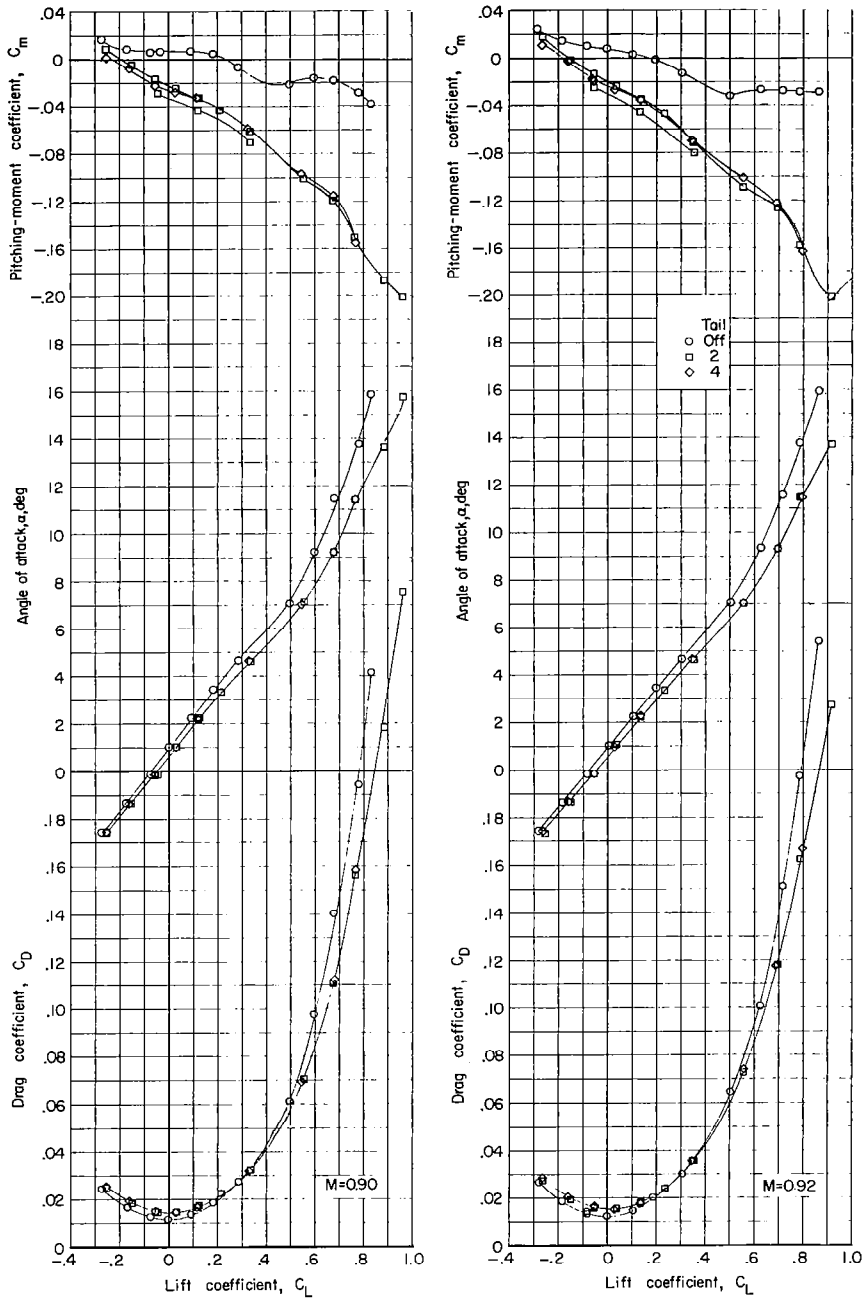

(b) M = 0.90 and 0.92.

Figure 16.- Continued.

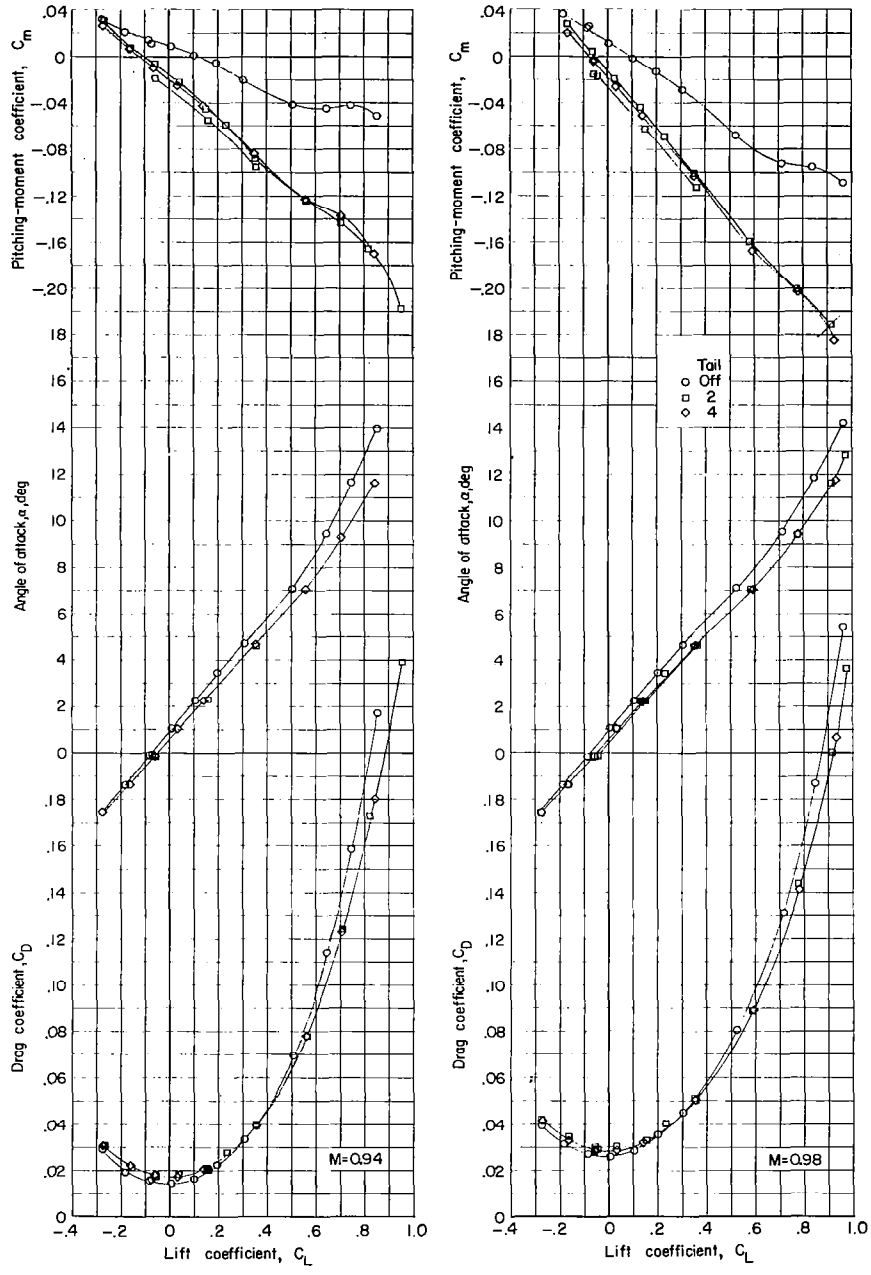

(c) M = 0.94 and 0.98.

Figure 16.- Continued.

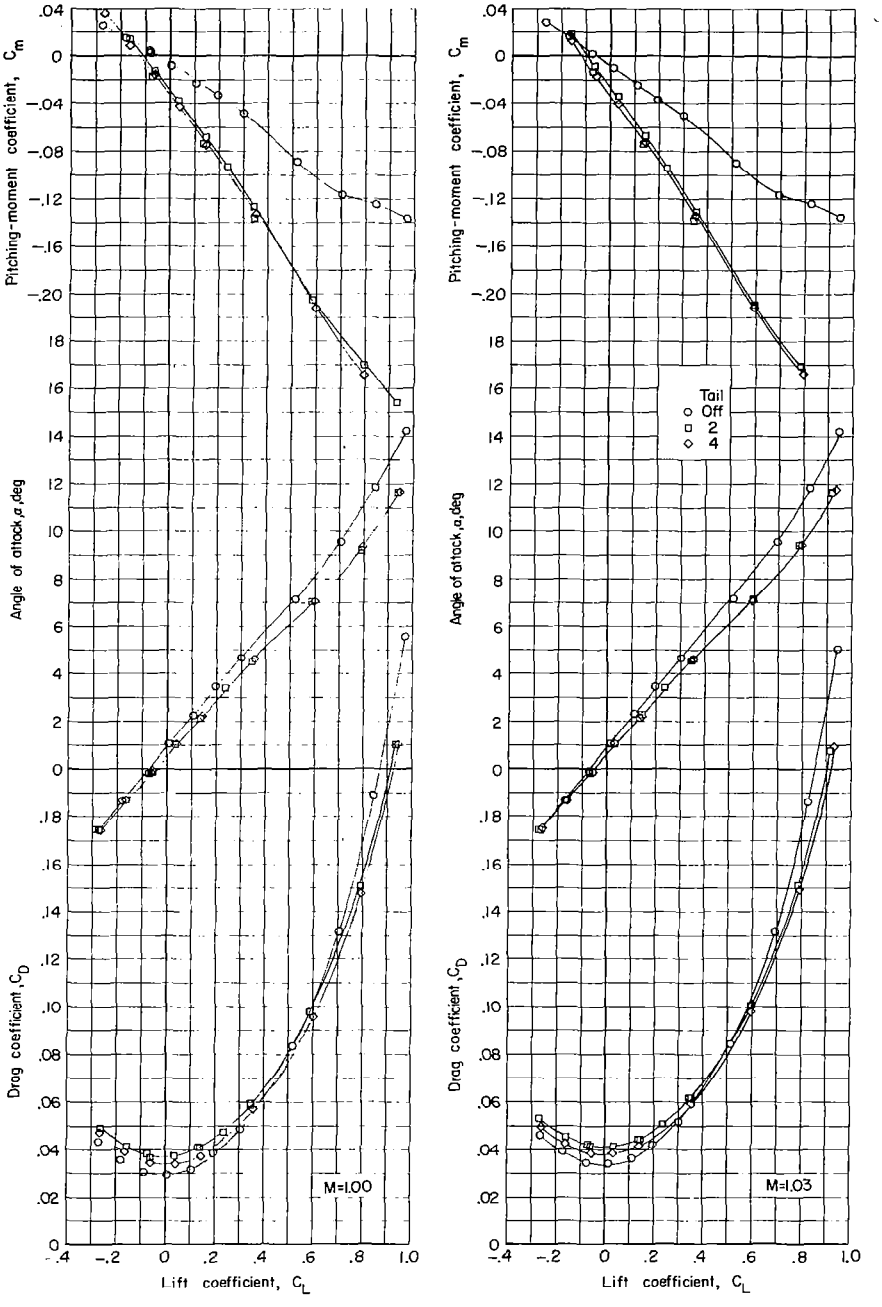

(d) M = 1.00 and 1.03.

Figure 16.- Continued.

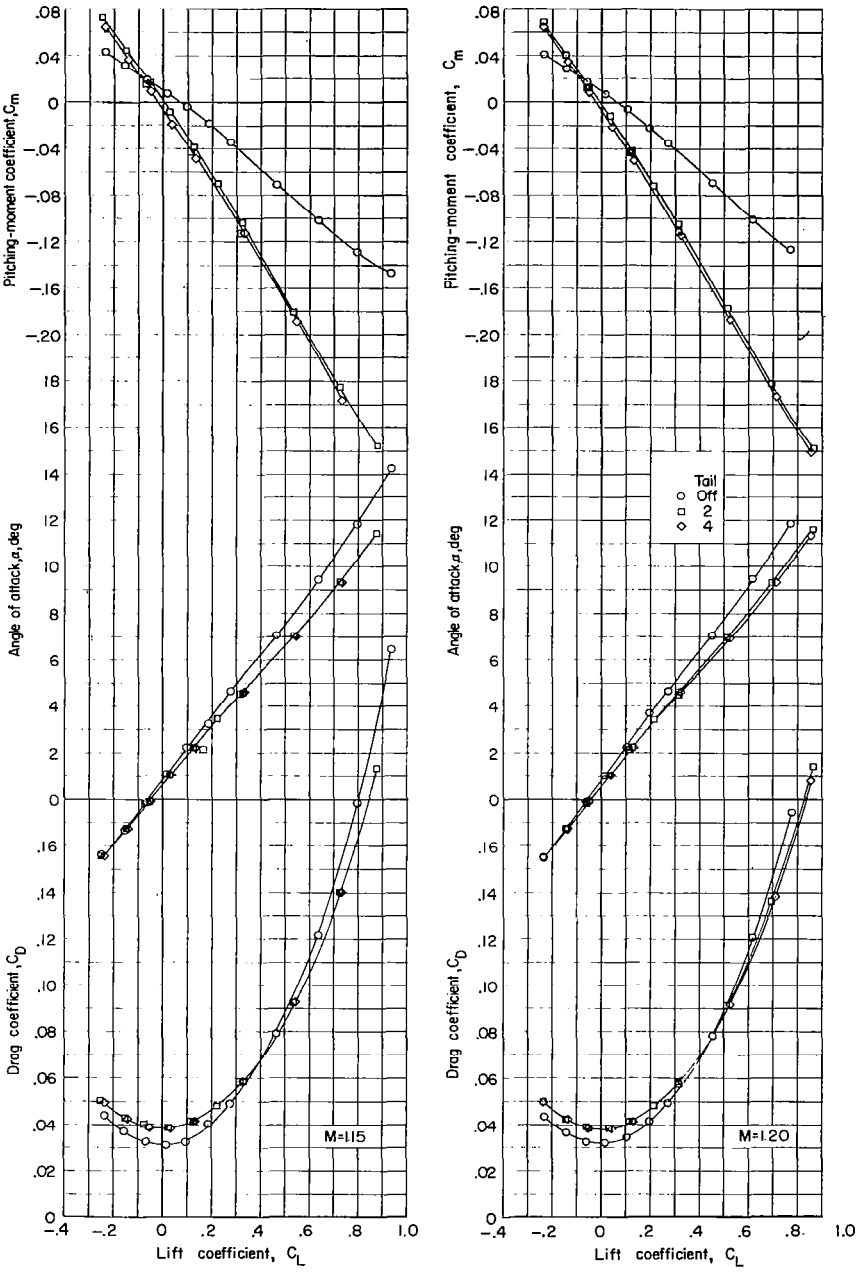

(e) M = 1.15 and 1.20.

Figure 16.- Concluded.

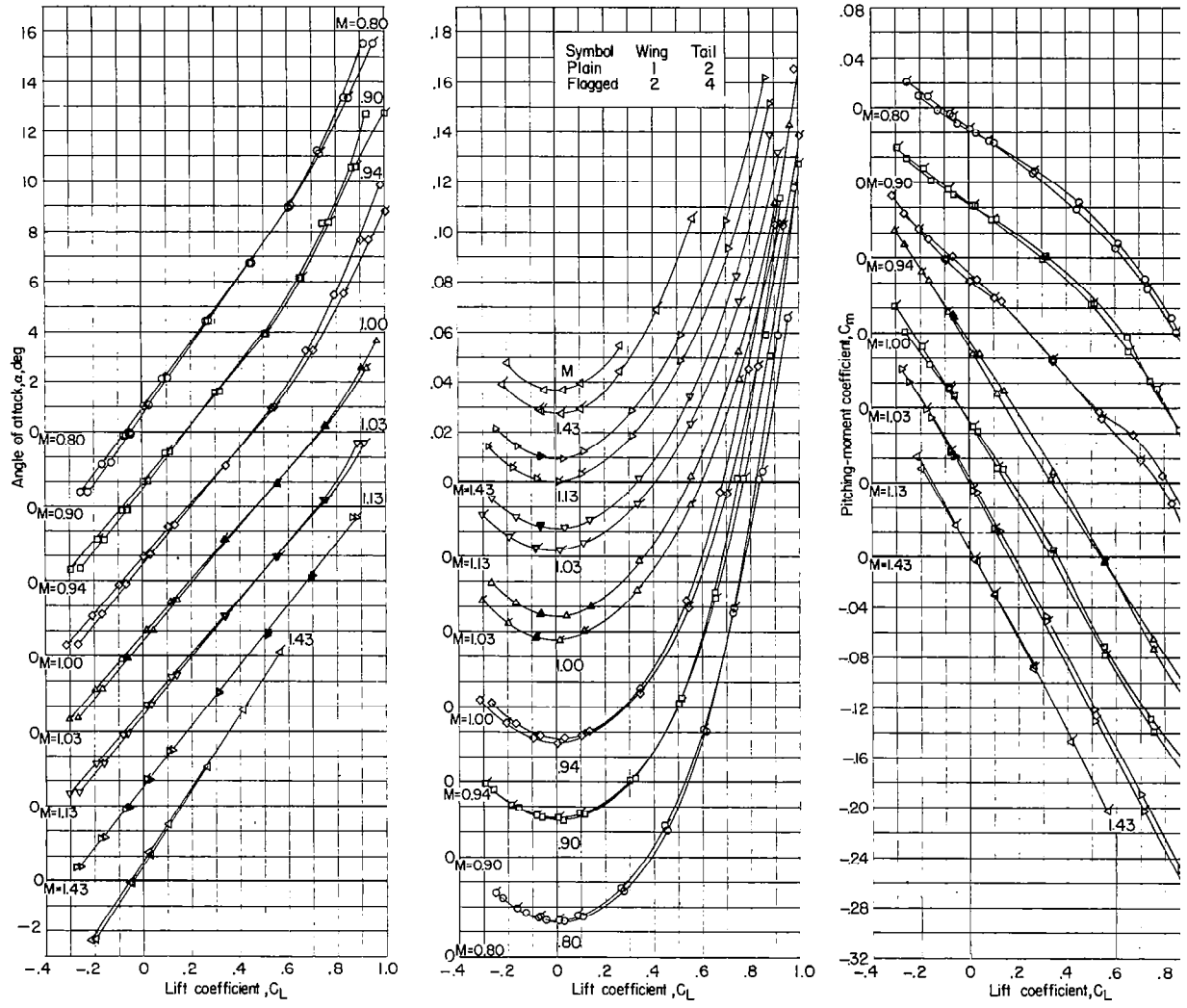

Figure 17.- Effects of wing and tail thicknesses on longitudinal characteristics; fuselage 2, $i_t = 0^o$.

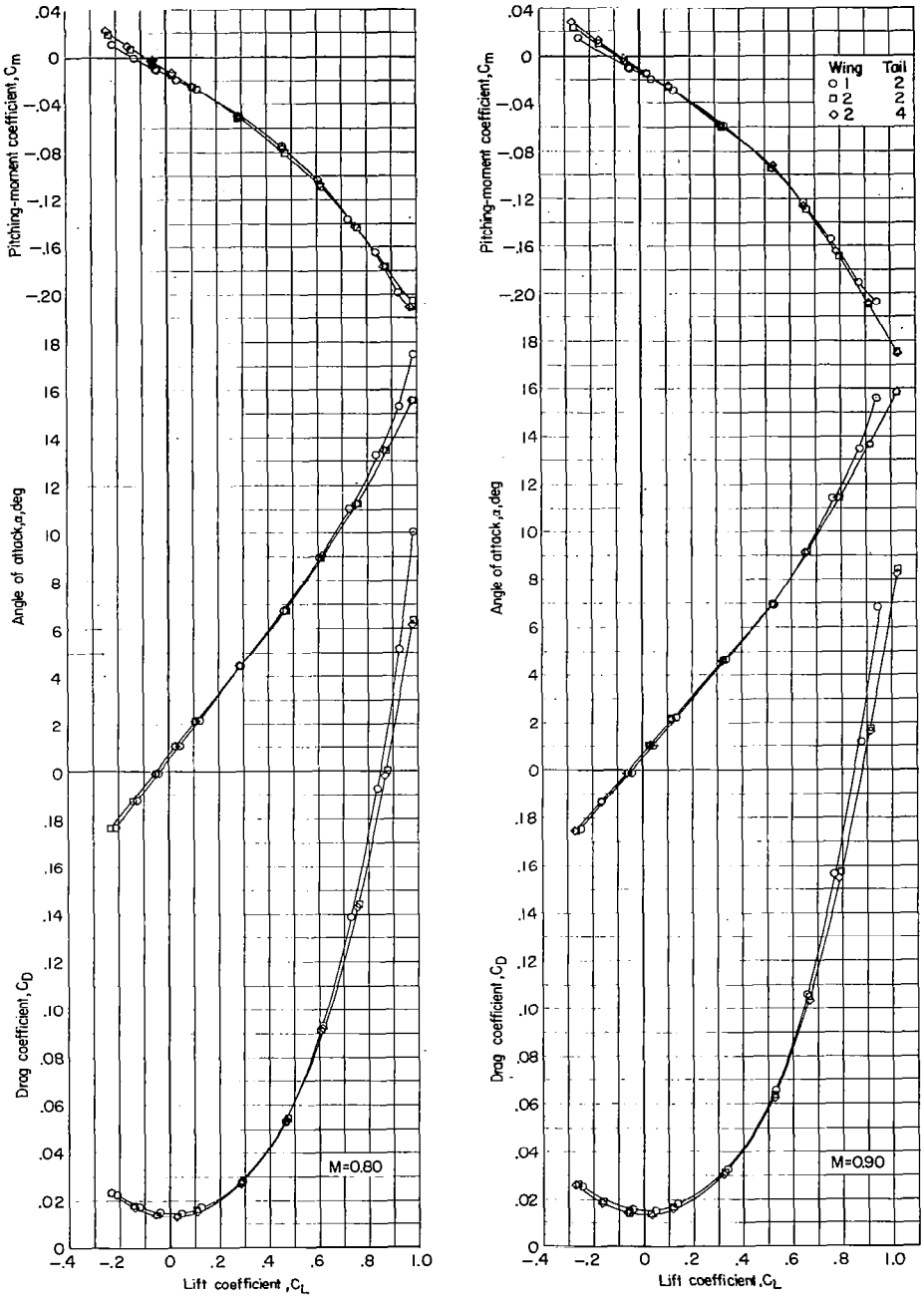

(a) M = 0.80 and 0.90.

Figure 18.- Effects of wing and tail thicknesses on longitudinal characteristics; fuselage 4, $i_t = 0^o$.

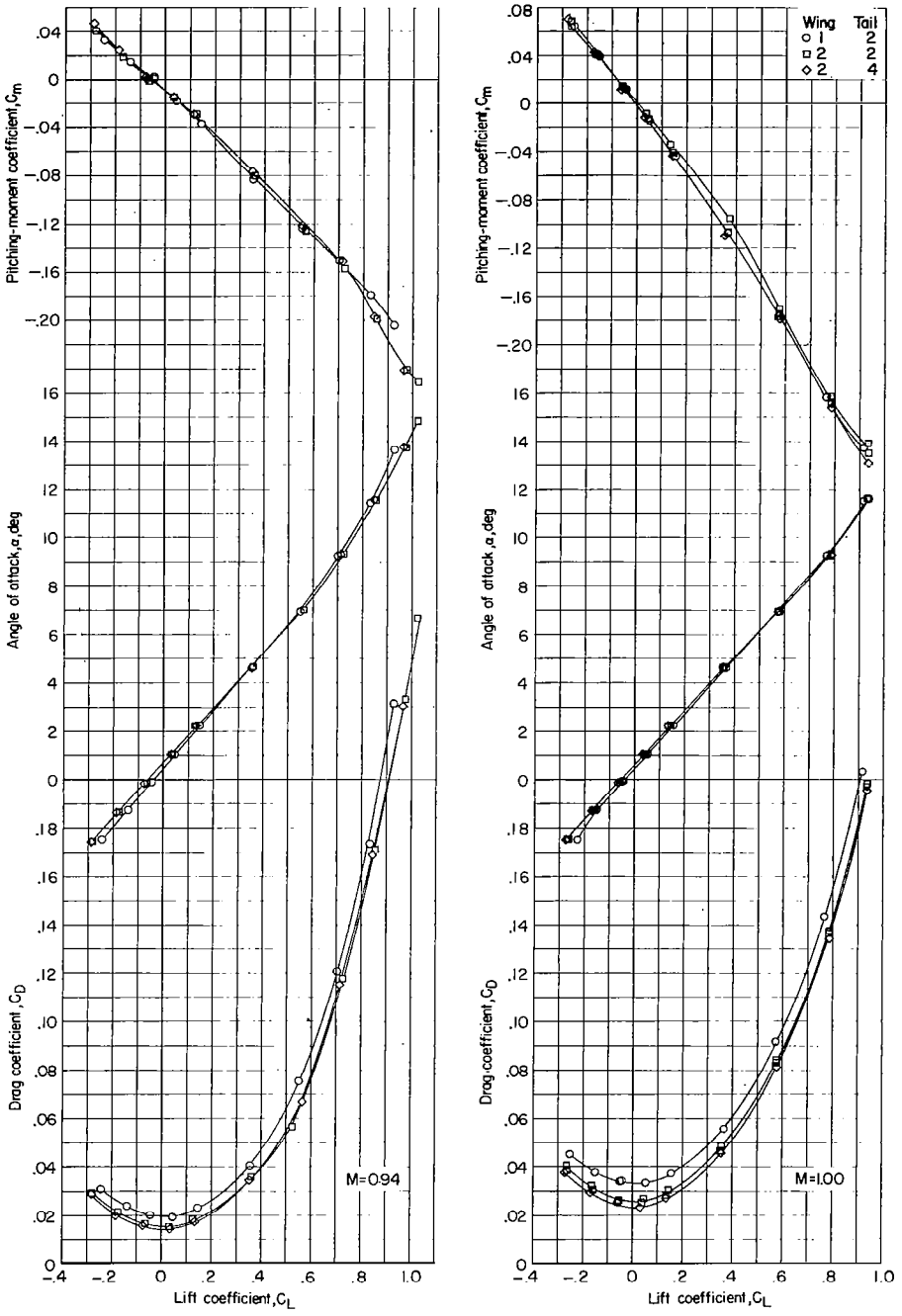

(b) M = 0.94 and 1.00.

Figure 18.- Continued.

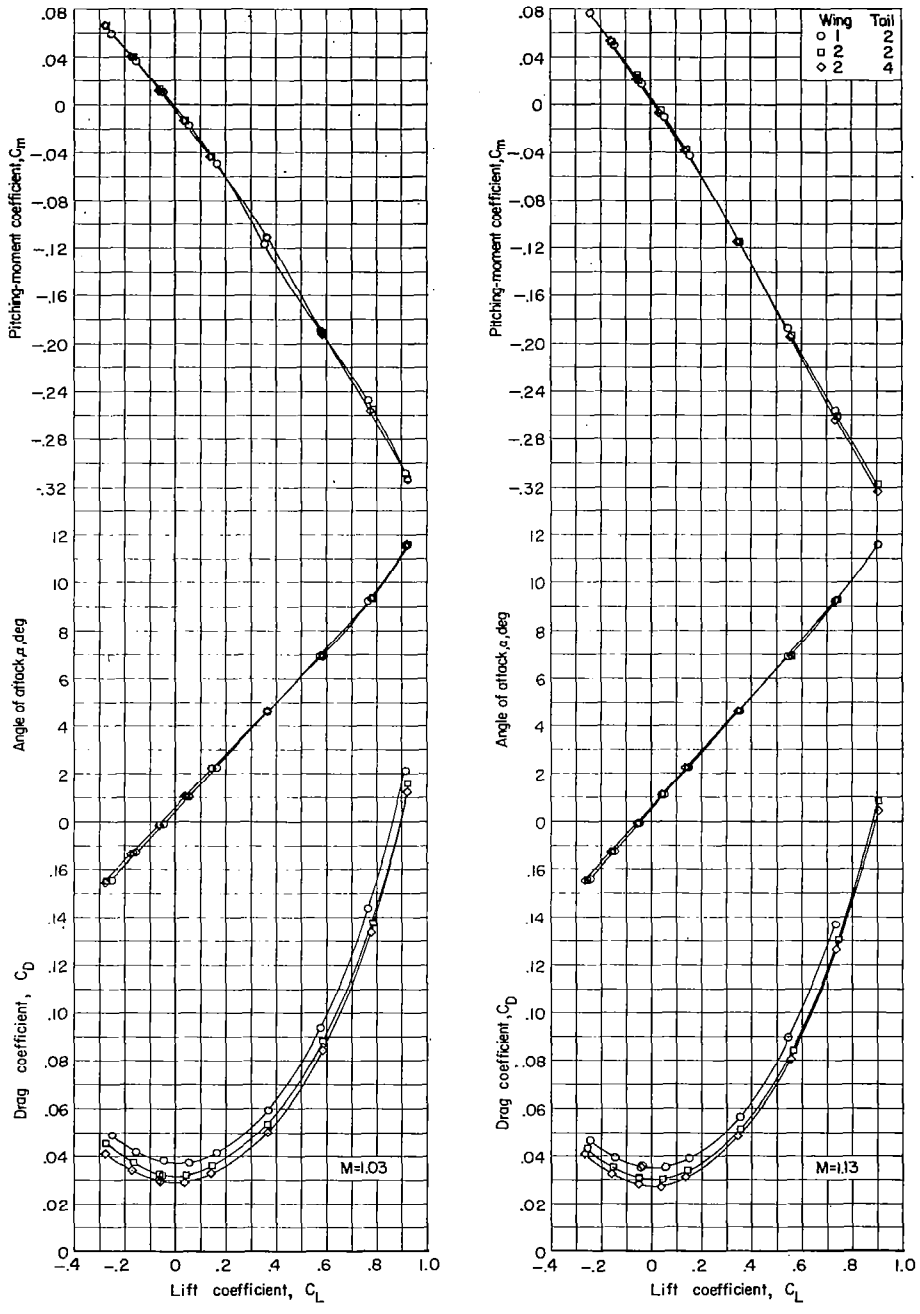

(c) M = 1.03 and 1.13.

Figure 18.- Continued.

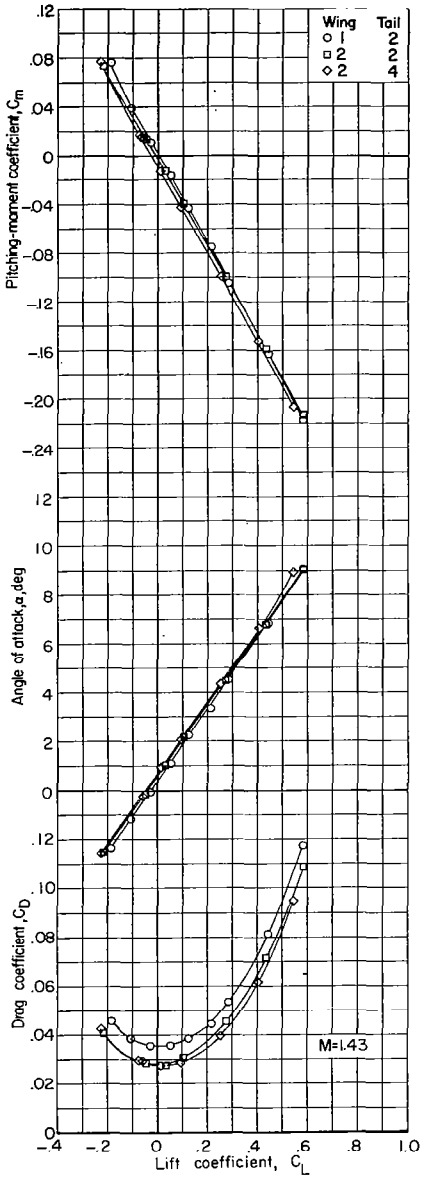

(d) M = 1.43.

Figure 18.- Concluded.

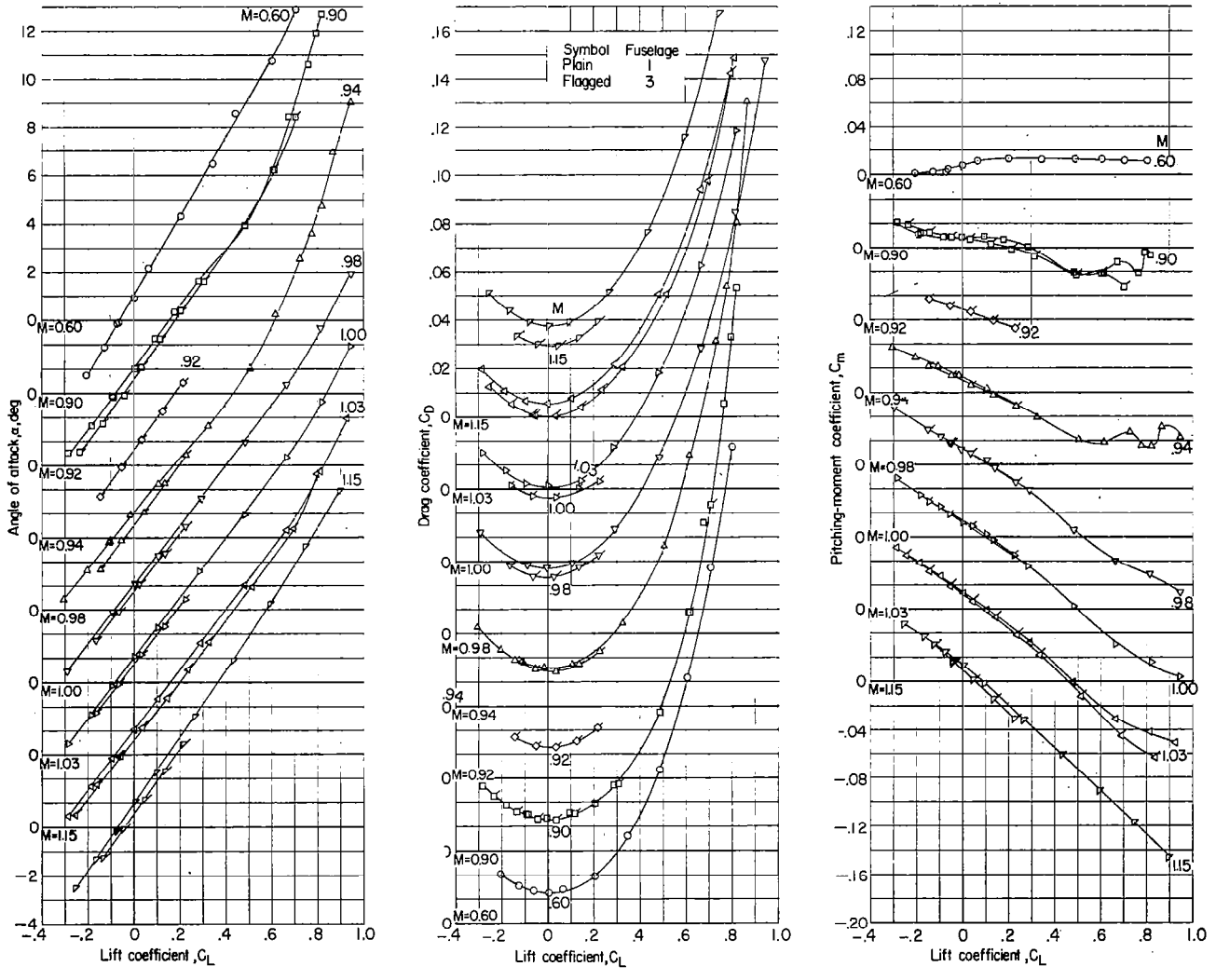

Figure 19.- Effect of fuselage modifications on longitudinal characteristics of wing-body combination; wing 1.

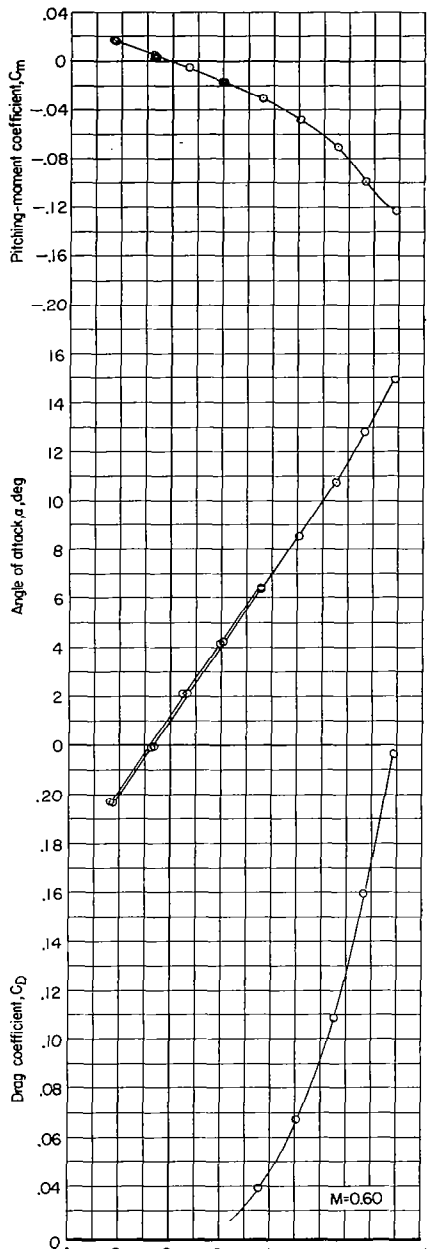
Pitching-moment coefficient, C_m
.04
0
-.04
-.08
-.12
-.16
-.20
Angle of attack, α, deg
16
14
12
10
8
6
4
2
0
Drag coefficient, C_D
.20
.18
.16
.14
.12
.10
.08
.06
.04
0
M=0.60

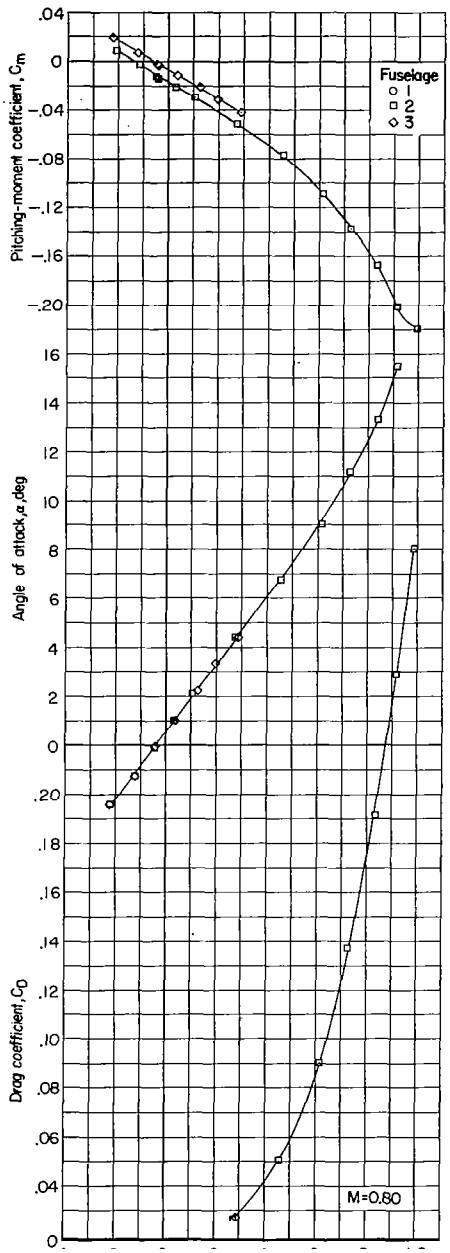
Pitching-moment coefficient, C_m
Fuselage
1
2
3
.04
0
-.04
-.08
-.12
-.16
-.20
Angle of attack, α, deg
16
14
12
10
8
6
4
2
0
Drag coefficient, C_D
.20
.18
.16
.14
.12
.10
.08
.06
.04
0
M=0.80

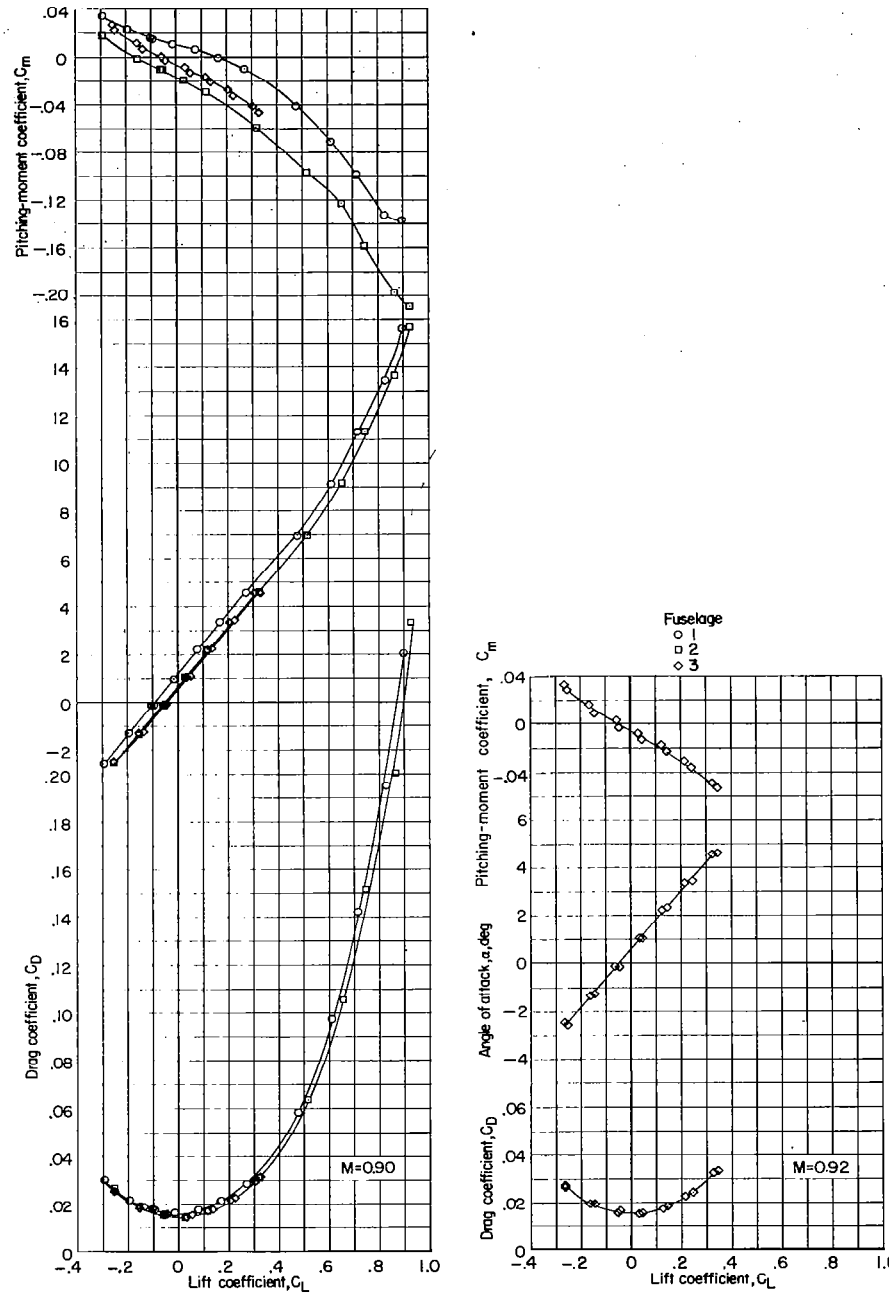

(b) M = 0.90 and 0.92.

Figure 20.- Continued.

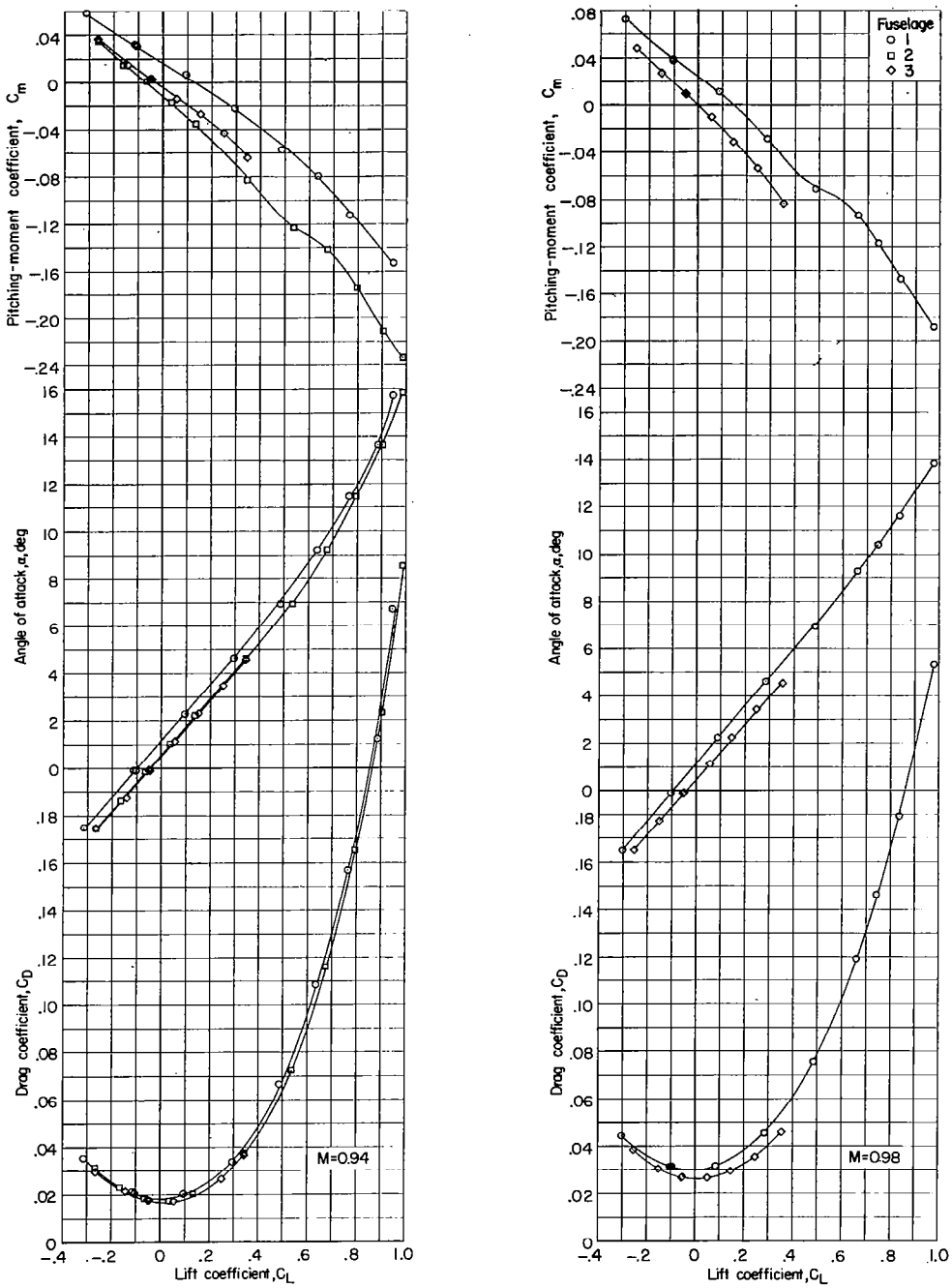

(c) M = 0.94 and 0.98.

Figure 20.- Continued.

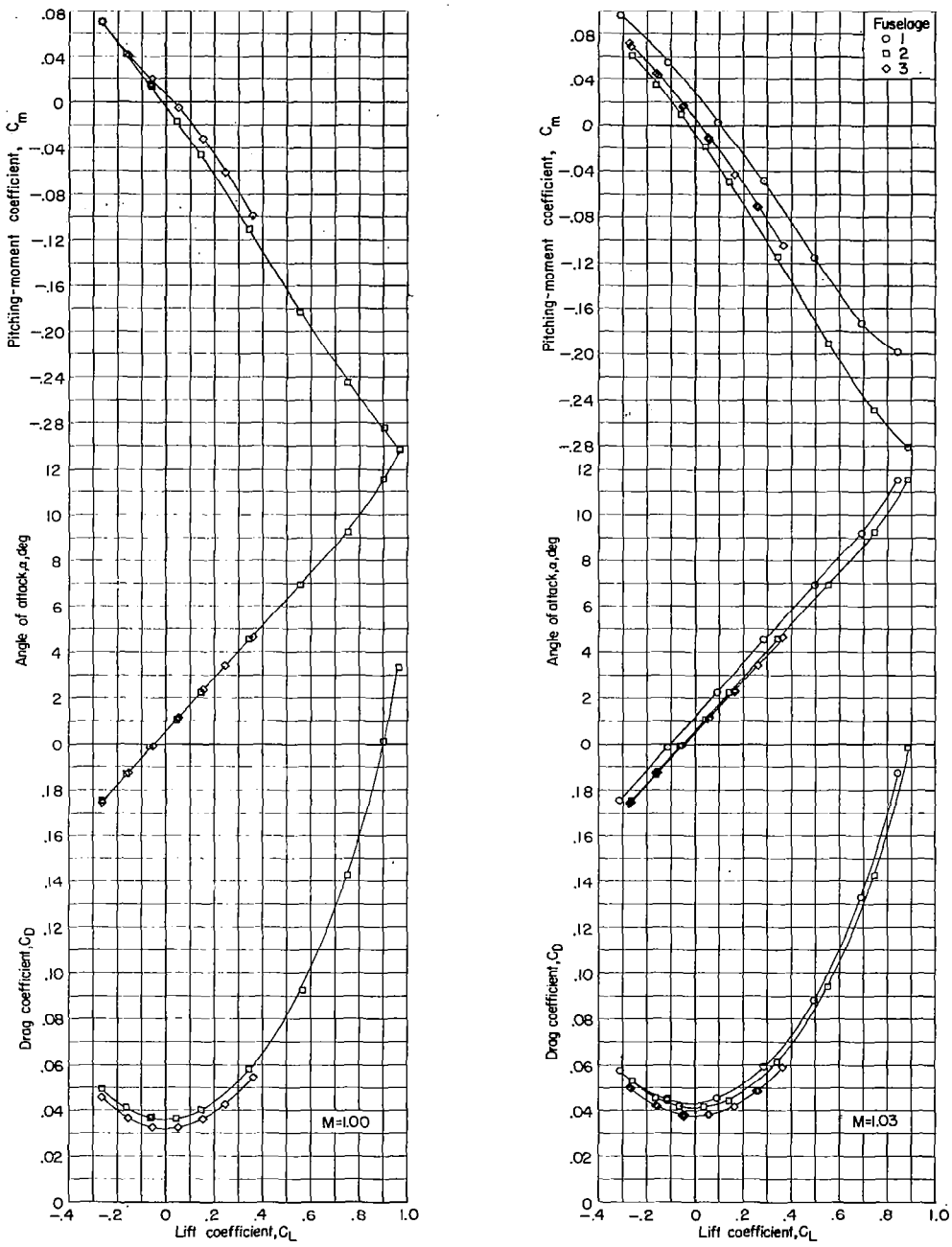

(d) M = 1.00 and 1.03.

Figure 20.- Continued.

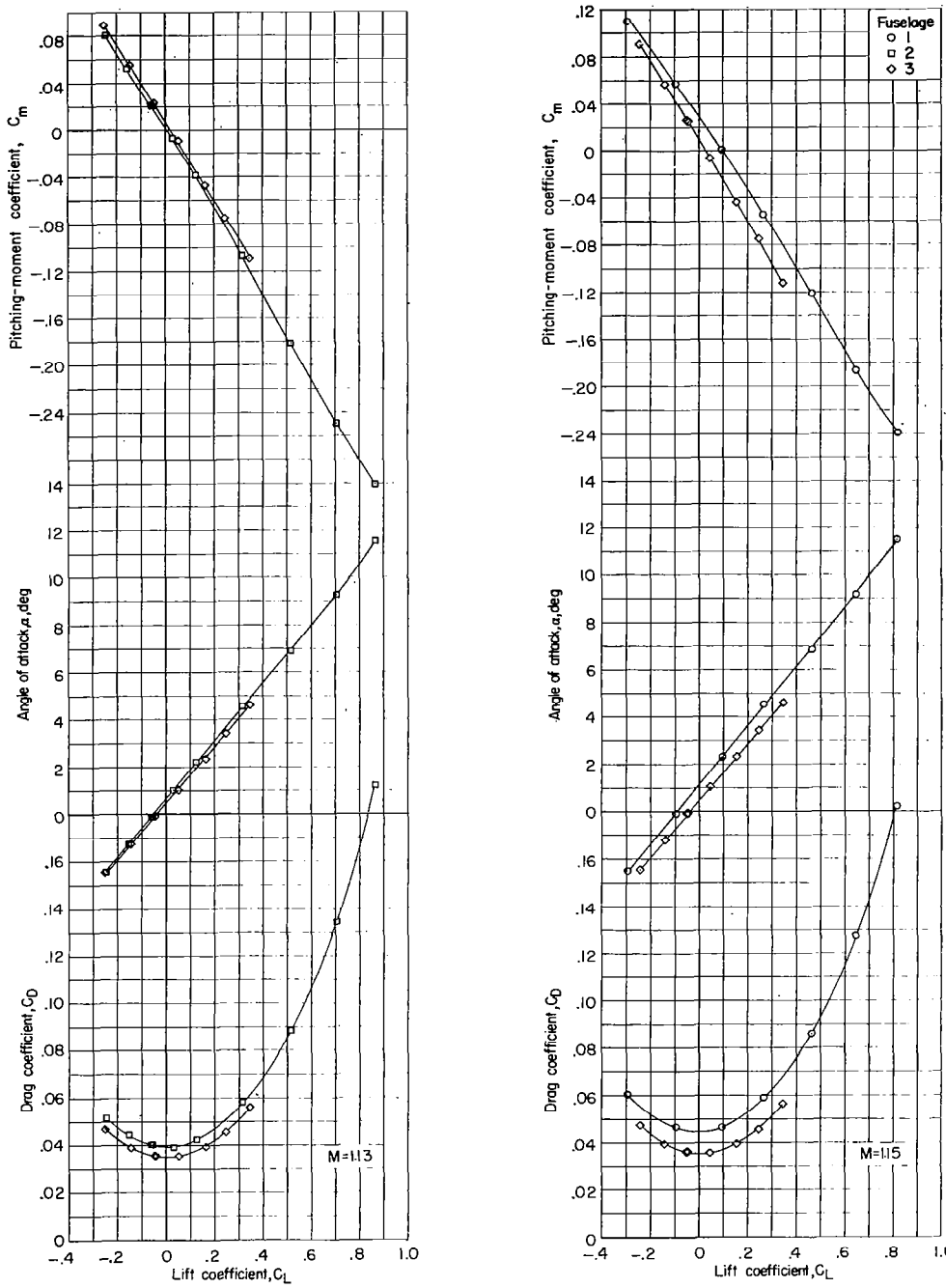

(e) M = 1.13 and 1.15.

Figure 20.- Continued.

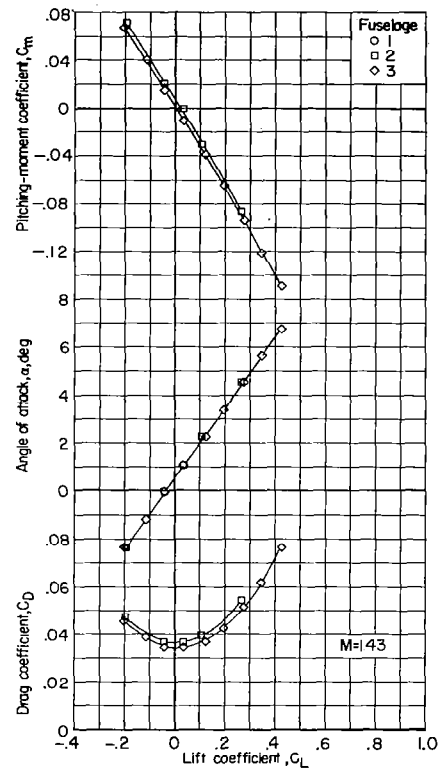

(f) M = 1.43.

Figure 20.- Concluded.

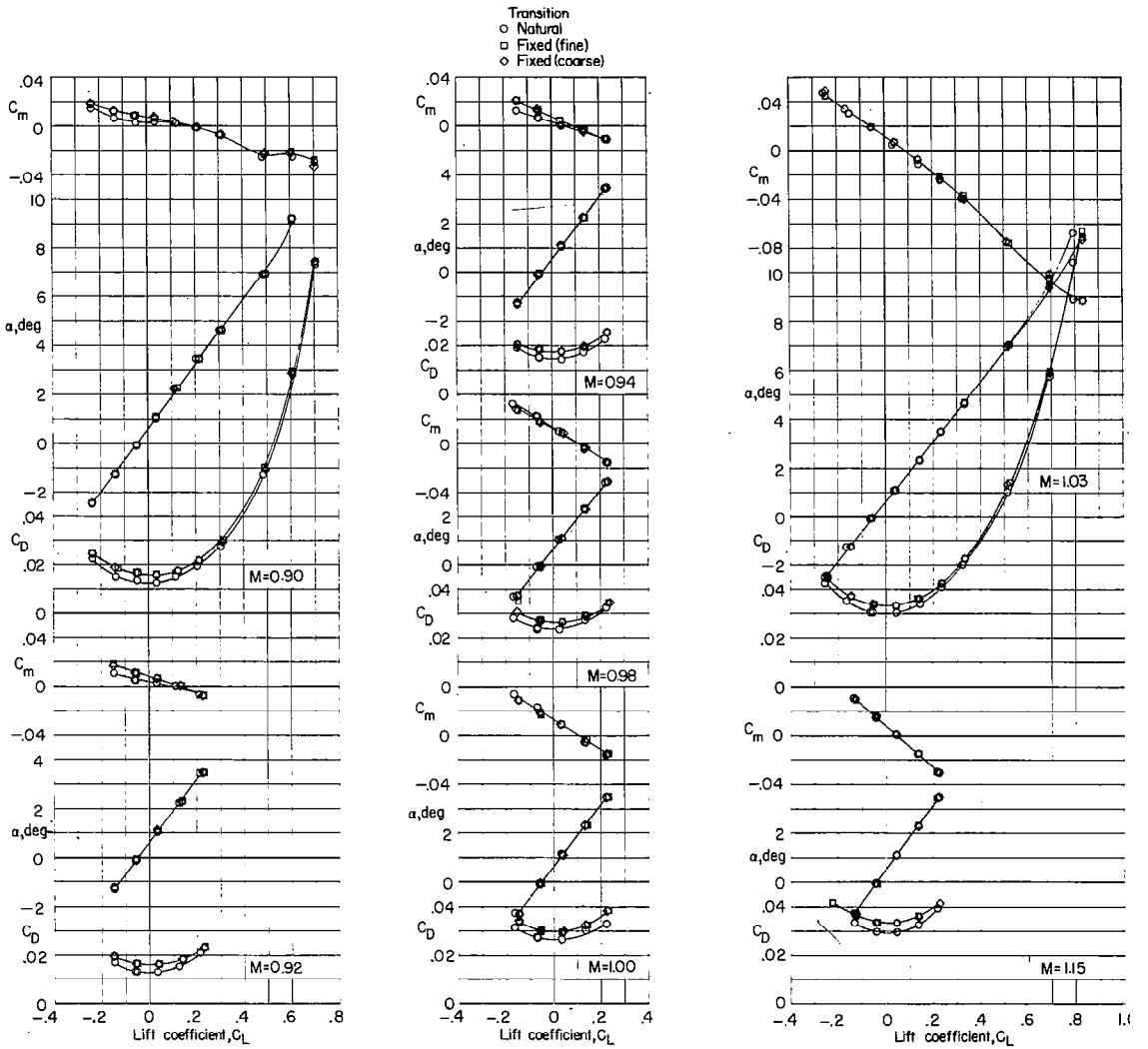

Figure 21.- Effect of fixed transition on longitudinal characteristics of the wing and body; fuselage 3, wing 1.

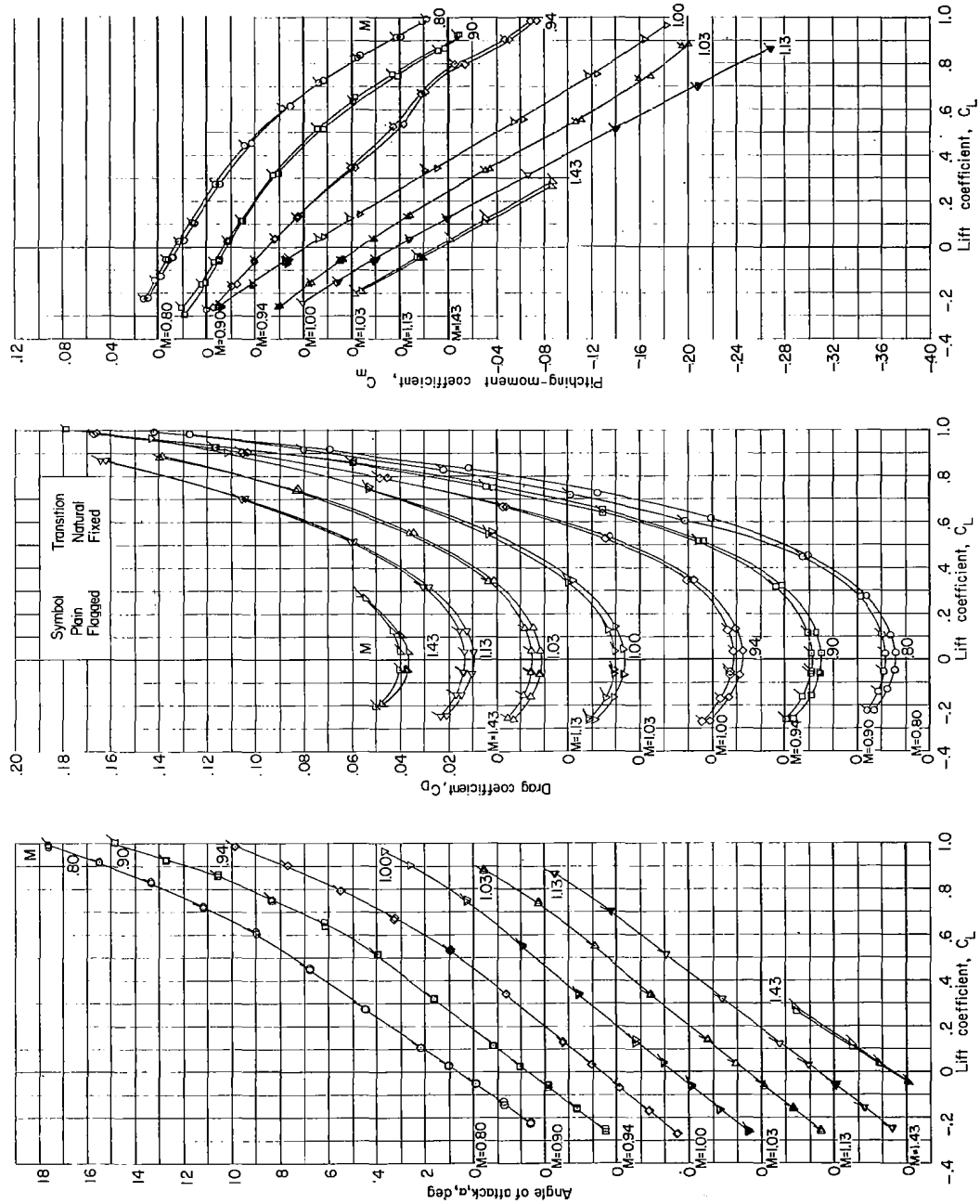

Figure 22.- Effect of fixed transition on longitudinal characteristics of complete model; fuselage 2, wing 1, tail 2; $i_t = 0^\circ$.

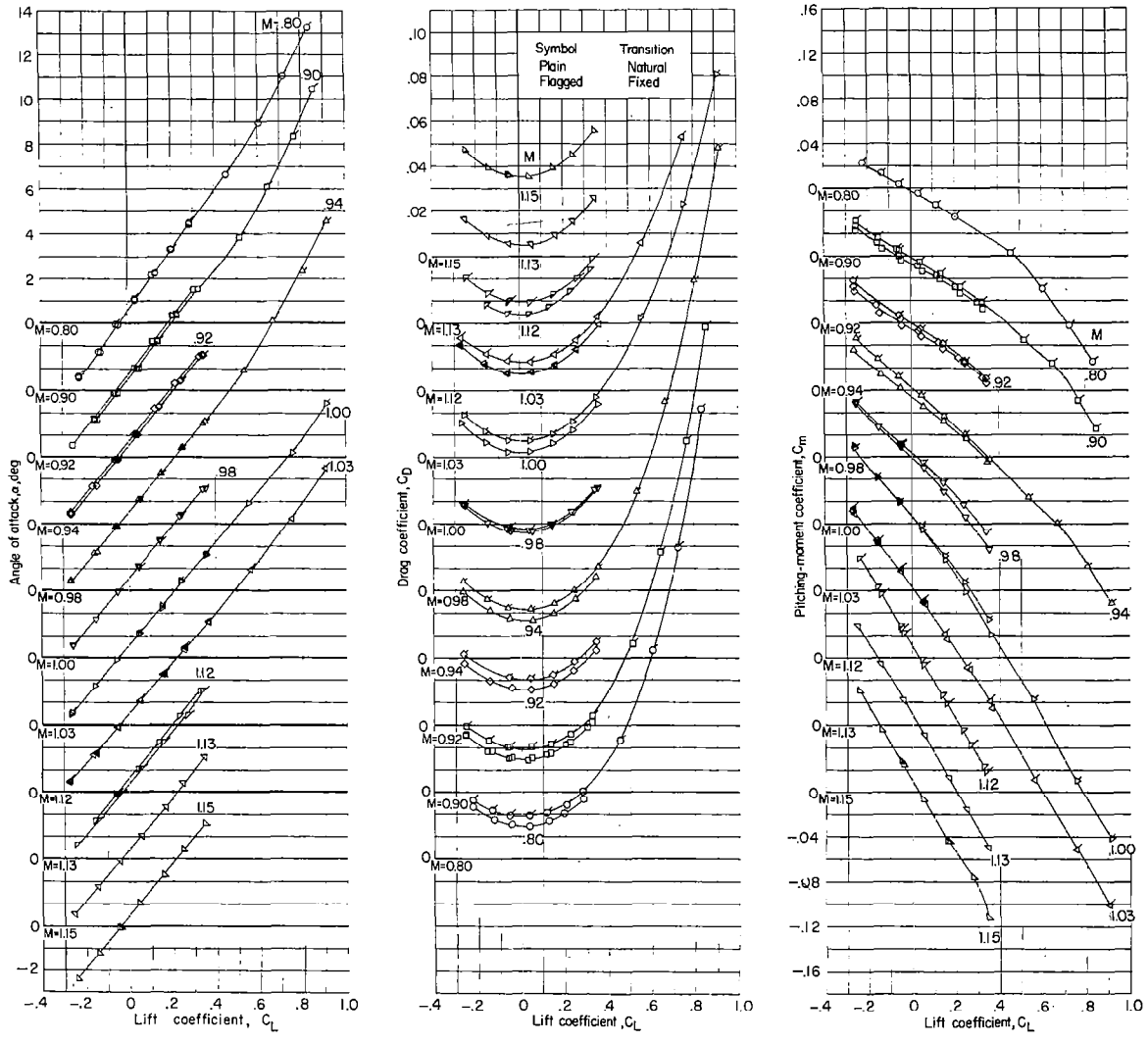

Figure 23.- Effect of fixed transition on longitudinal characteristics of complete model; fuselage 3, wing 1, tail 2, $i_t = 0^\circ$.

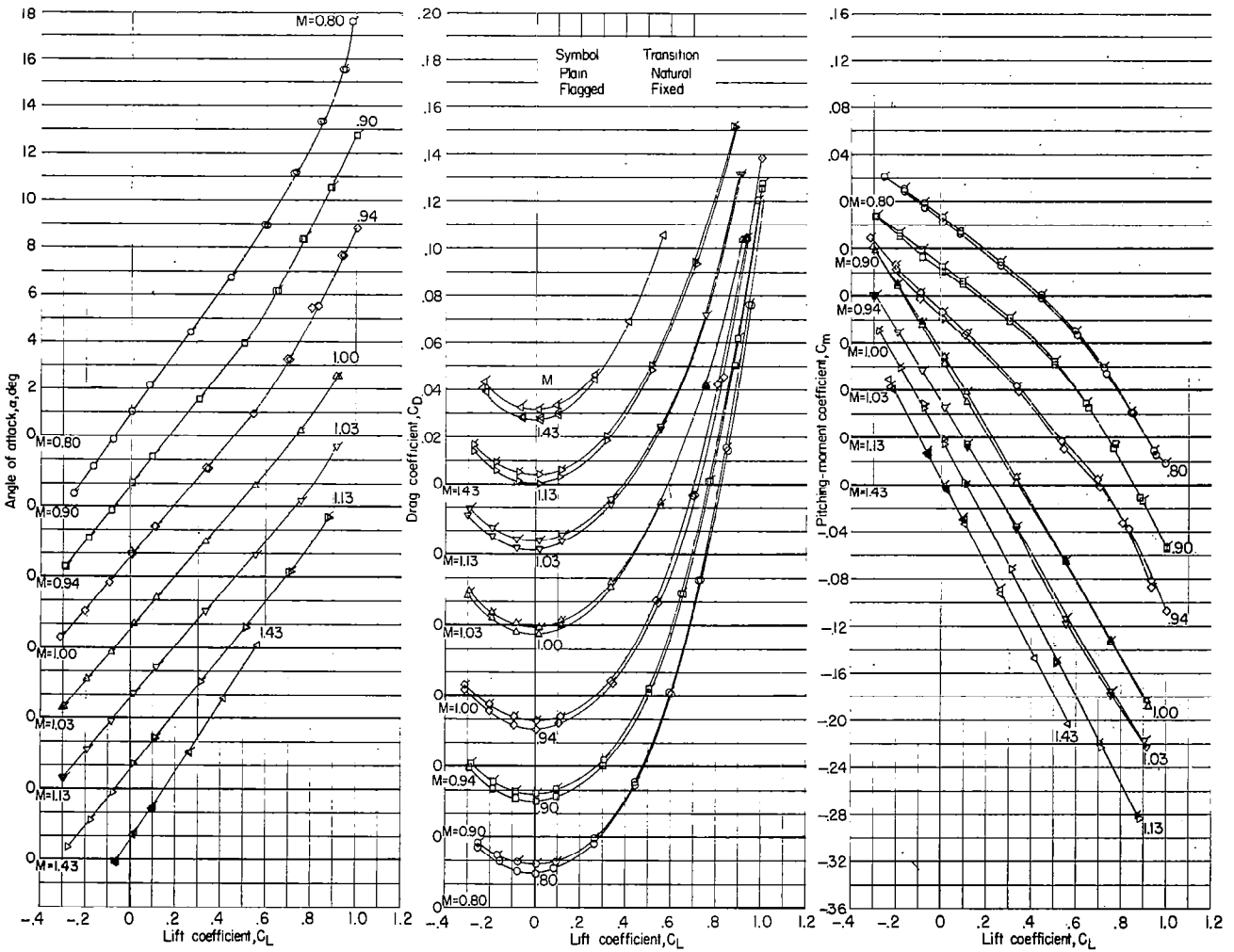

Figure 24.- Effect of fixed transition on longitudinal characteristics of complete model with 4-percent-thick surfaces, fuselage 2, wing 2, tail 4, $i_t = 0^\circ$.

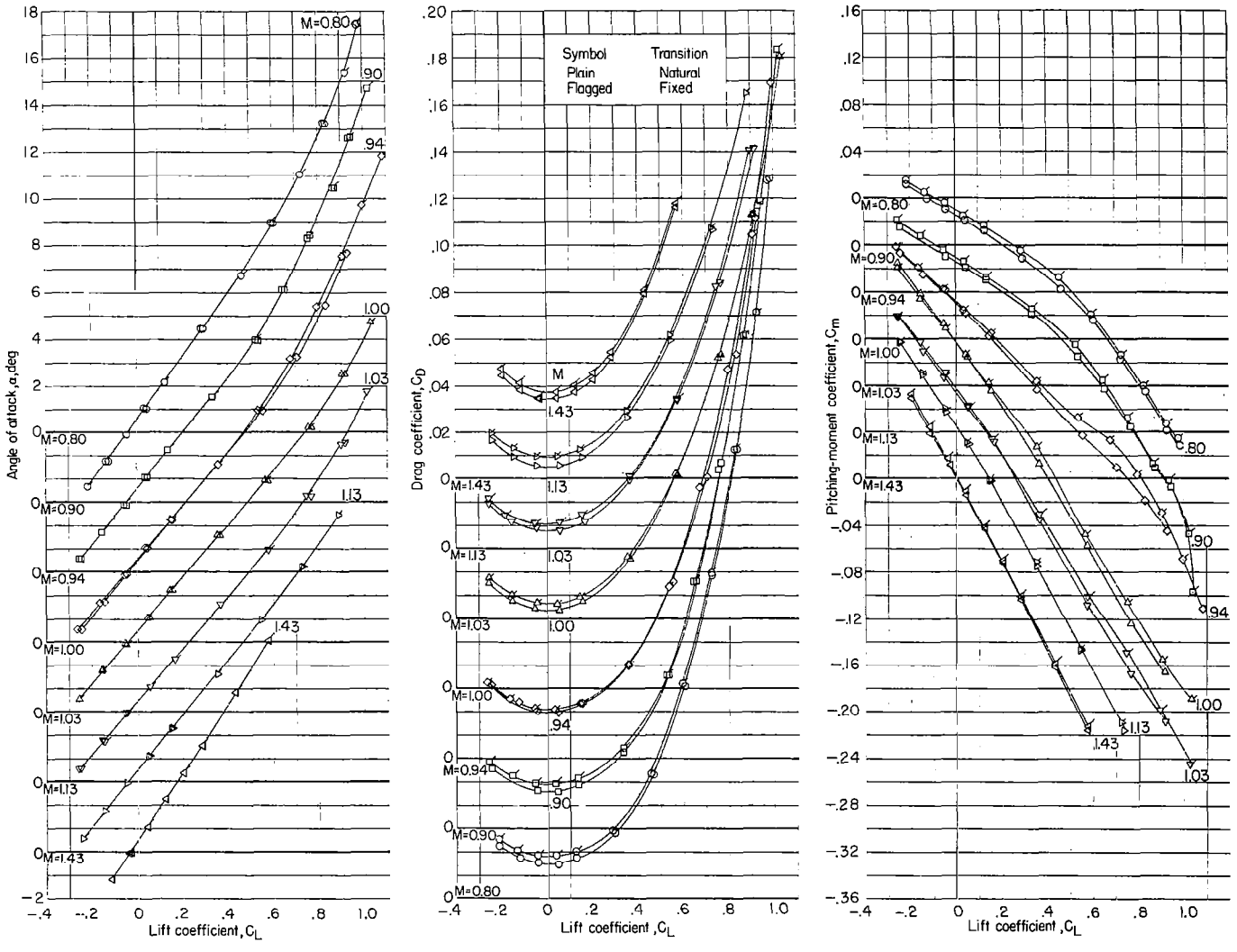

Figure 25.- Effect of fixed transition on longitudinal characteristics of complete model; fuselage 4, wing 1, tail 2, $i_t = 0^o$.

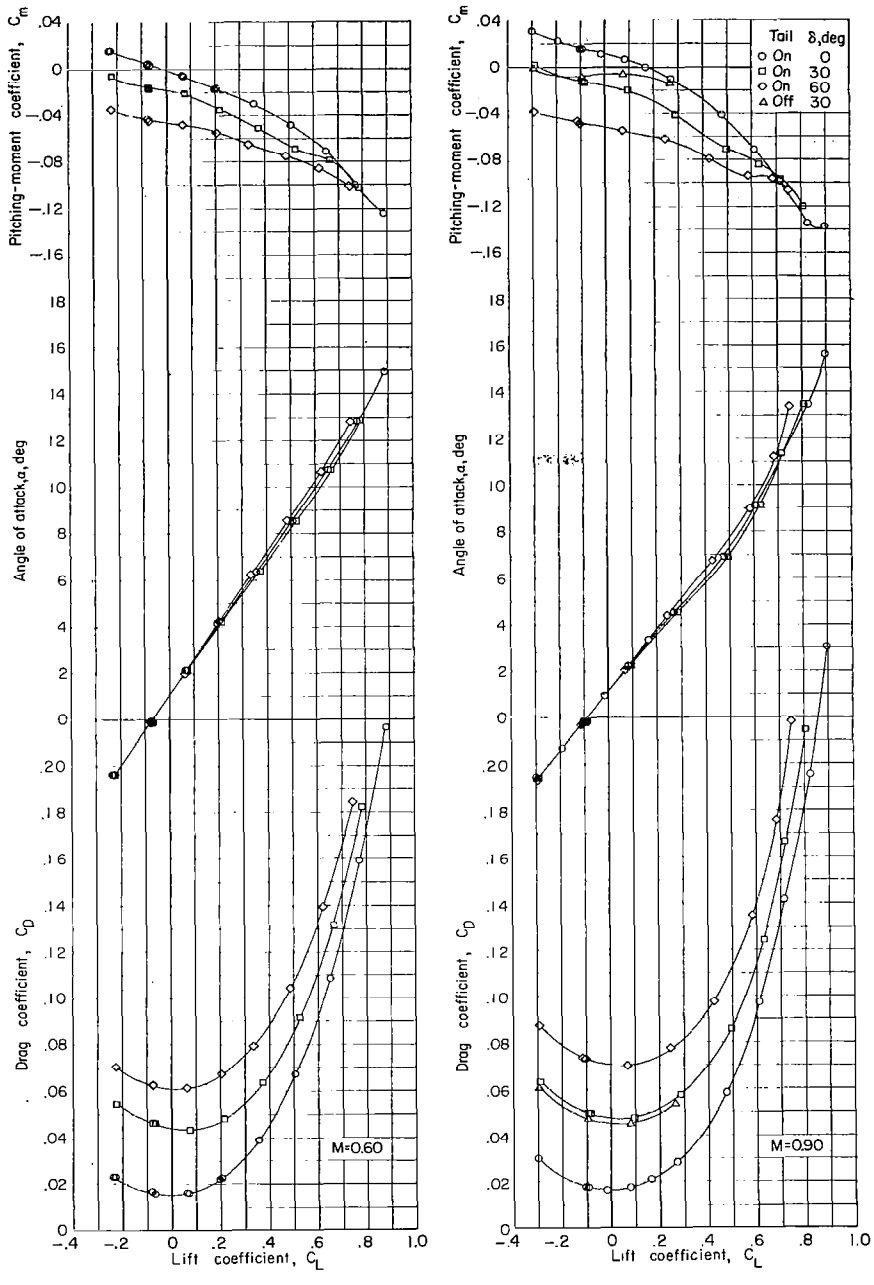

(a) M = 0.60 and 0.90.

Figure 26.- Longitudinal characteristics of model with speed brake 1, fuselage 1, wing 1, tail 2, $i_t = 0^o$.

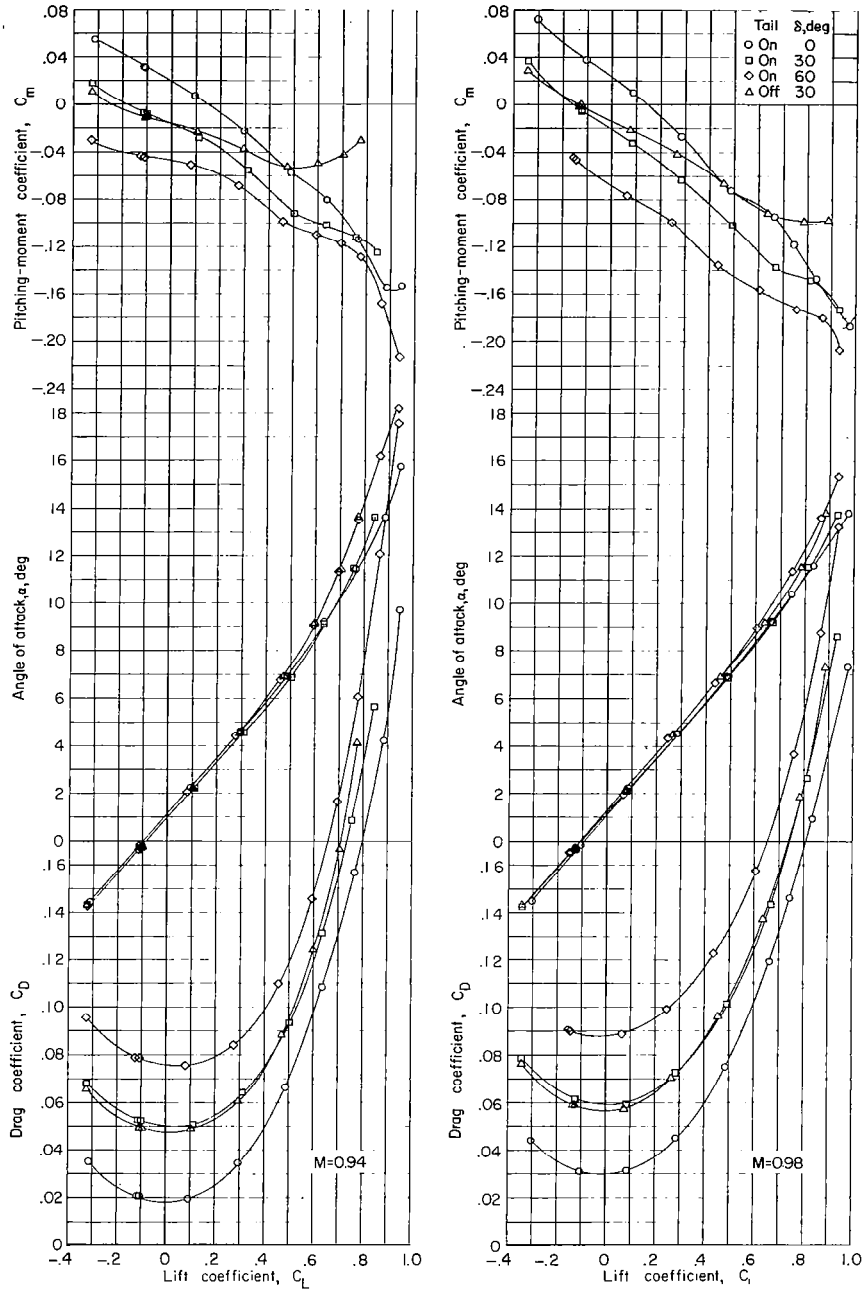

(b) M = 0.94 and 0.98.

Figure 26.- Continued.

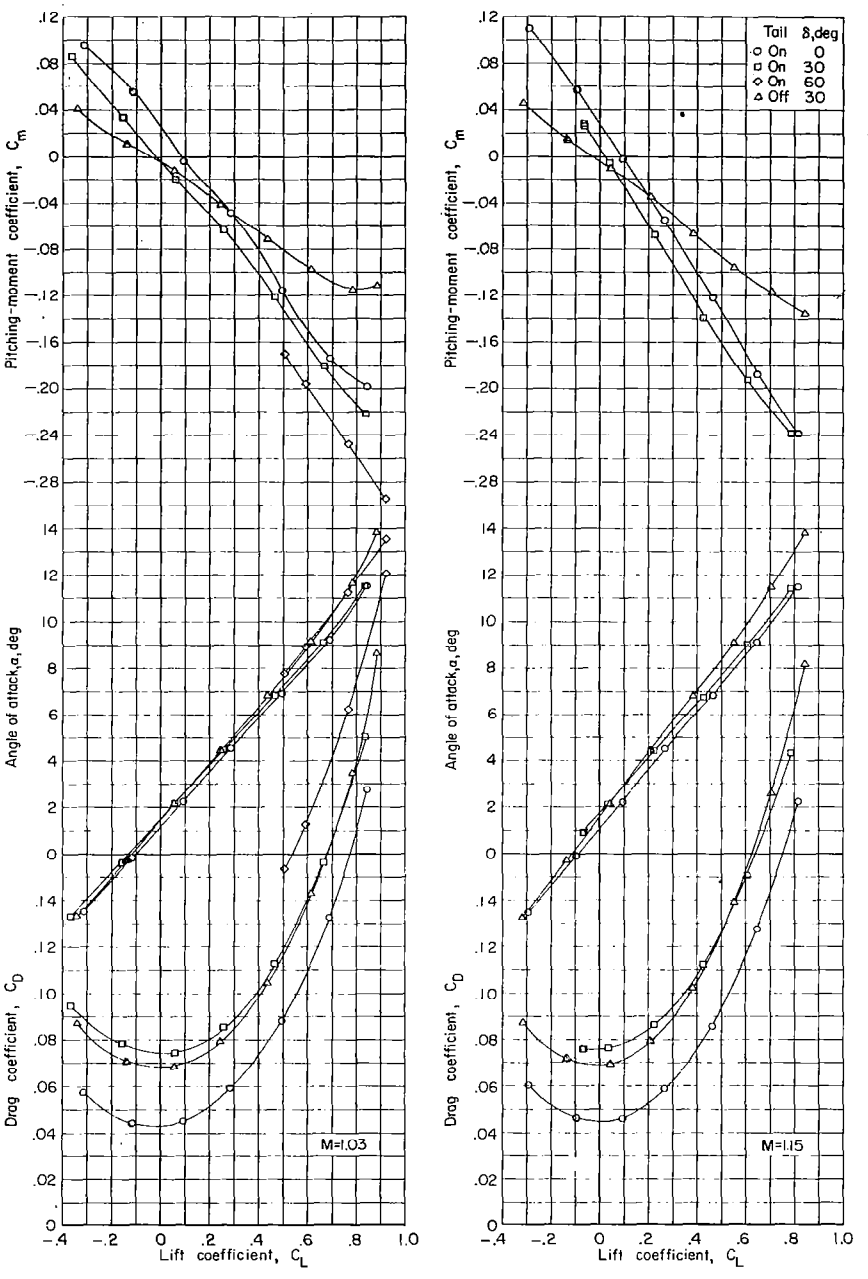

(c) M = 1.03 and 1.15.

Figure 26.- Concluded.

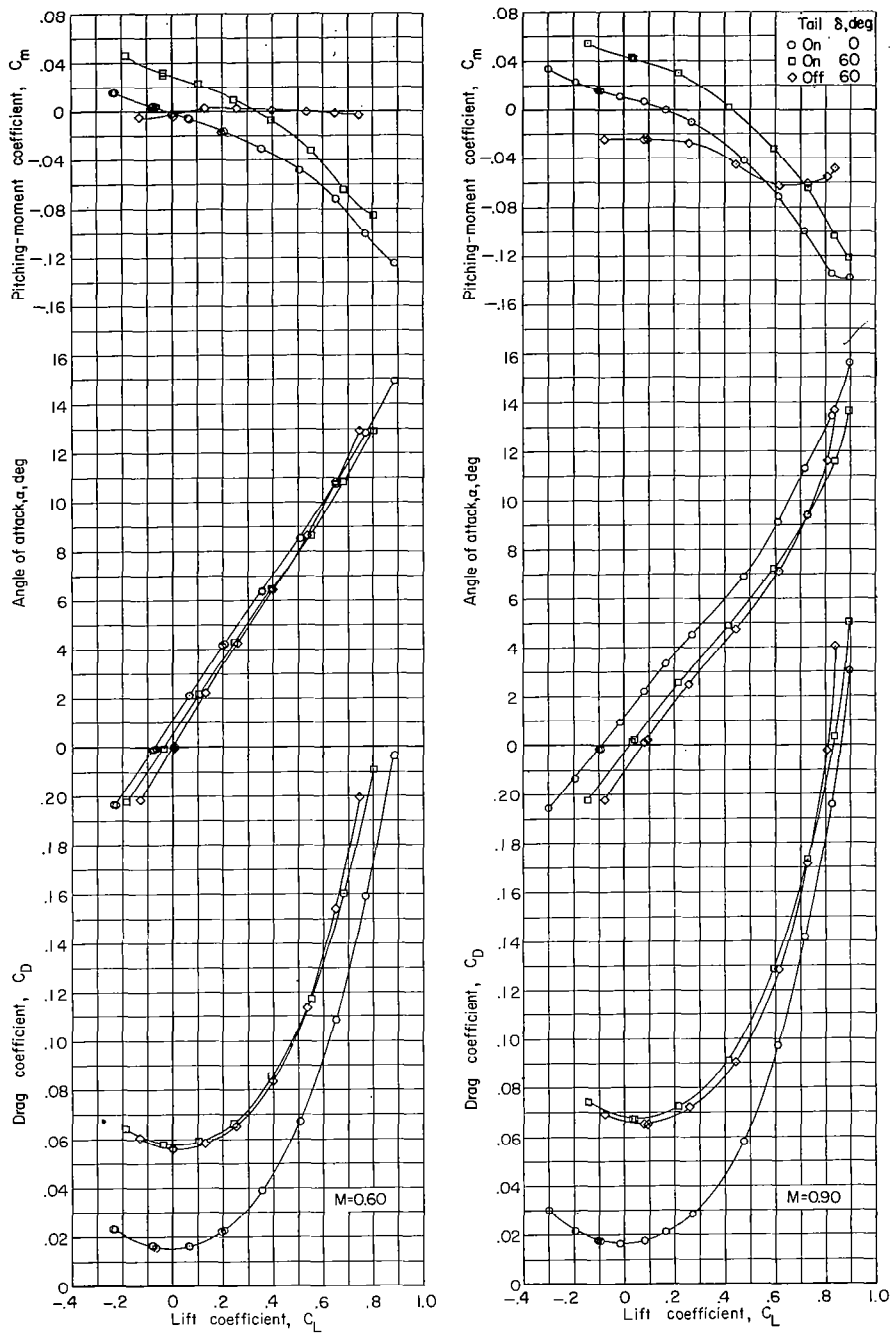

(a) M = 0.60 and 0.90.

Figure 27.- Longitudinal characteristics of model equipped with speed brake 2, fuselage 1, wing 1, tail 2, $i_t = 0^\circ$.

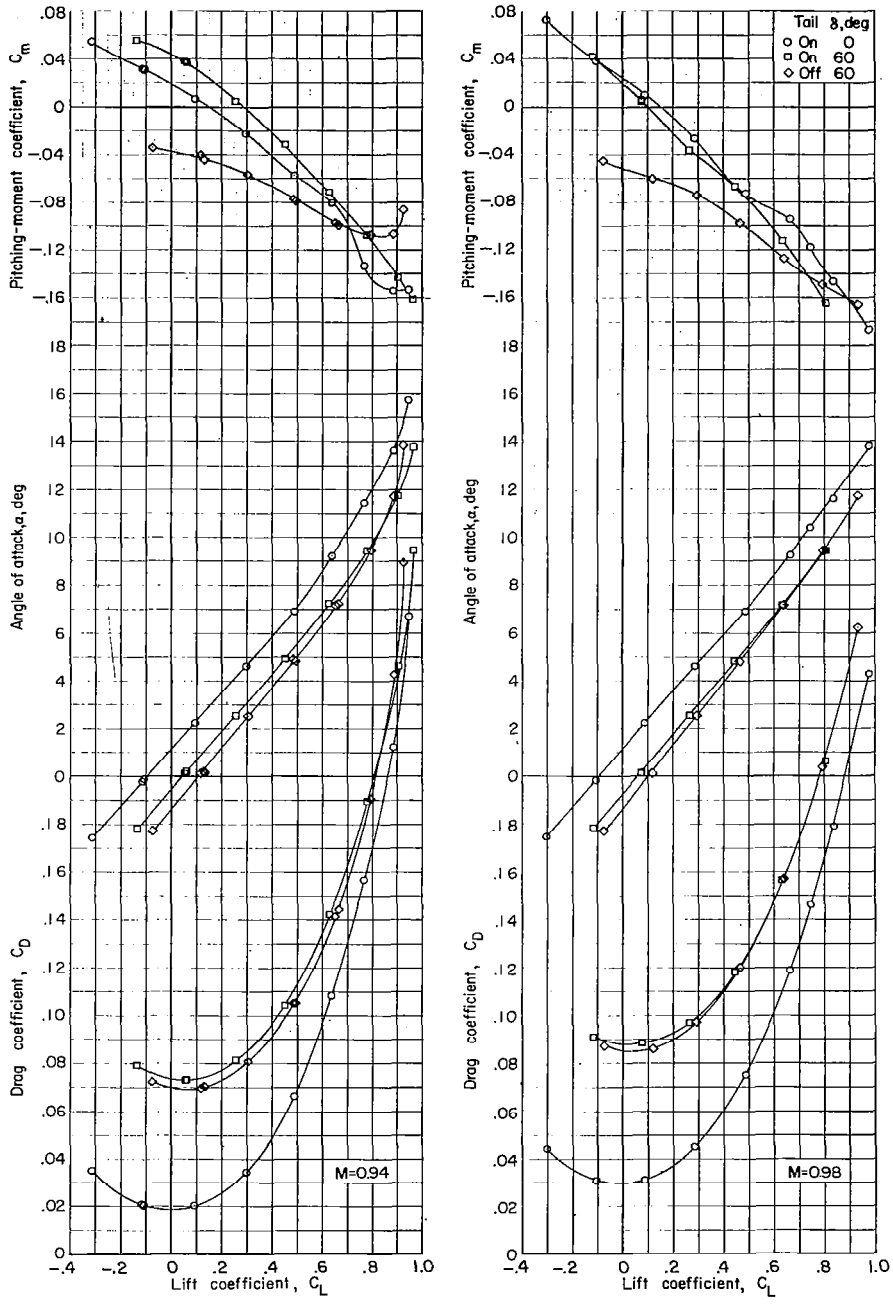

(b) M = 0.94 and 0.98.

Figure 27.- Continued.

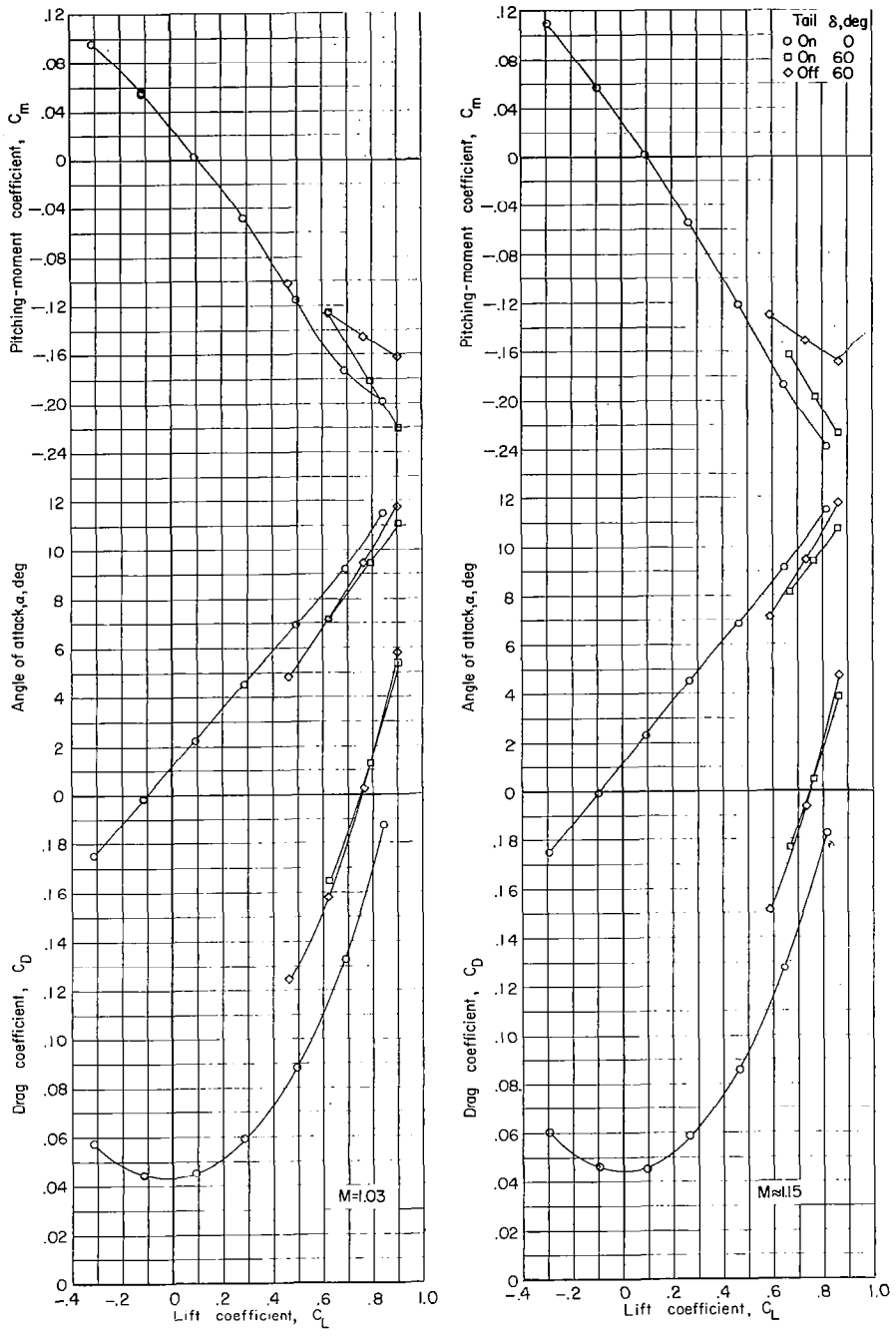

(c) M = 1.03 and 1.15.

Figure 27.- Concluded.

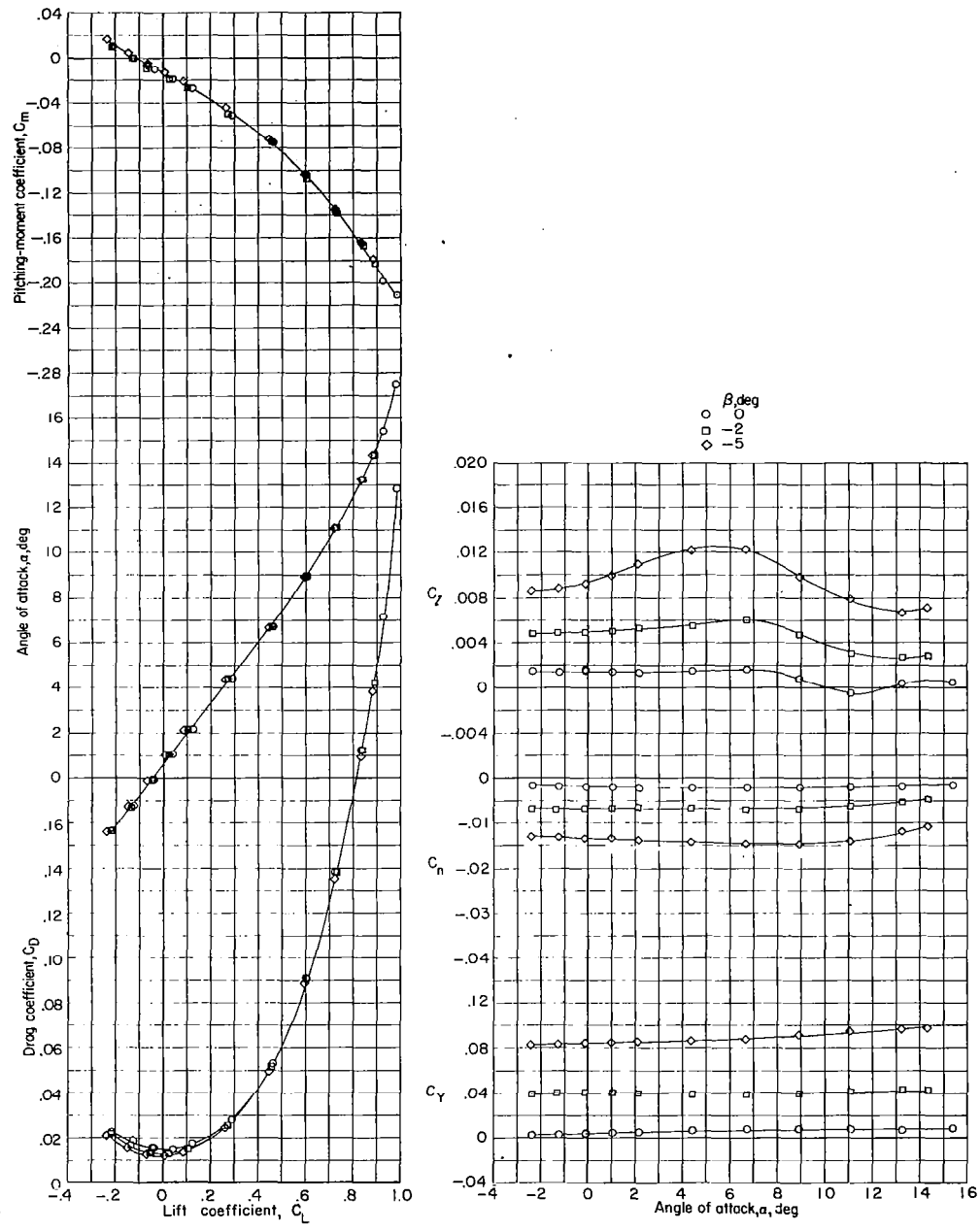

(a) M = 0.80.

Figure 28.- Effect of sideslip on aerodynamic characteristics in pitch; fuselage 4, wing 1, tail 2, $i_t = 0^o$.

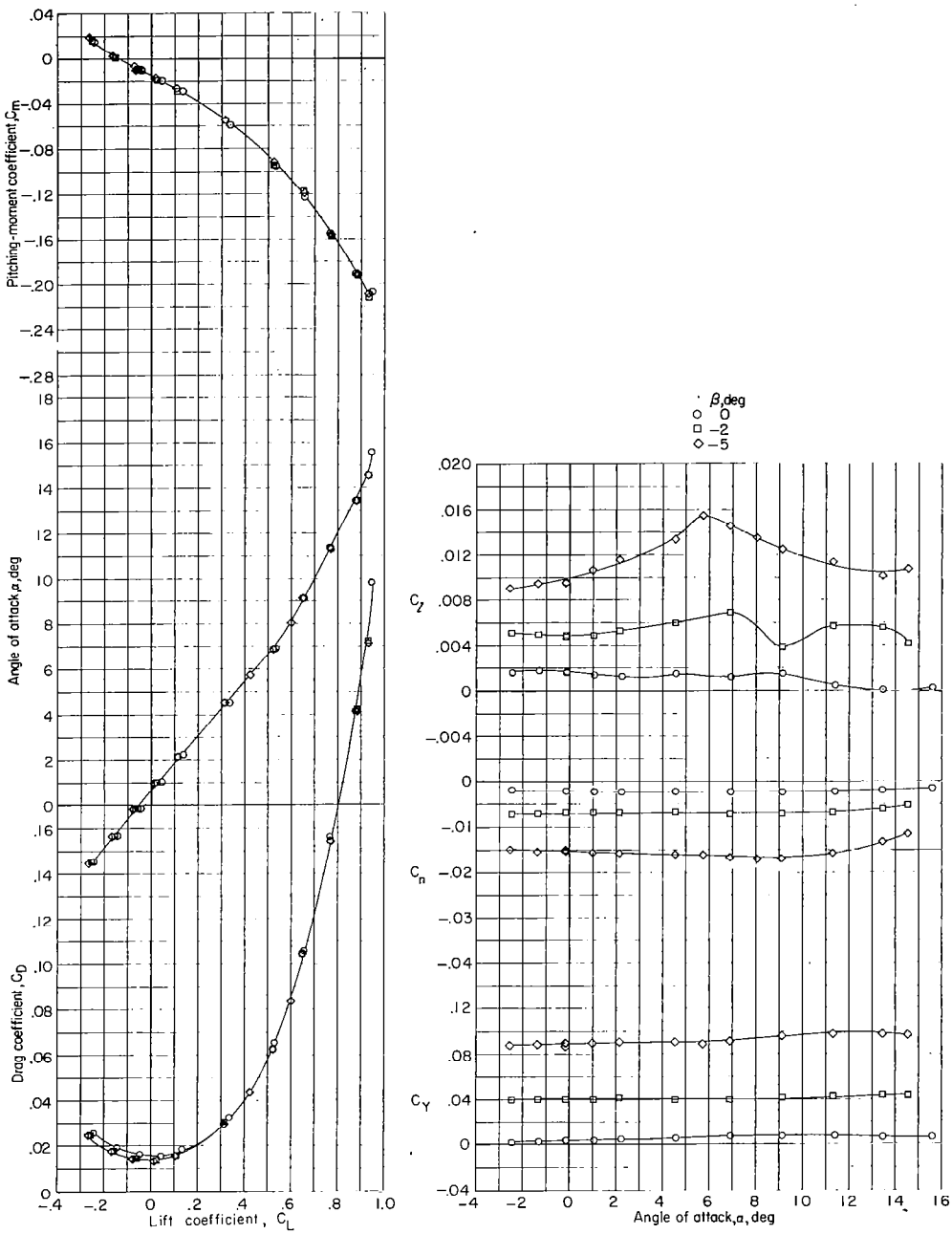

(b) M = 0.90.

Figure 28.- Continued.

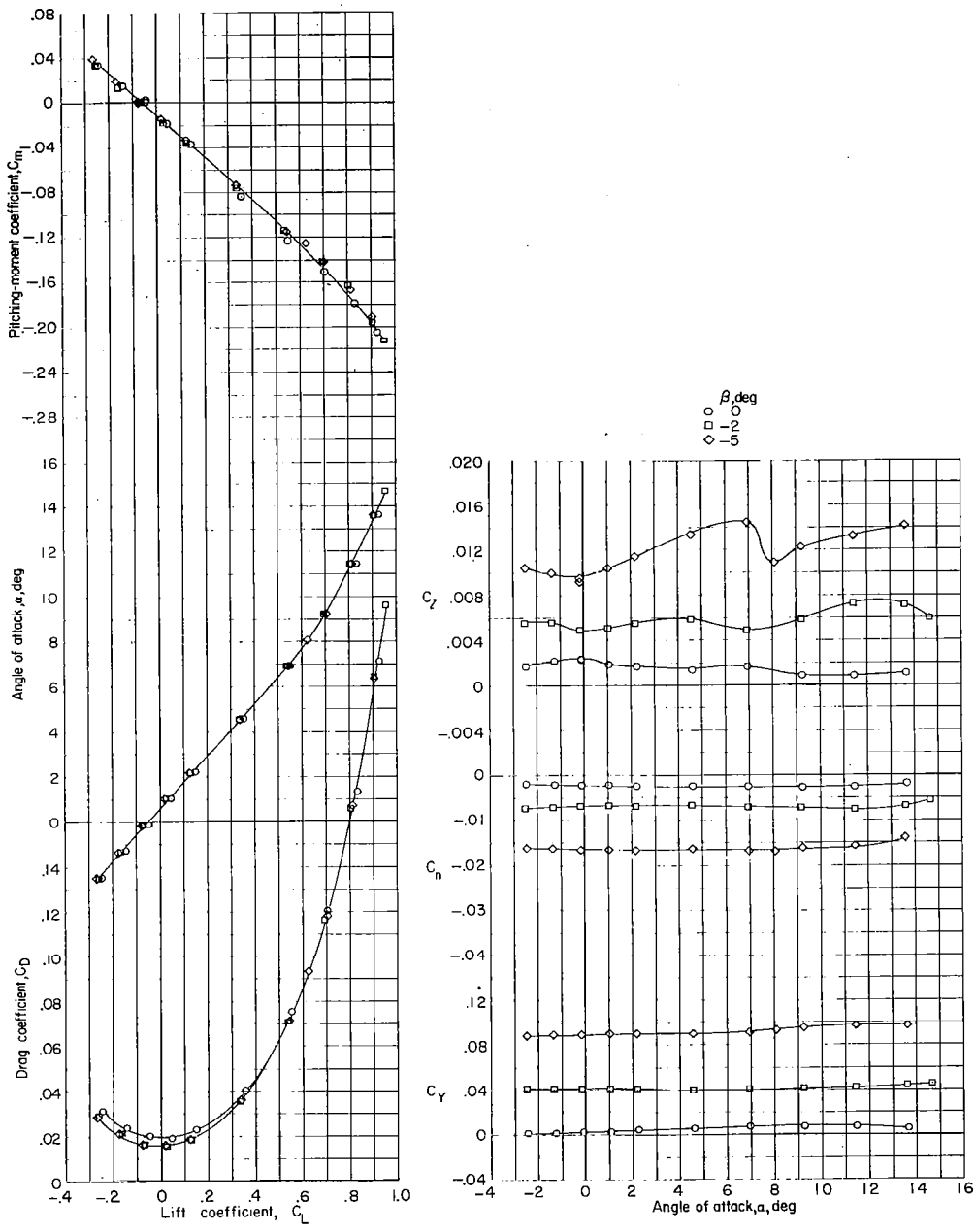

(c) M = 0.94.

Figure 28.- Continued.

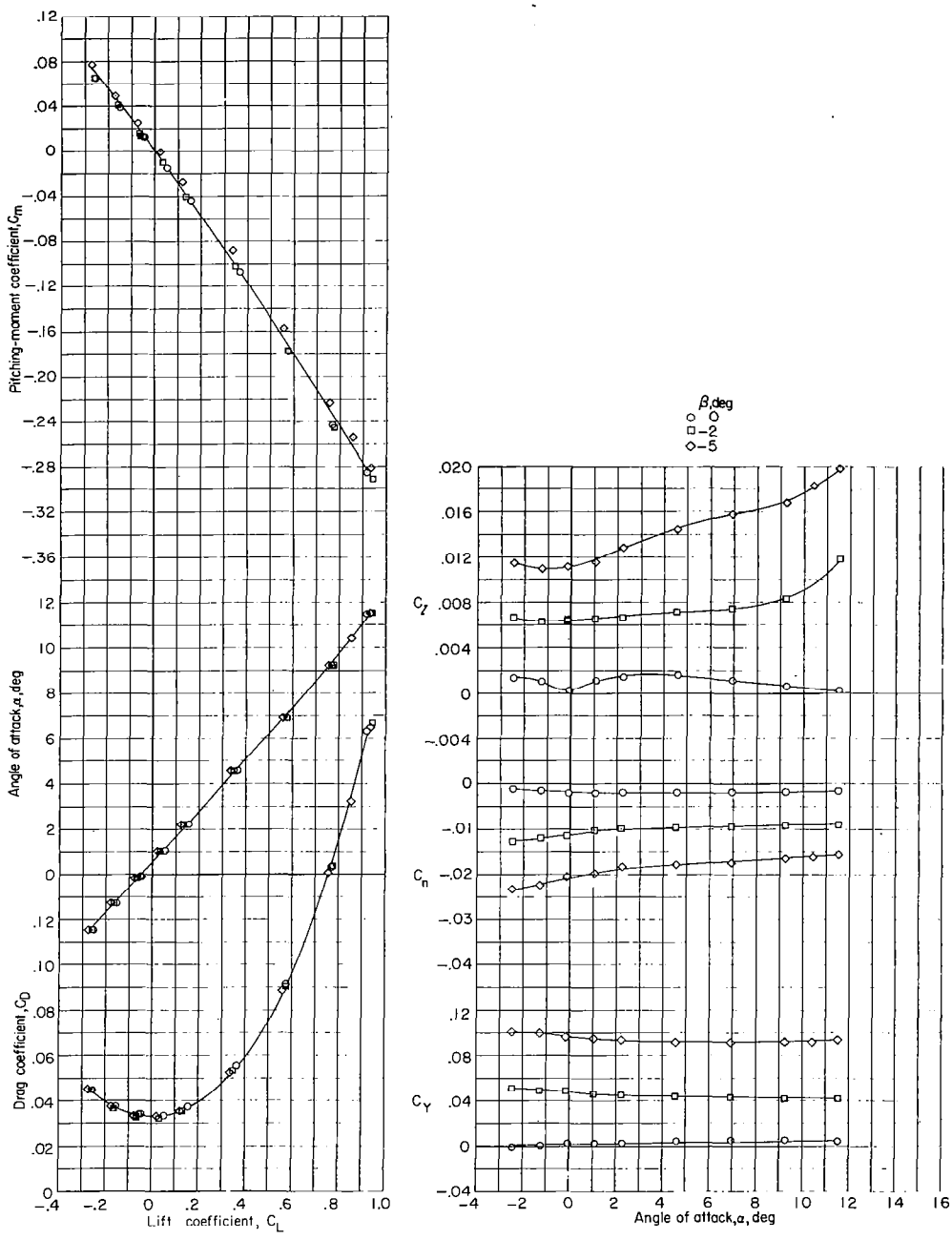

(d) M = 1.00.

Figure 28.- Continued.

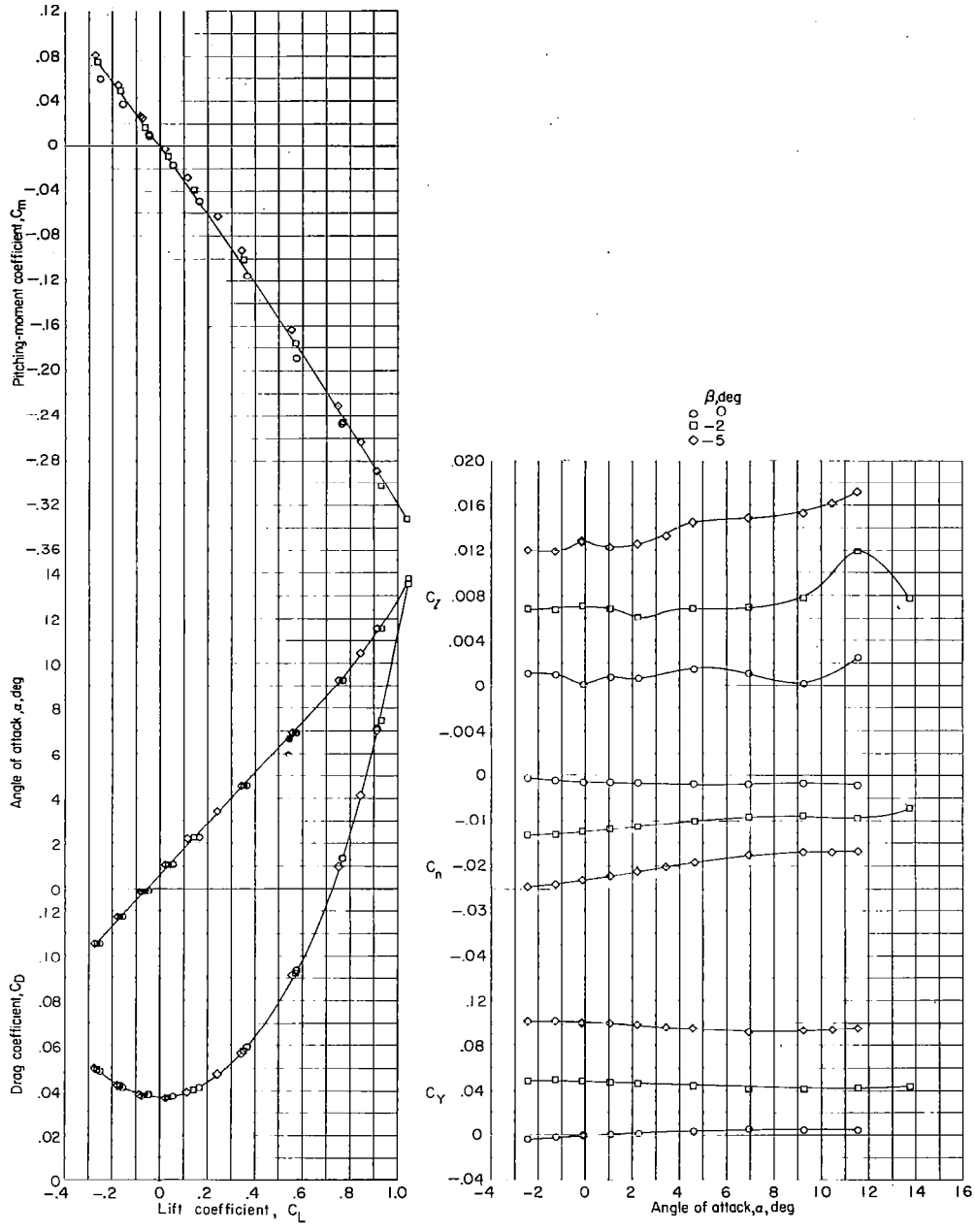

(e) M = 1.03.

Figure 28.- Continued.

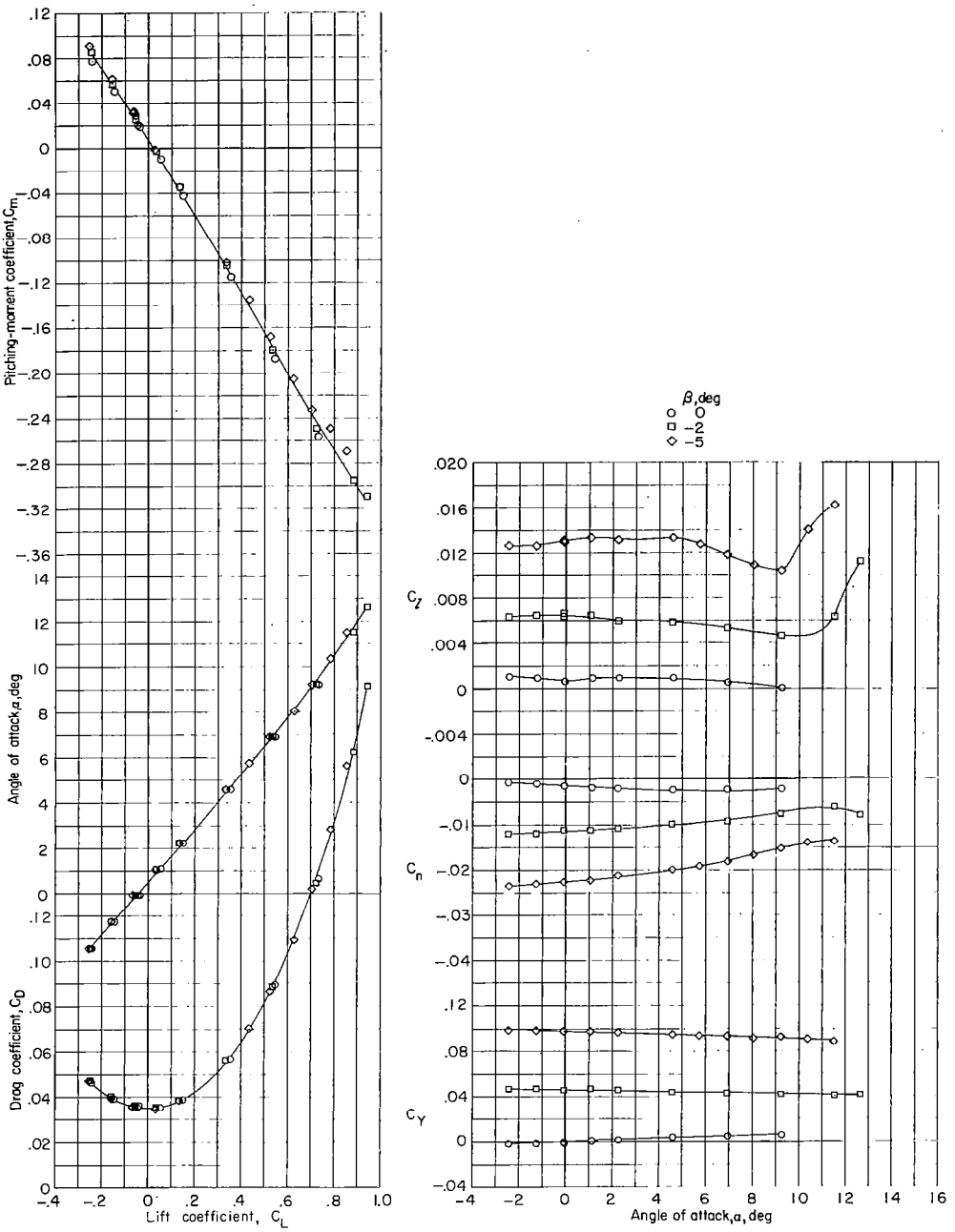

(f) M = 1.13.

Figure 28.- Continued.

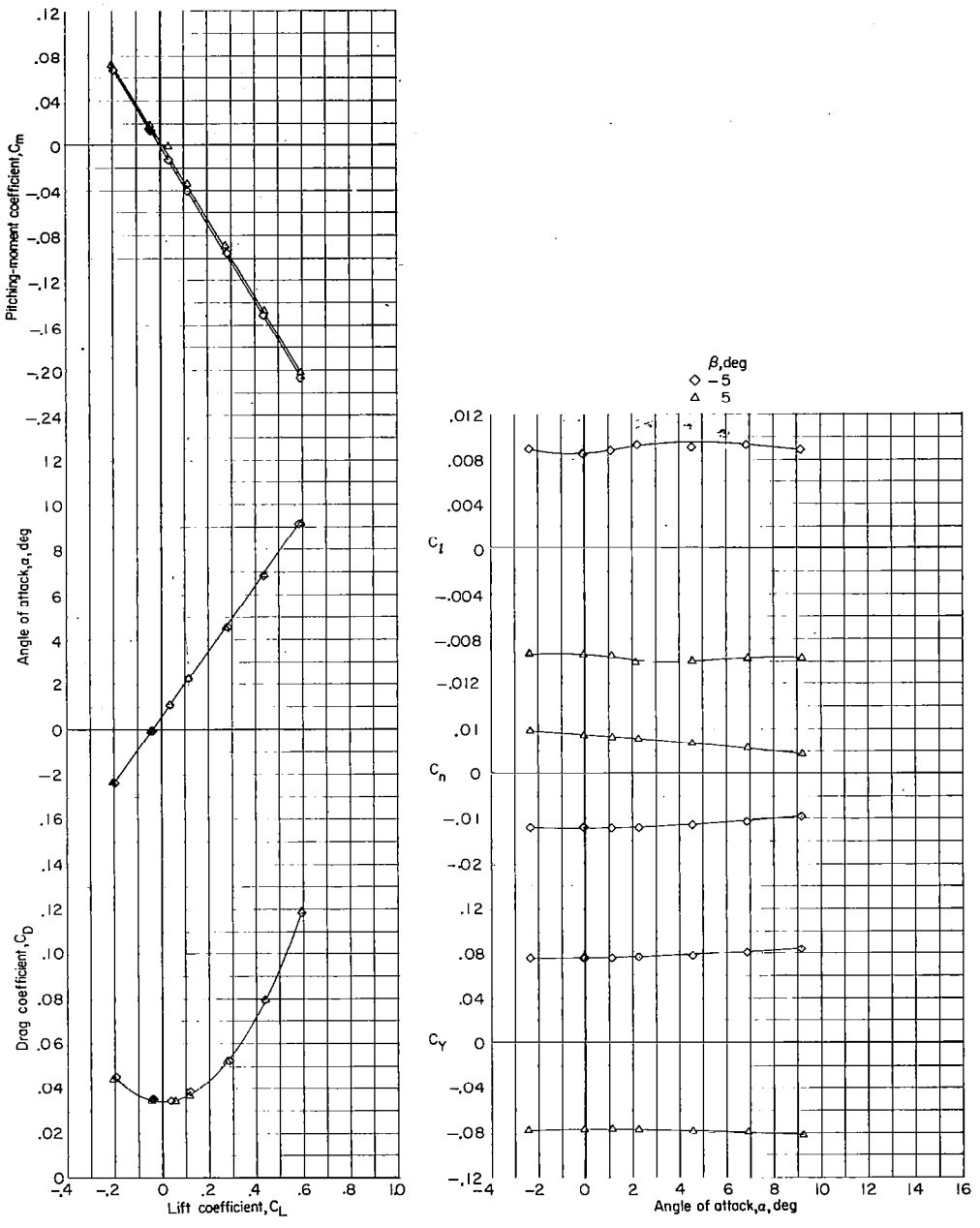

(g) M = 1.43.

Figure 28.- Concluded.

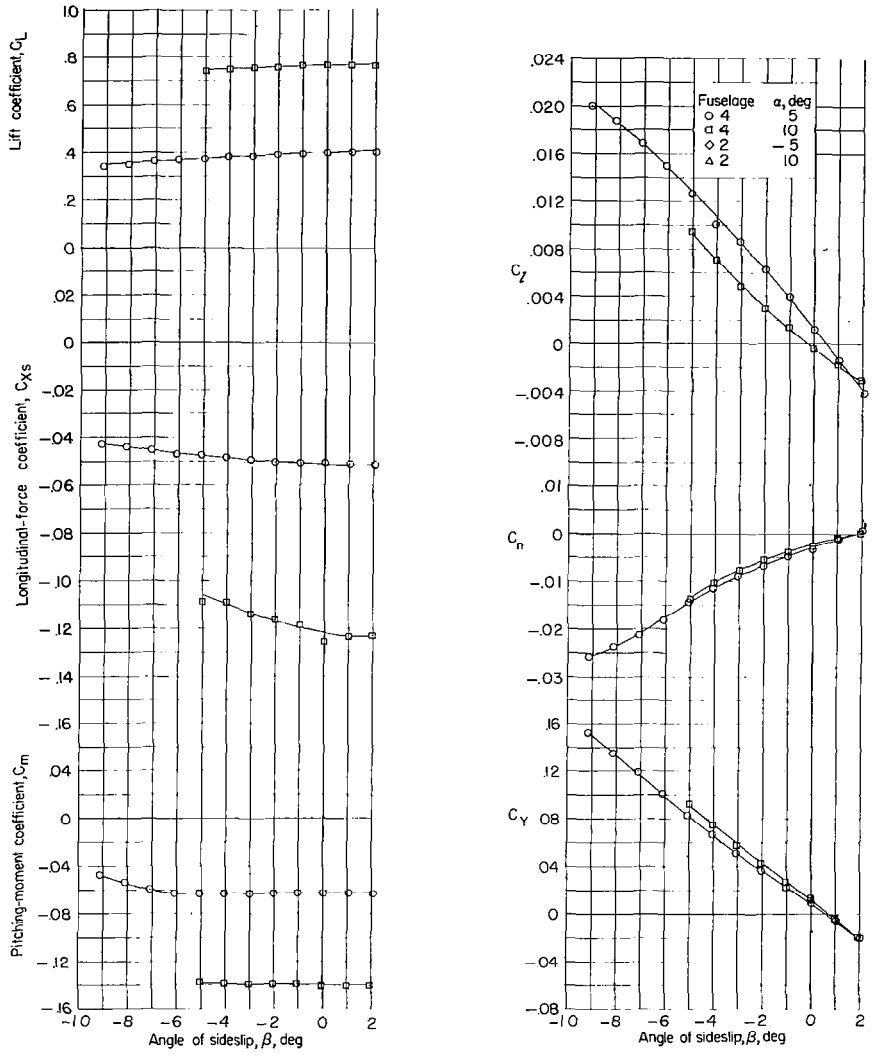

(a) M = 0.80.

Figure 29.- Effect of pitch on aerodynamic characteristics of model in sideslip; wing 1, tail 2, $i_t = 0^o$.

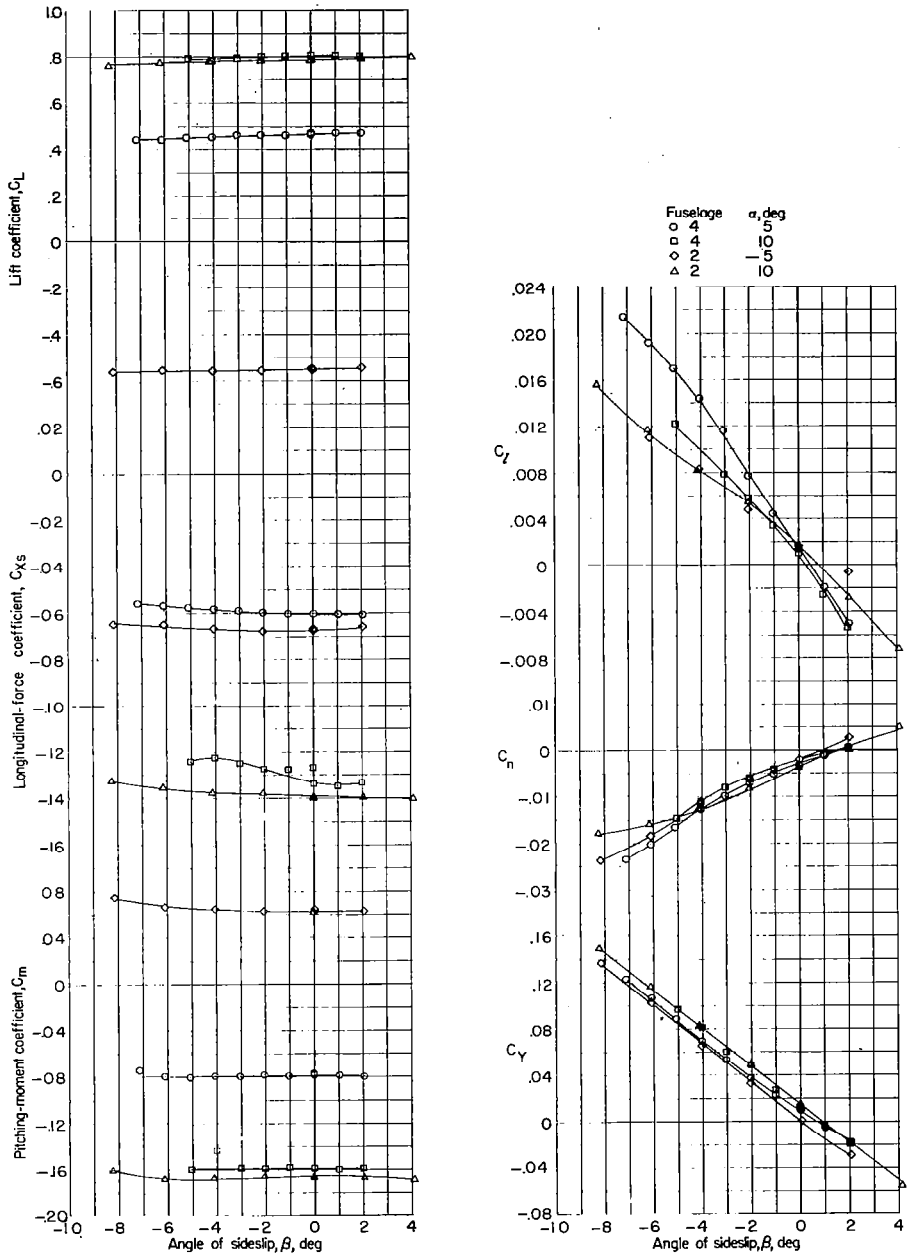

(b) M = 0.90.

Figure 29.- Continued.

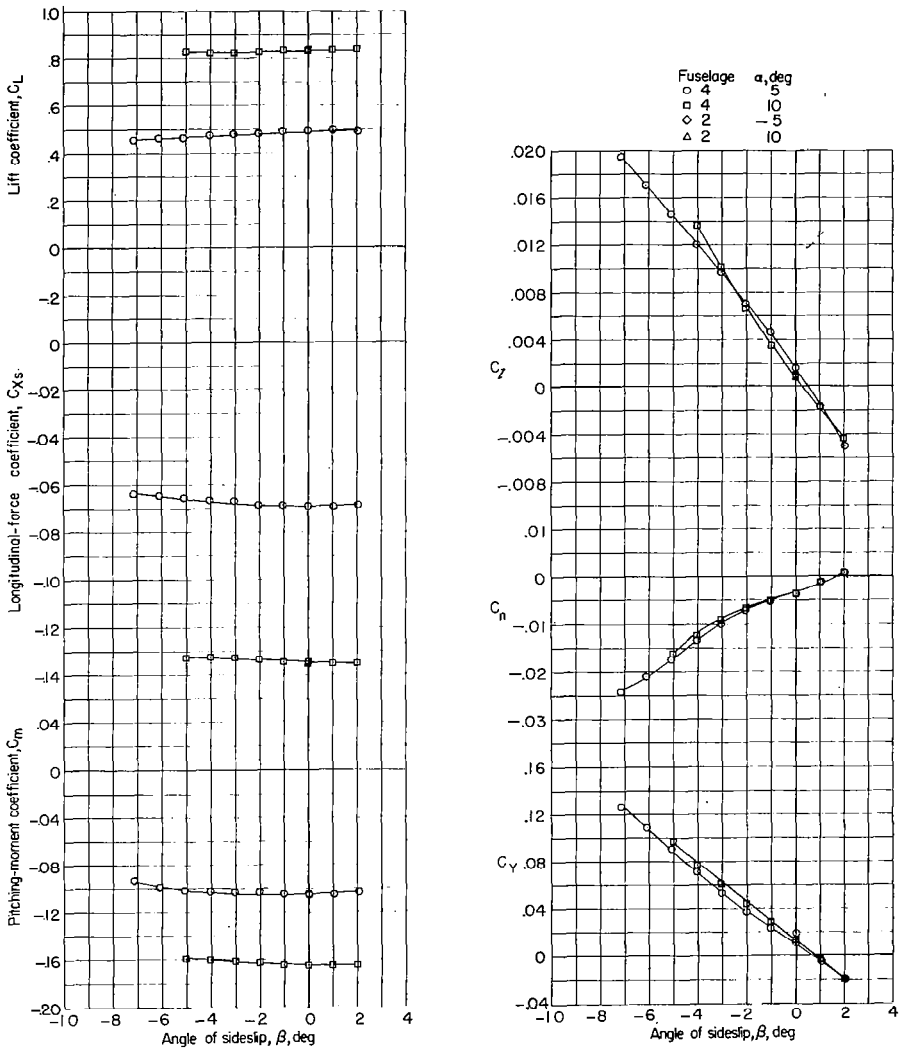

(c) M = 0.94.

Figure 29.- Continued.

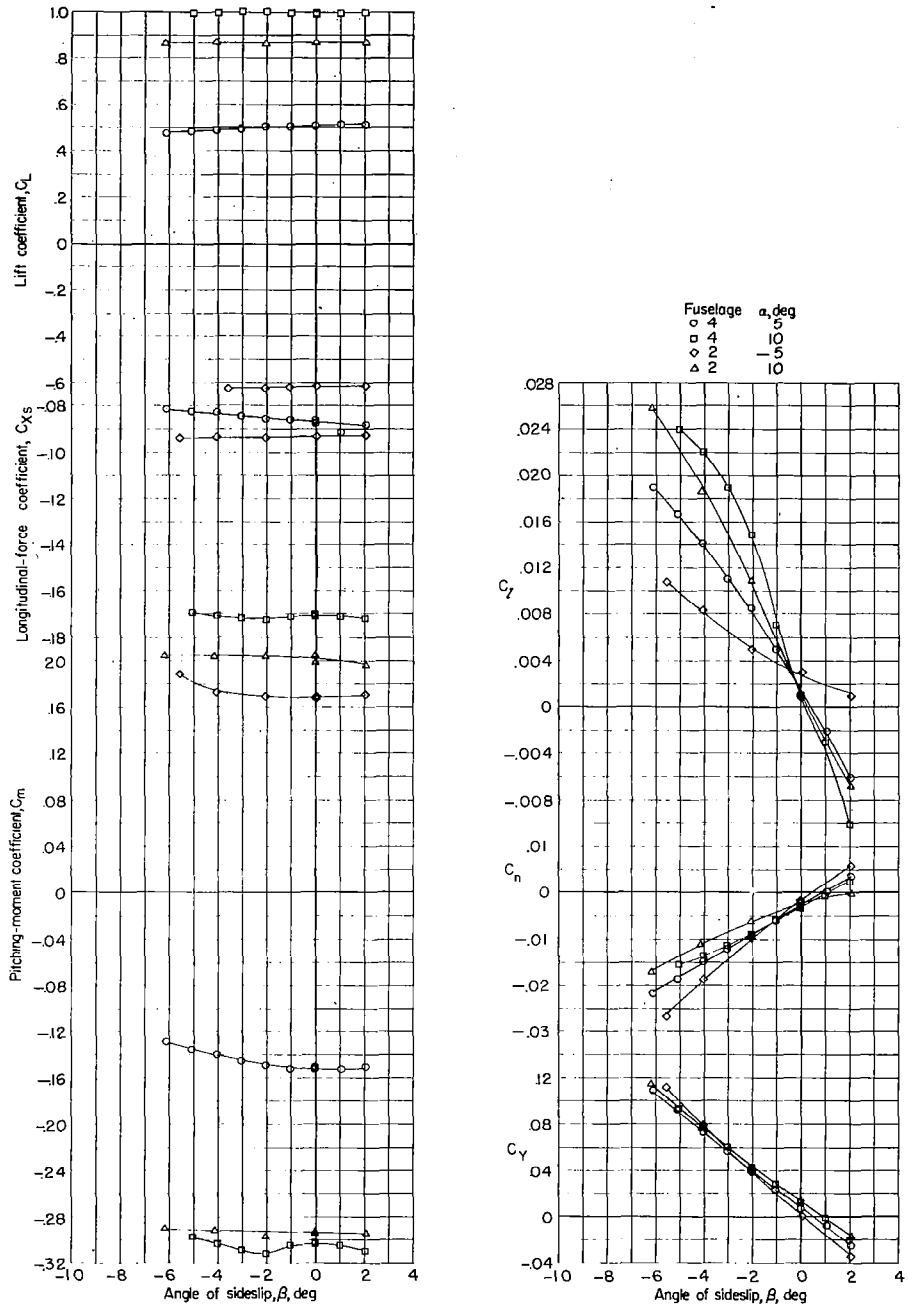

(d) M = 1.00.

Figure 29.- Continued.

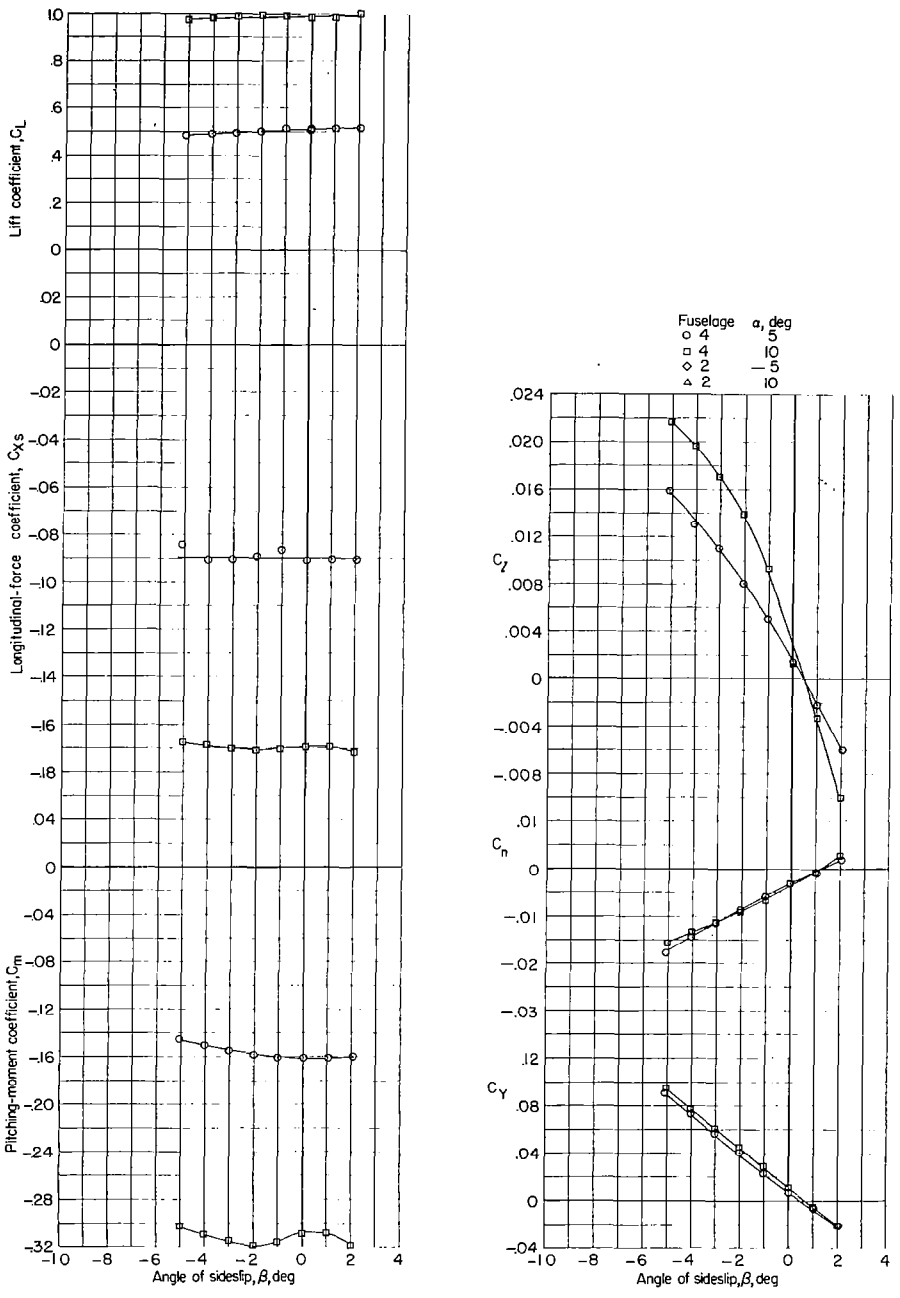

(e) M = 1.03.

Figure 29.- Continued.

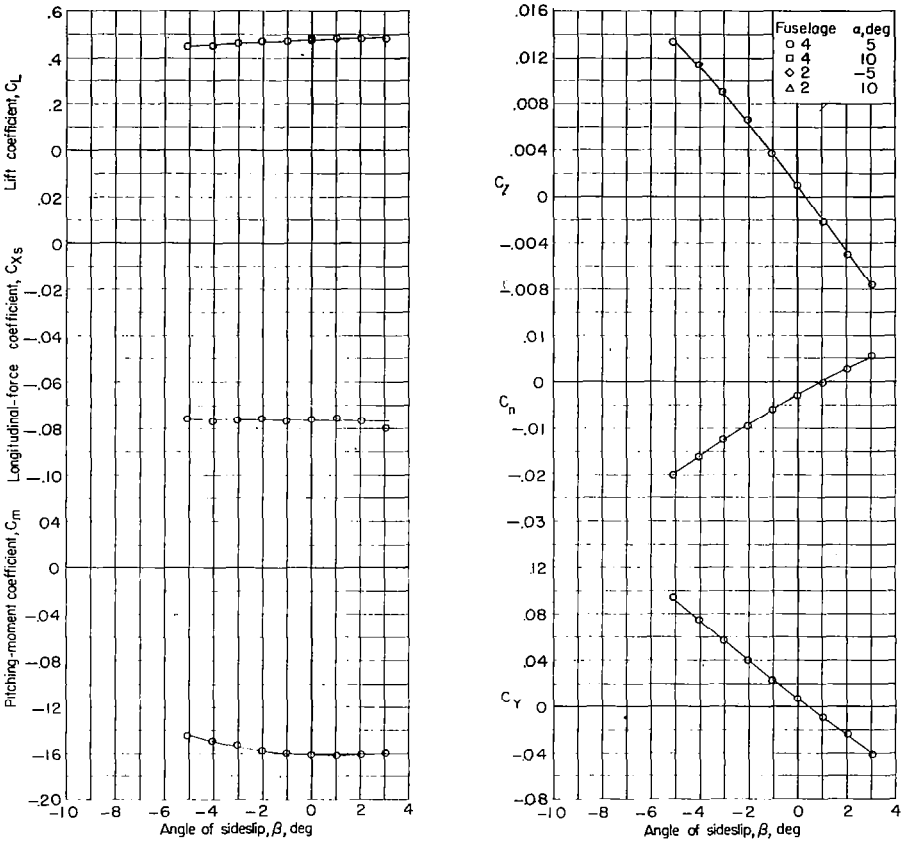

(f) M = 1.13.

Figure 29.- Concluded.

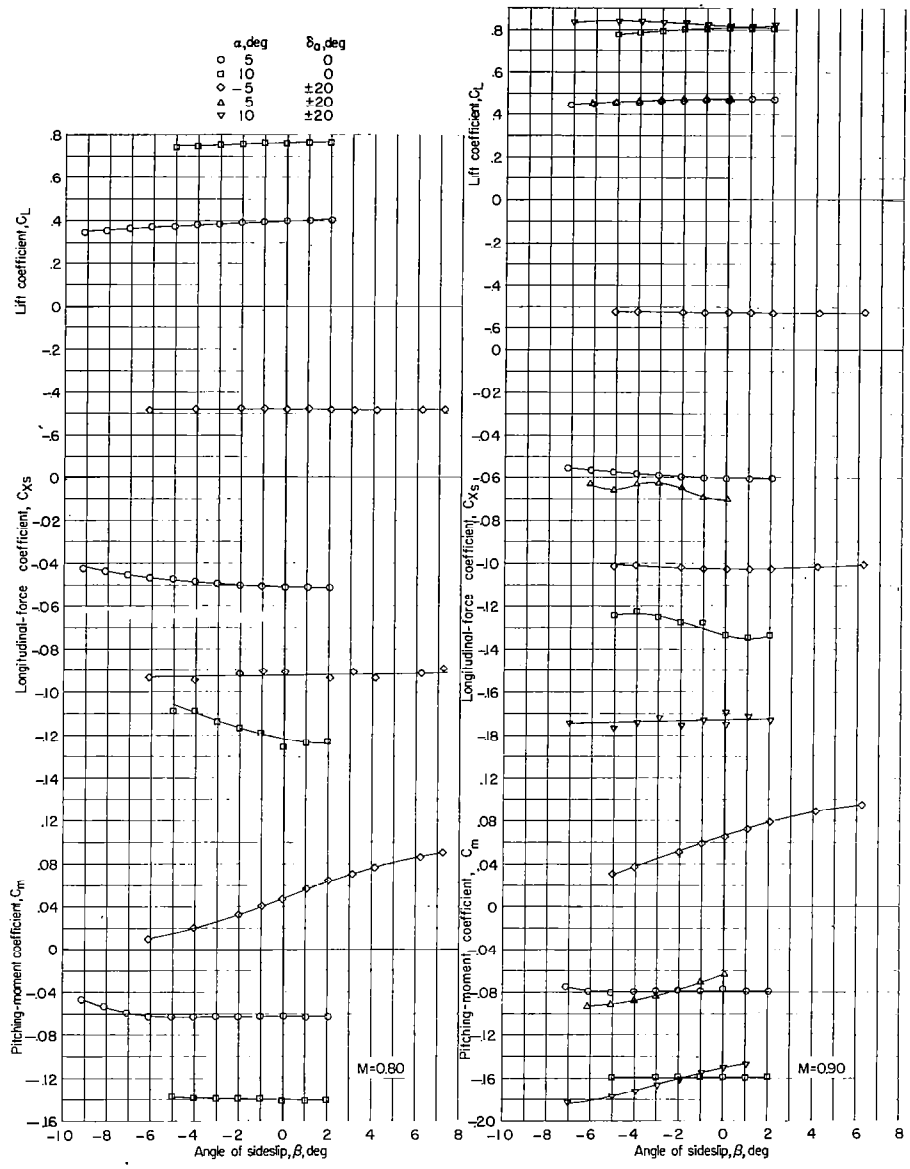

(a) M = 0.80 and 0.90.

Figure 30.- Longitudinal characteristics of model in sideslip with ailerons deflected 20°, fuselage 4, wing 1, tail 2, $i_t = 0°$.

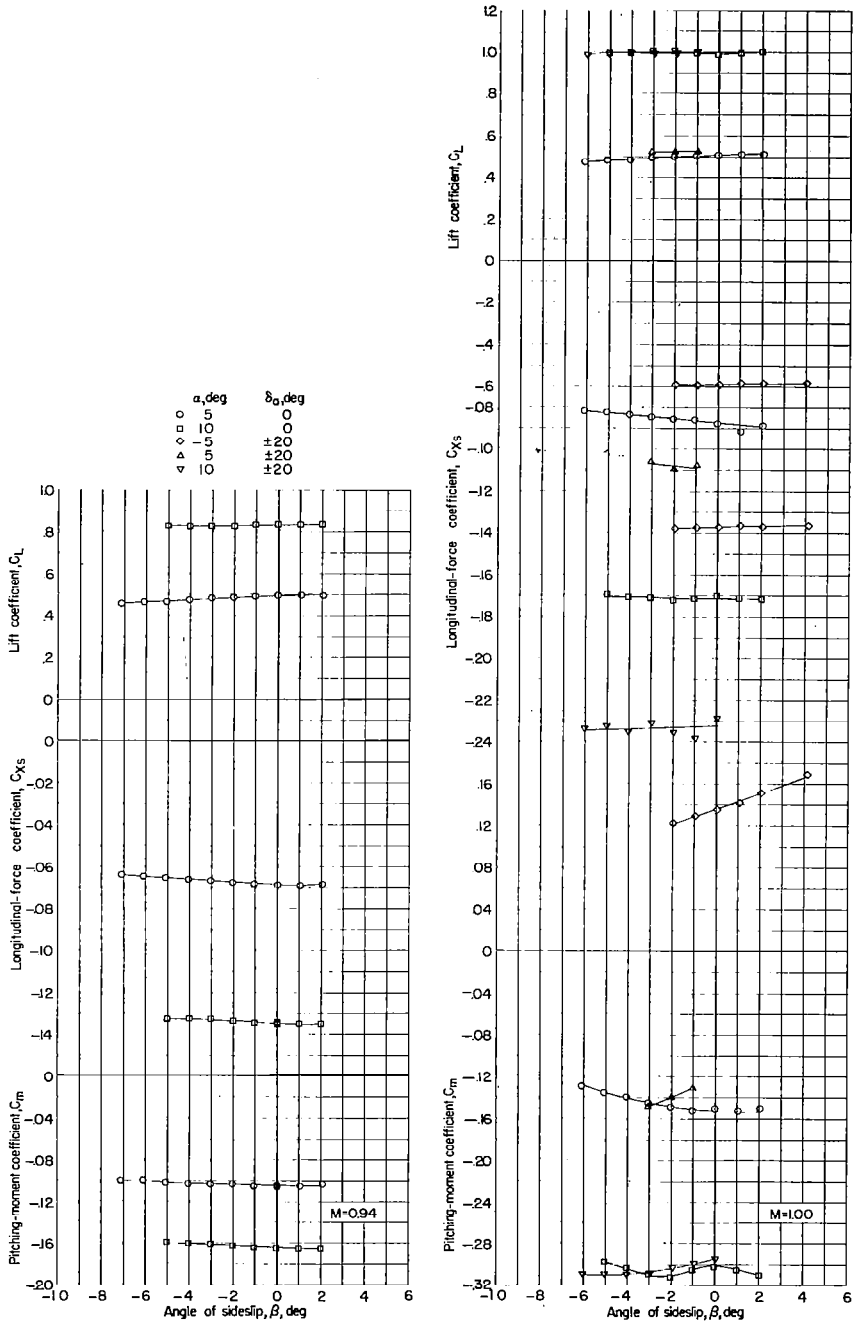

(b) M = 0.94 and 1.00.

Figure 30.- Continued.

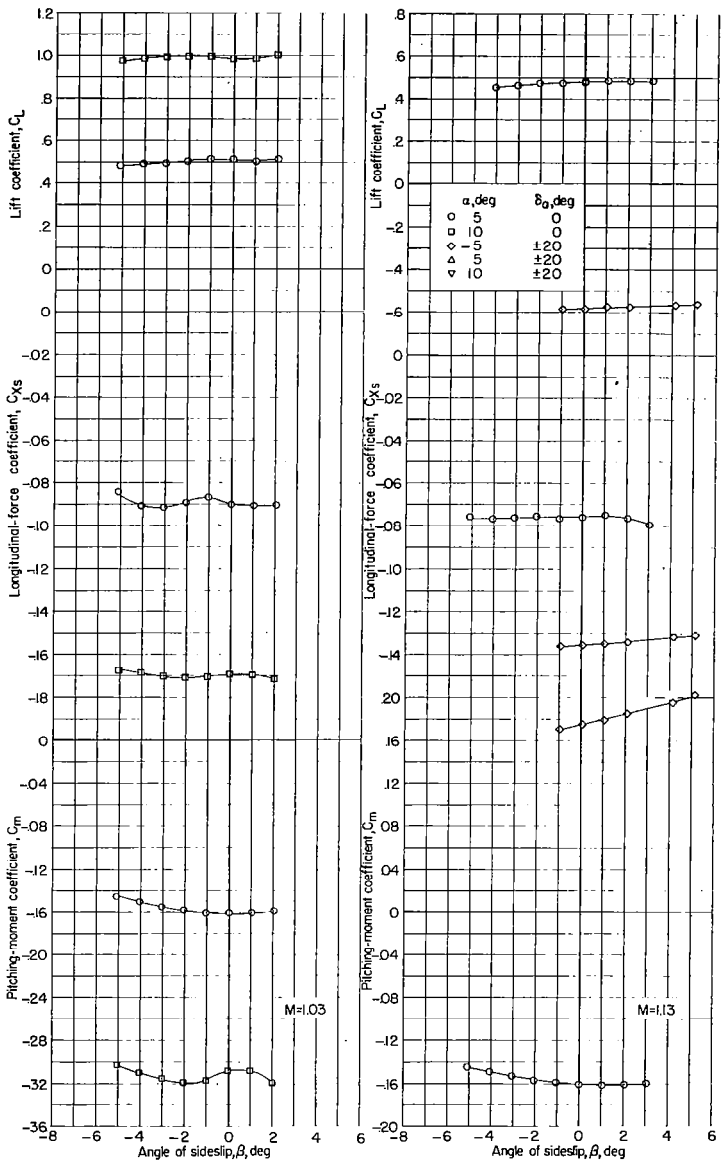

(c) M = 1.03 and 1.13.

Figure 30.- Concluded.

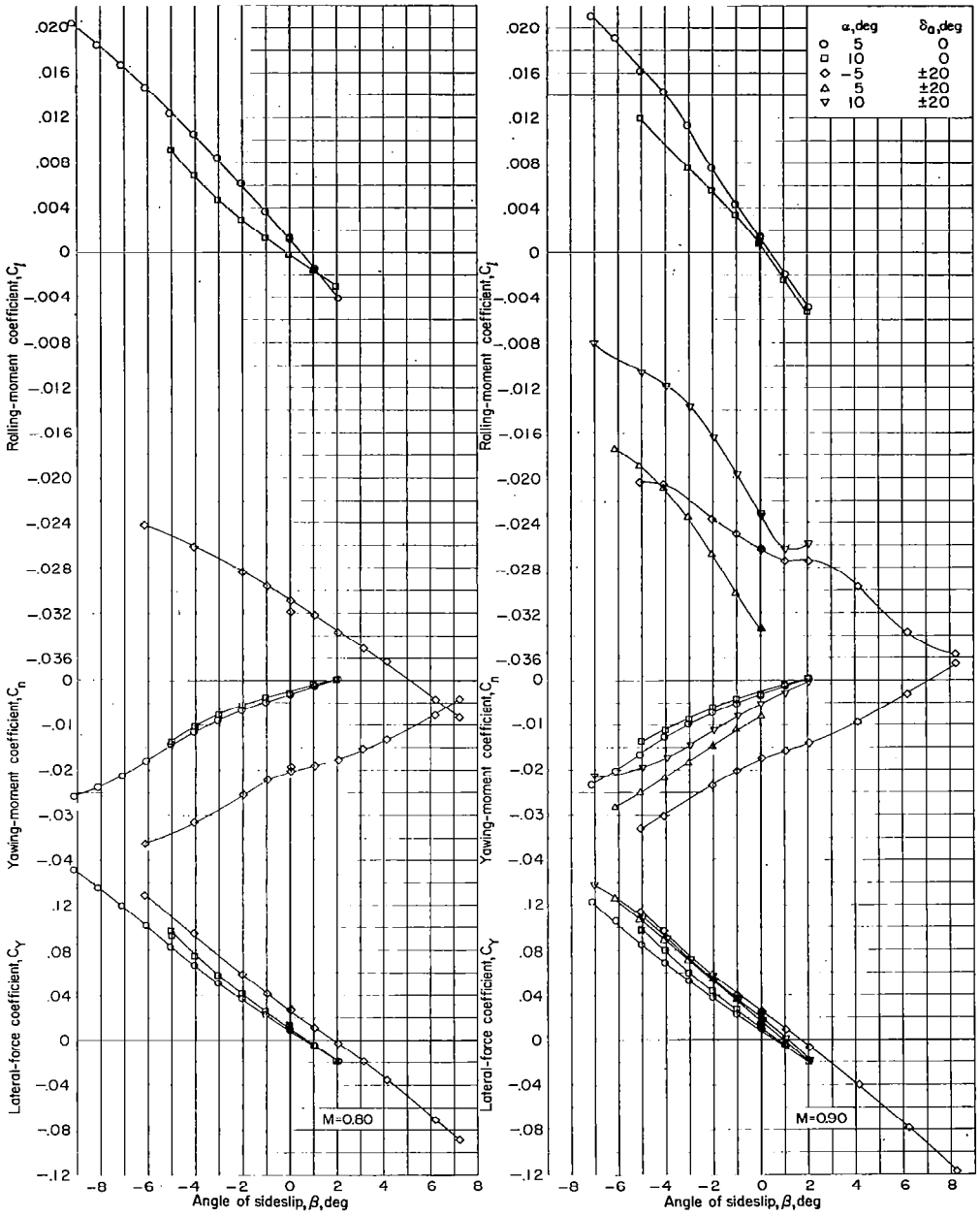

(a) M = 0.80 and 0.90.

Figure 31.- Lateral characteristics of complete model in sideslip with ailerons deflected 20°, fuselage 4, wing 1, tail 2, $i_t = 0°$.

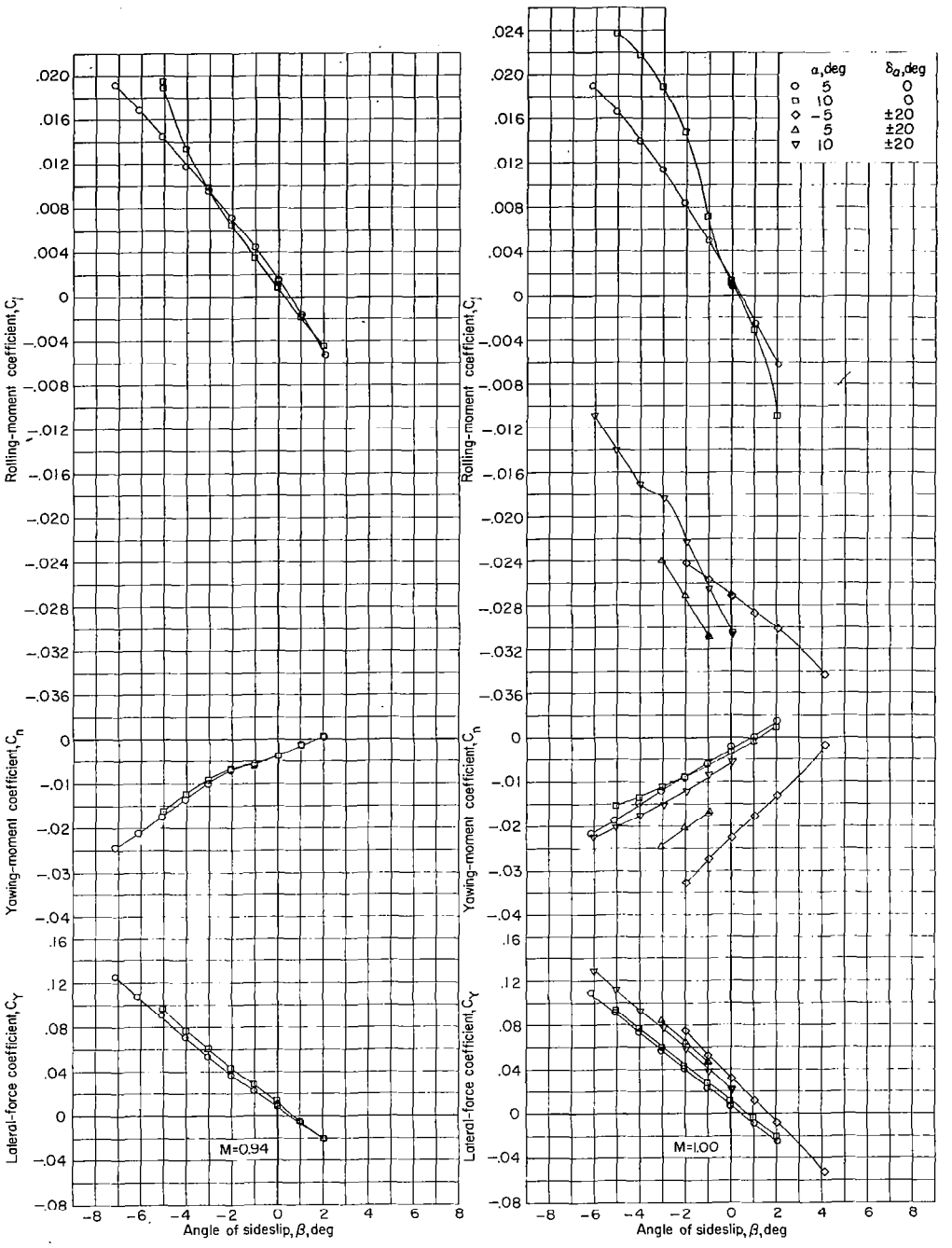

(b) M = 0.94 and 1.00.

Figure 31.- Continued.

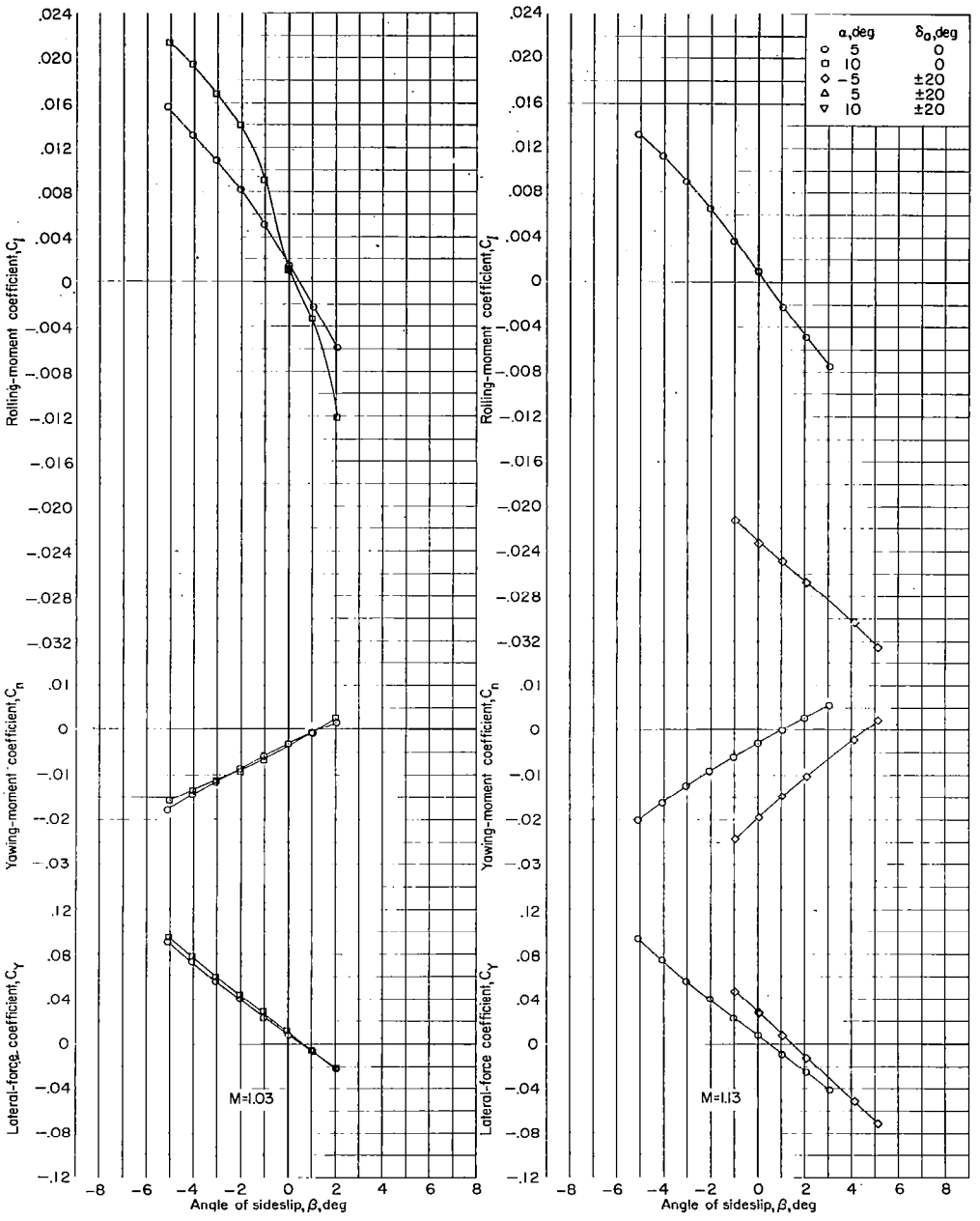

(c) M = 1.03 and 1.13.

Figure 31.- Concluded.

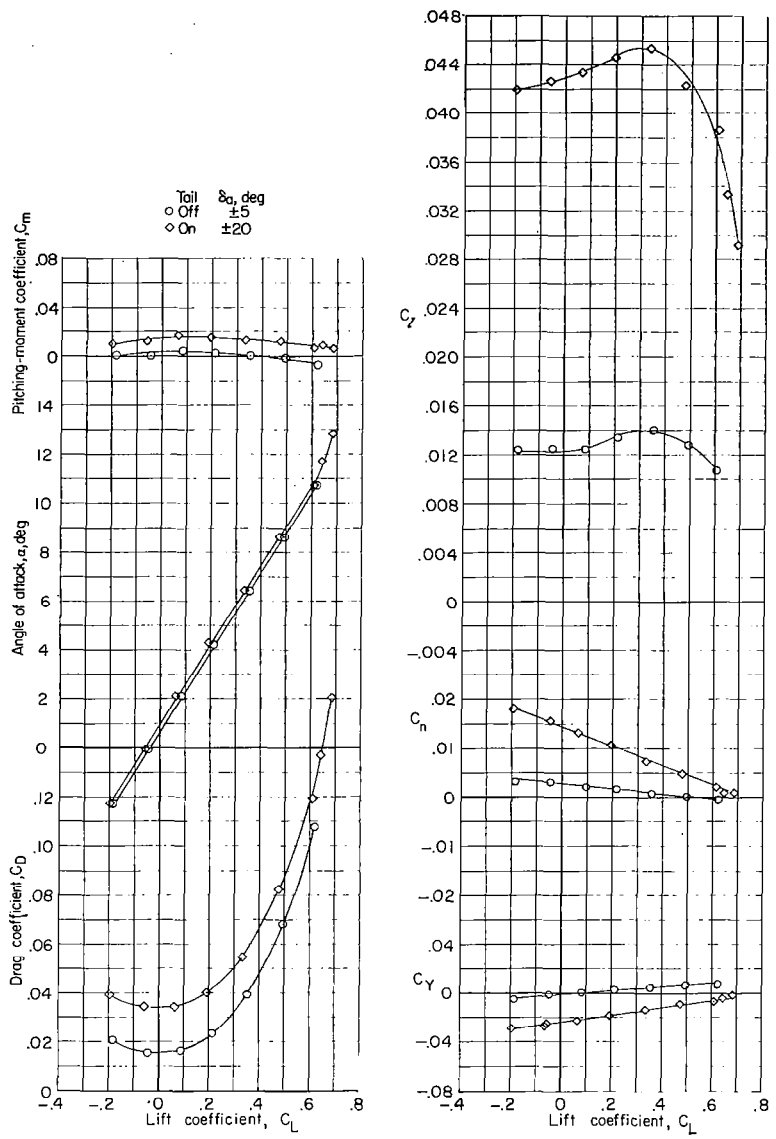

(a) M = 0.60.

Figure 32.- Effect of tail on aerodynamic characteristics in pitch of model with ailerons deflected, fuselage 4, wing 1, tail 2, $i_t = 0^o$.

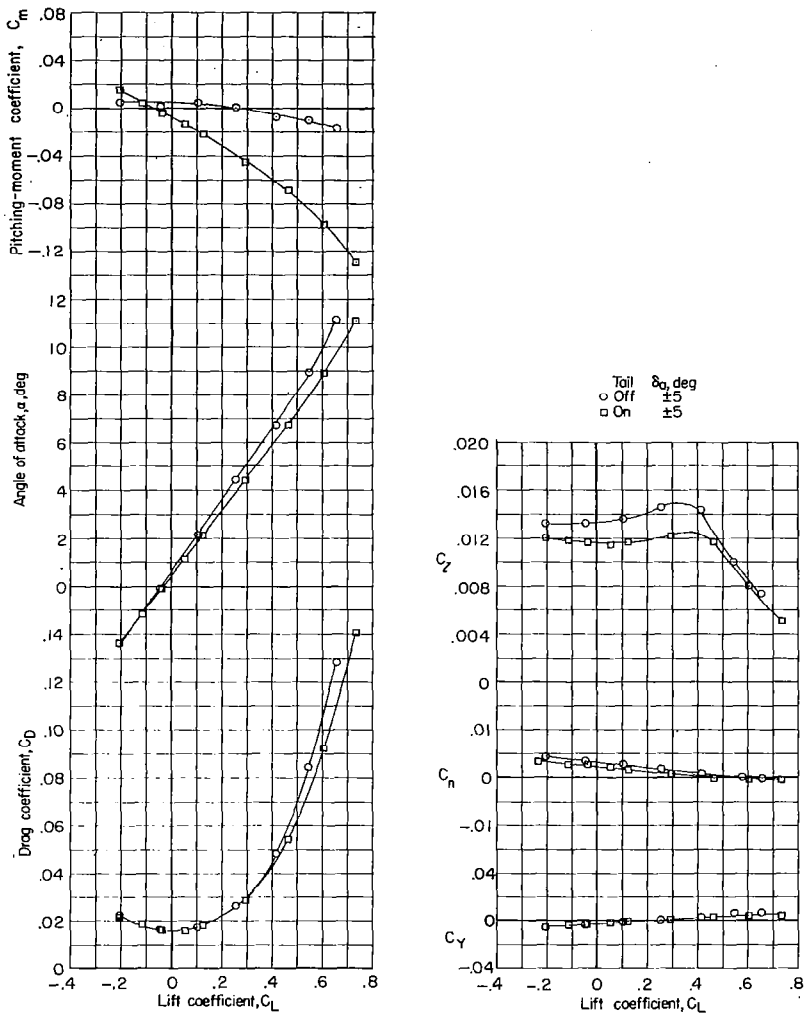

(b) M = 0.80.

Figure 32.- Continued.

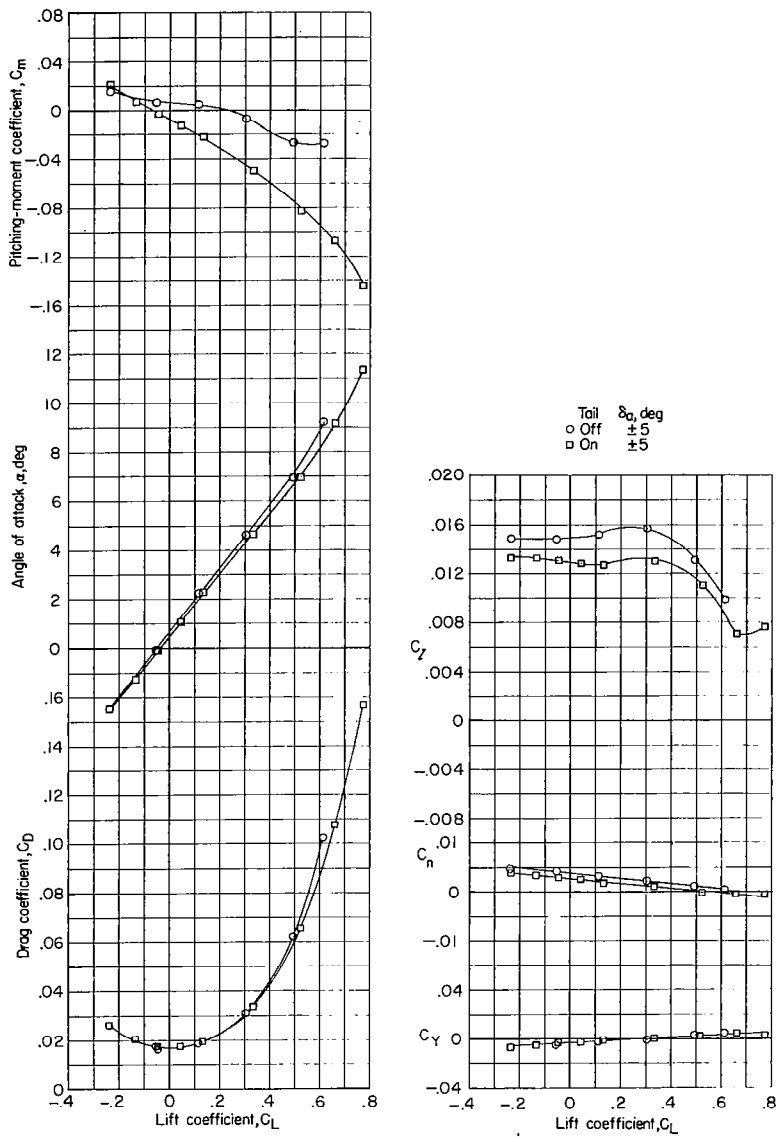

(c) M = 0.90.

Figure 32.- Continued.

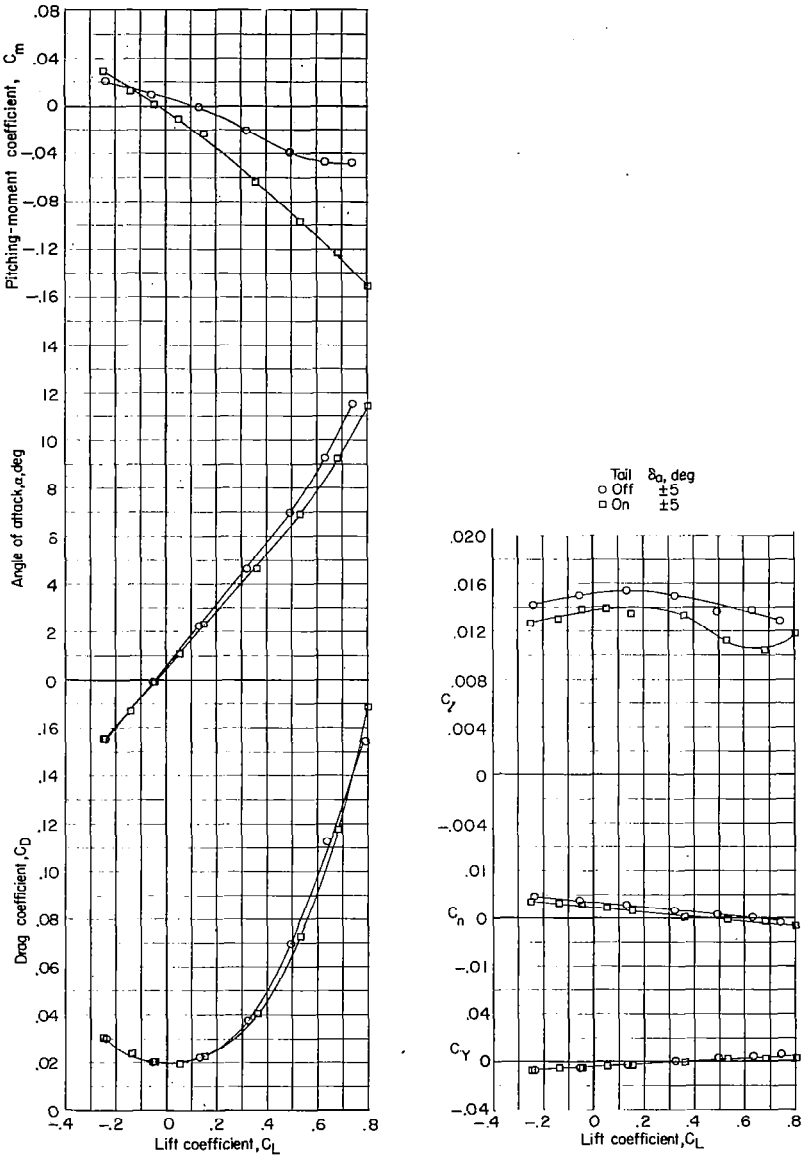

(d) M = 0.94.

Figure 32.- Continued.

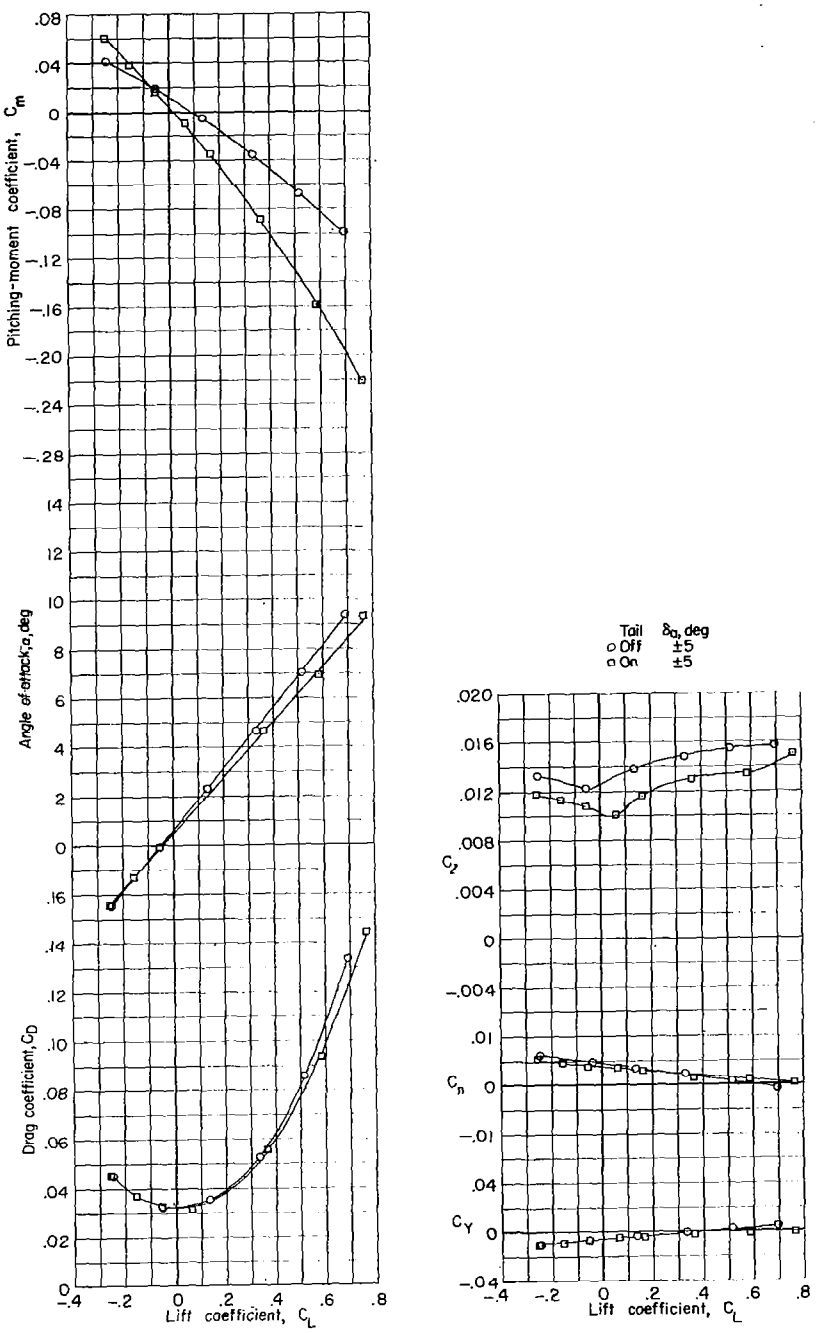

(e) M = 1.00.

Figure 32.- Continued.

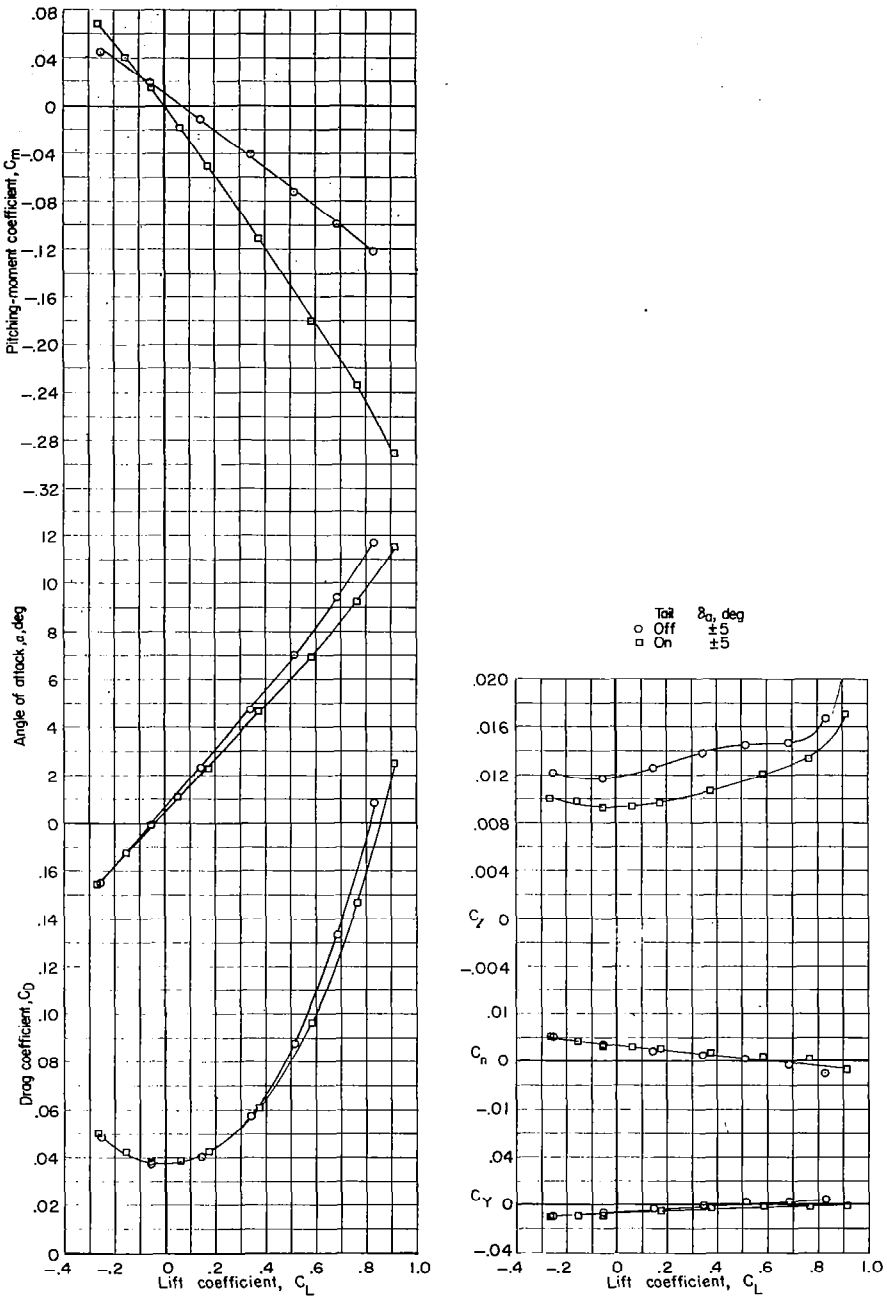

(f) M = 1.03.

Figure 32.- Continued.

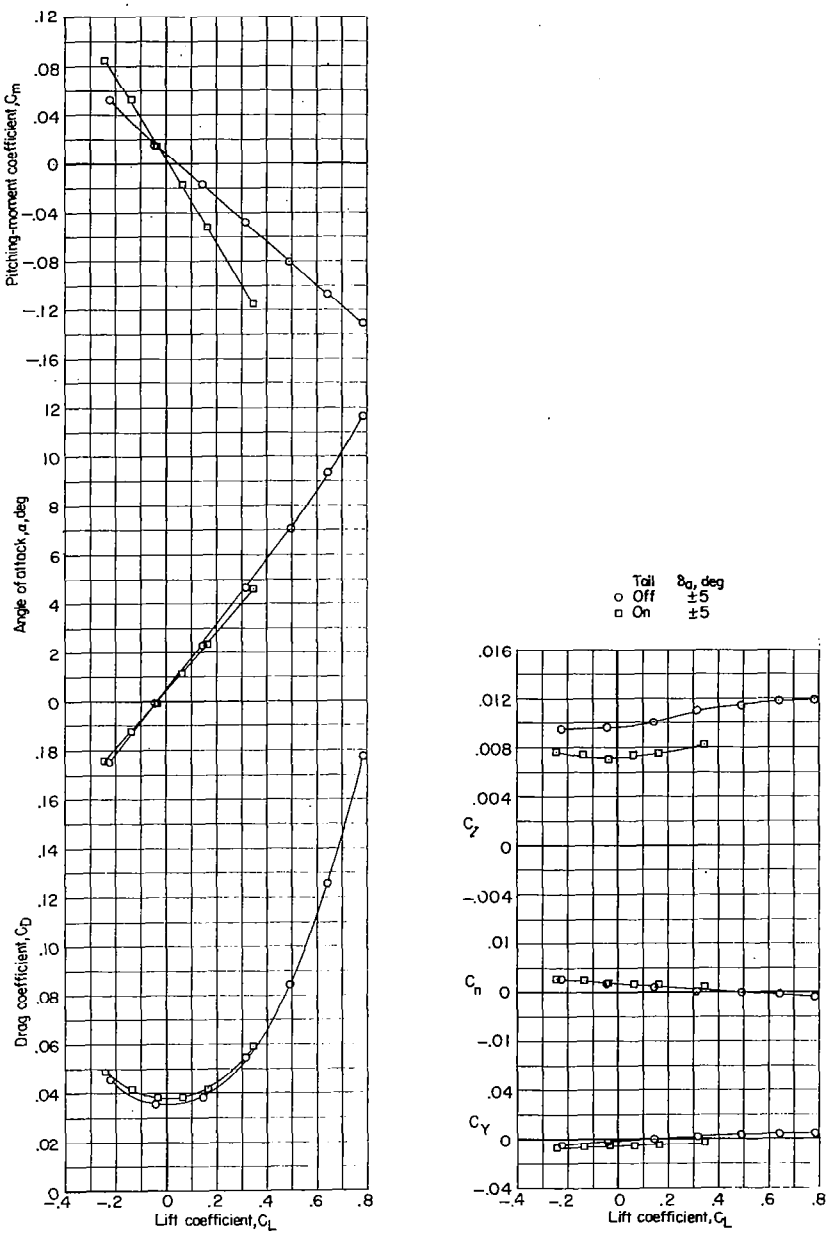

(g) M = 1.13.

Figure 32.- Concluded.

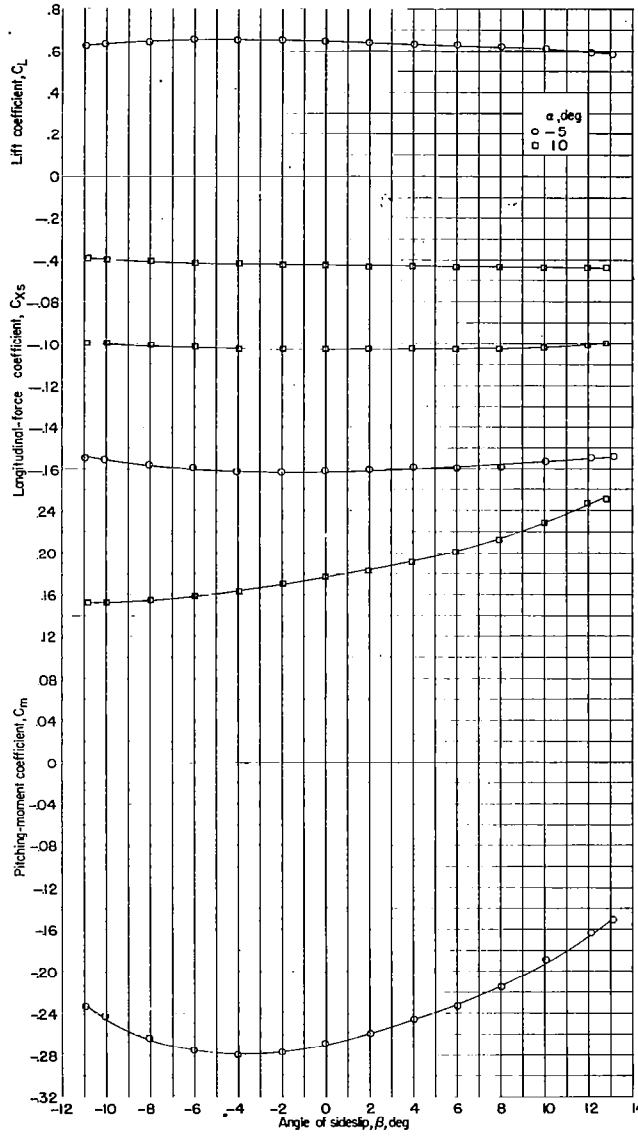

Figure 33.- Supersonic characteristics of model with ailerons deflected 20°, fuselage 2, wing 1, tail 2, $i_t = 0°$; M = 1.43, Langley 8-foot transonic pressure tunnel.

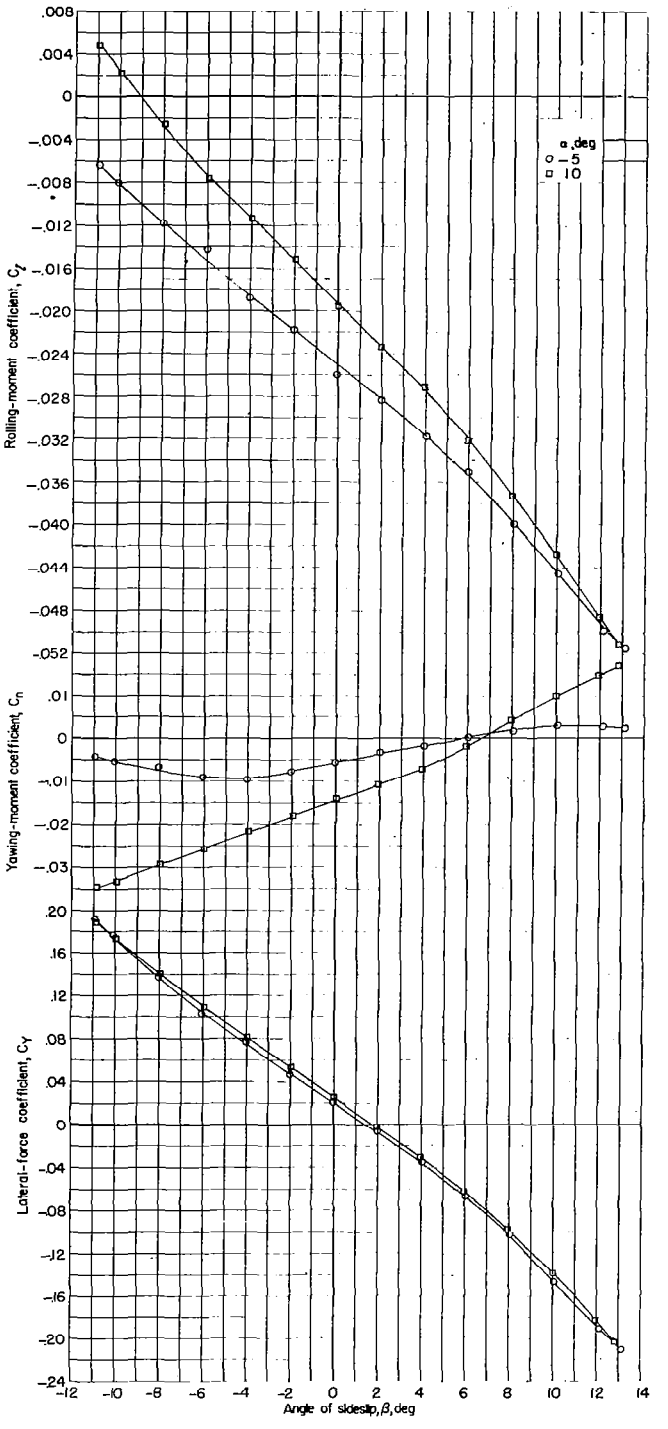

Figure 33.- Concluded.

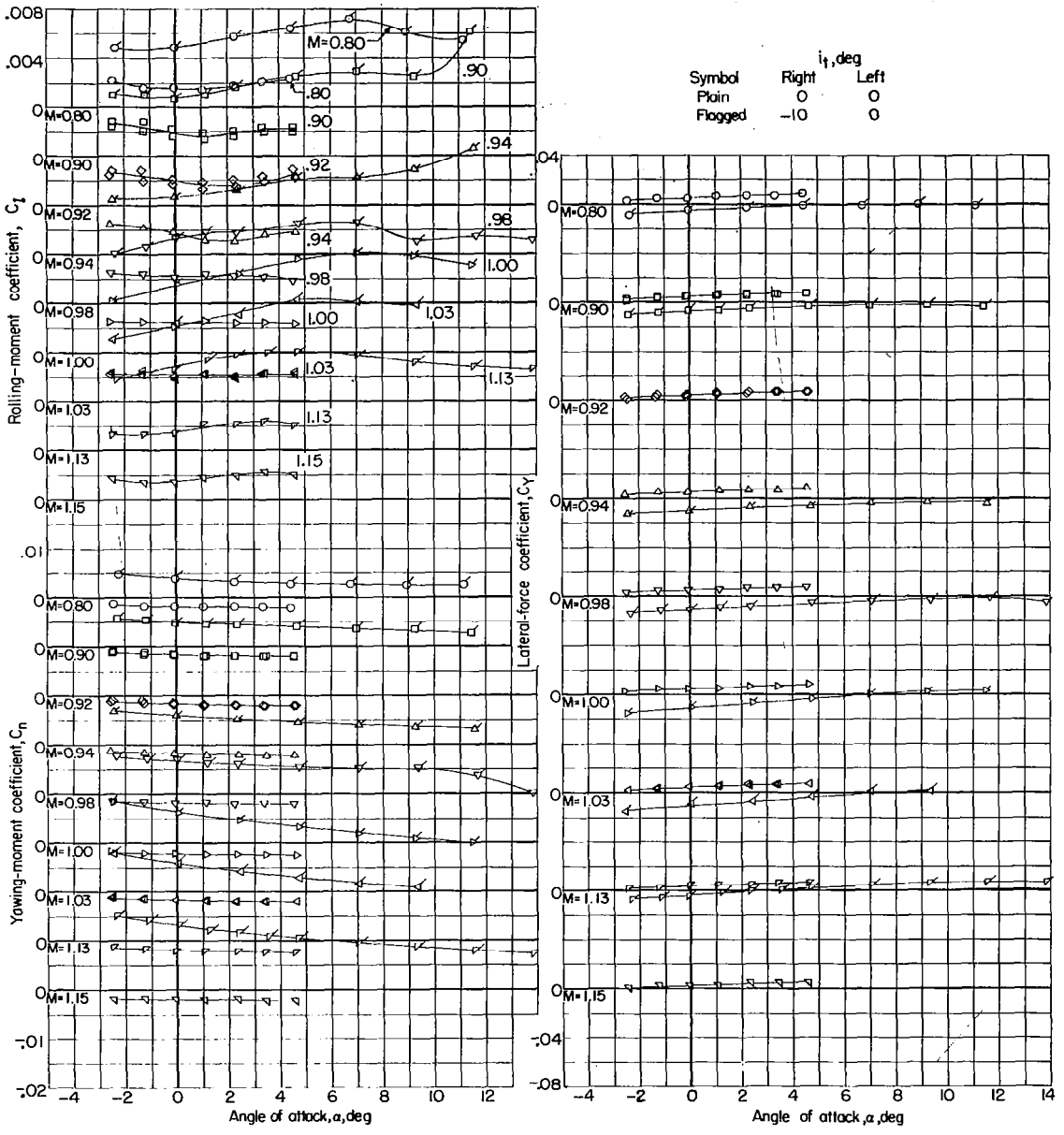

Figure 34.- Lateral characteristics of model in pitch with differential stabilizer for lateral control; fuselage 3, wing 1, tail 2, $i_t = 0^\circ$.

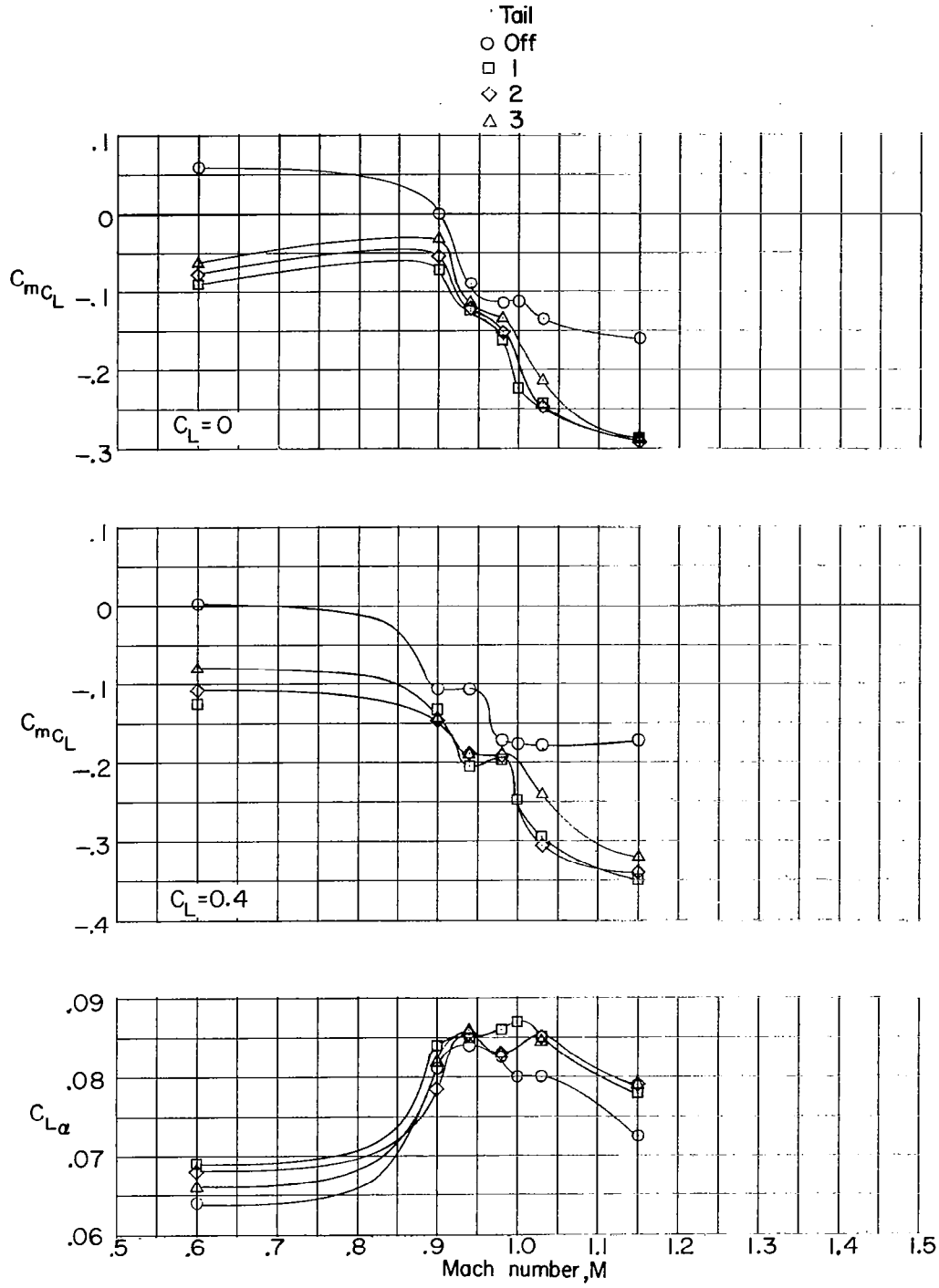

Figure 35.- Variation of longitudinal aerodynamic parameters with Mach number for several tail configurations, fuselage 1, wing 1, $i_t = 0^\circ$.

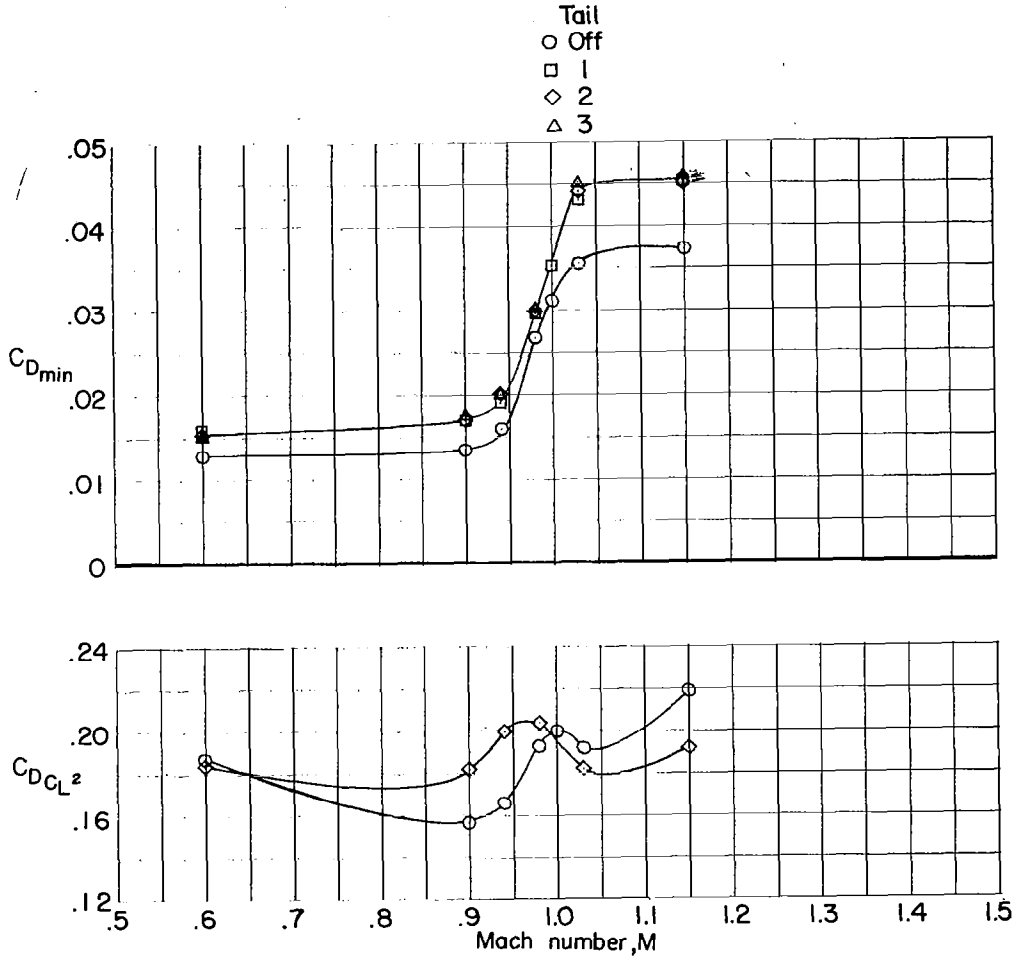

Figure 35.- Continued.

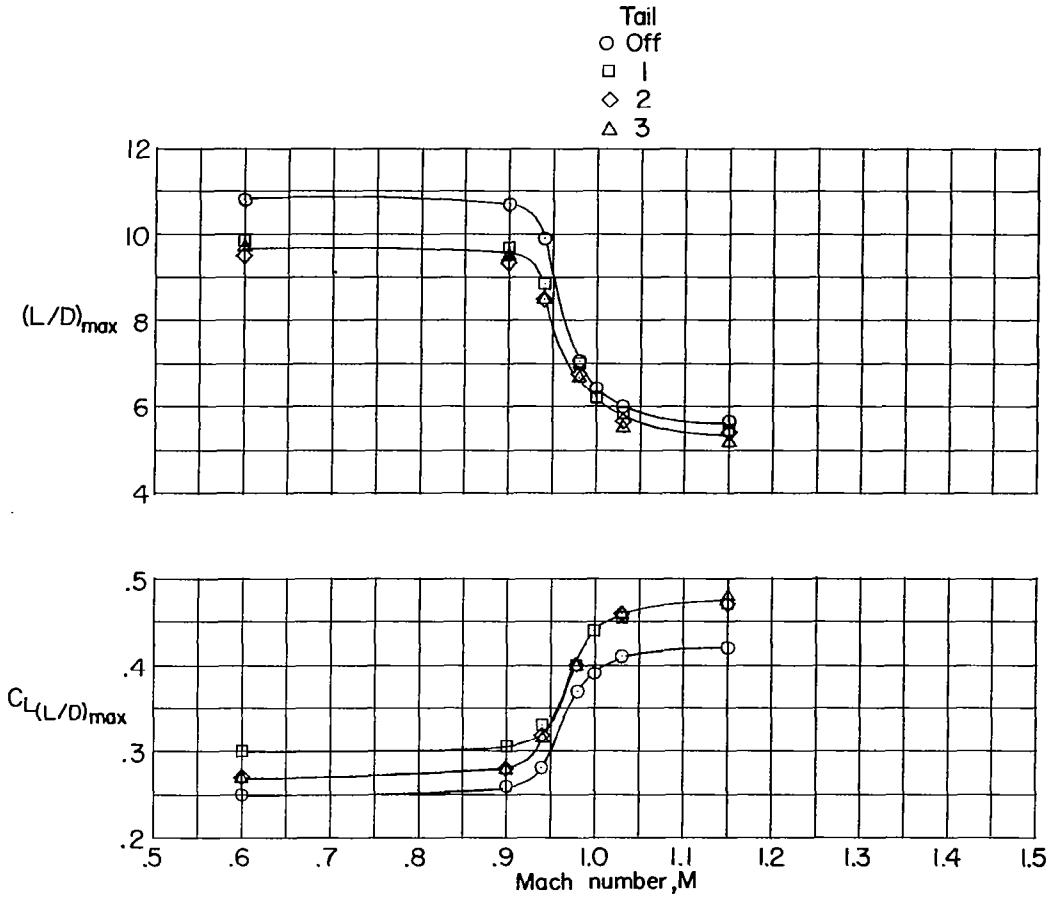

Figure 35.- Concluded.

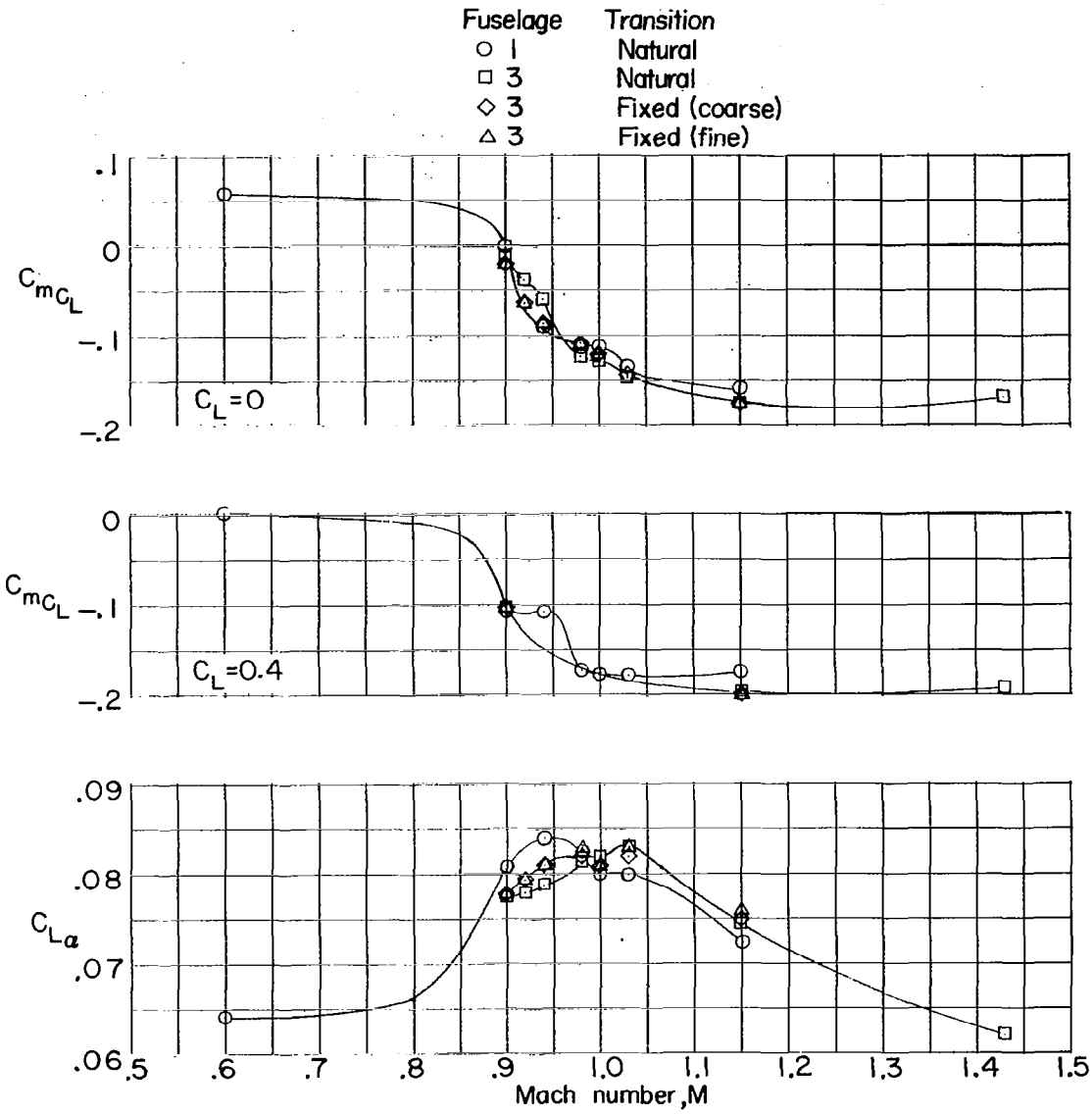

Figure 36.- Effects of fuselage modification and fixed transition on longitudinal parameters for wing and body alone; wing 1.

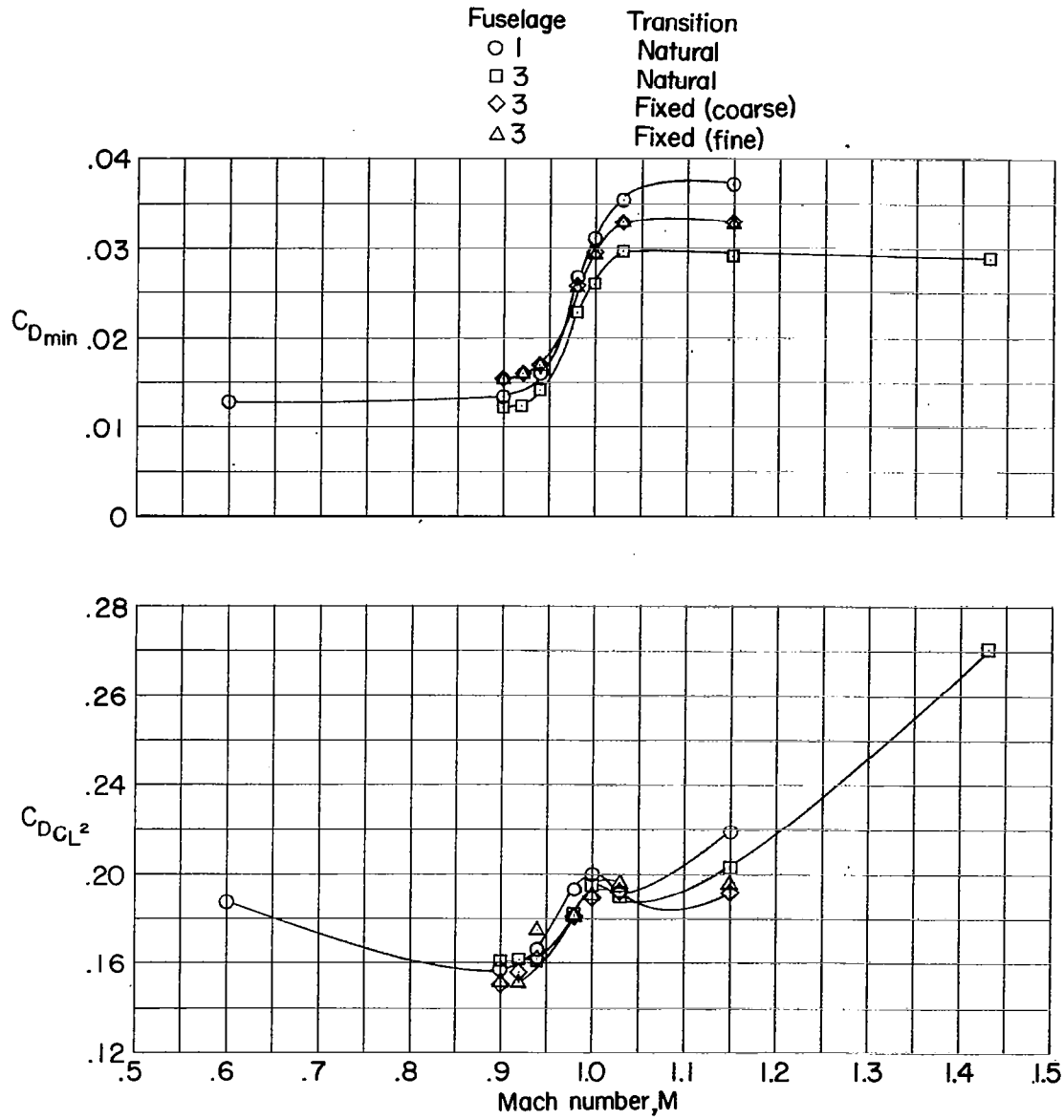

Figure 36.- Continued.

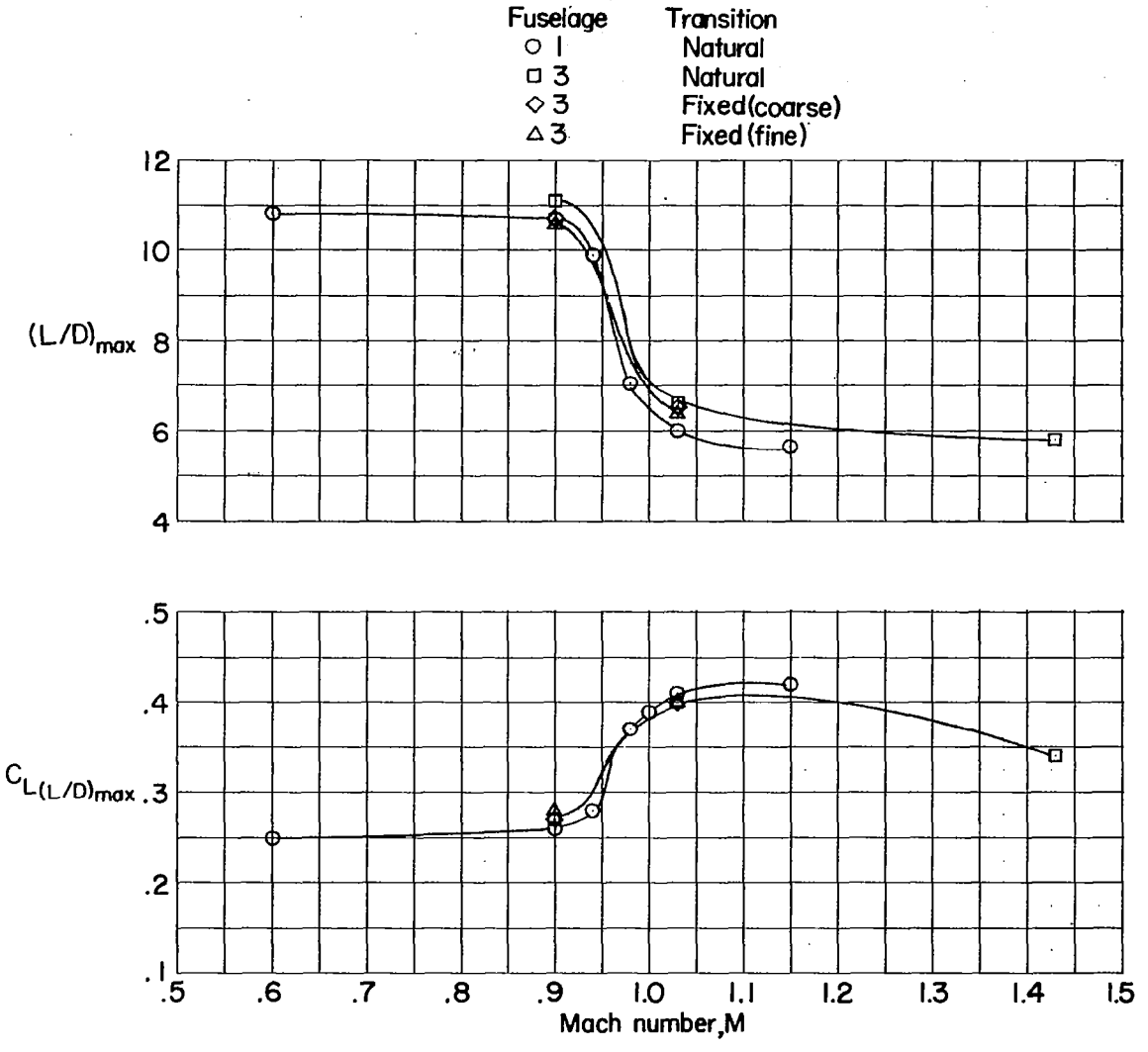

Figure 36.- Concluded.

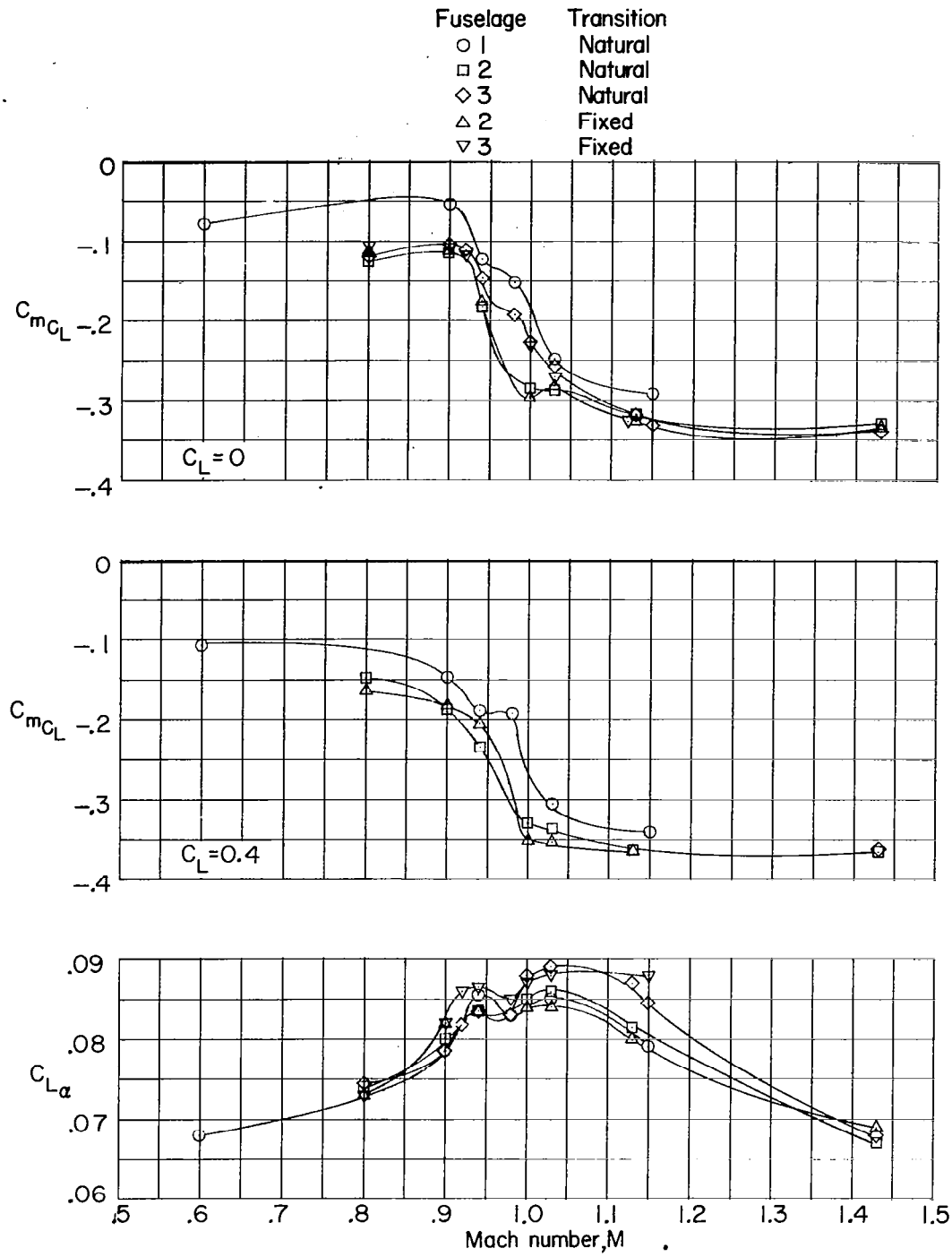

Figure 37.- Effects of body shape and fixed transition on longitudinal parameters of complete model; wing 1, tail 2, $i_t = 0^o$.

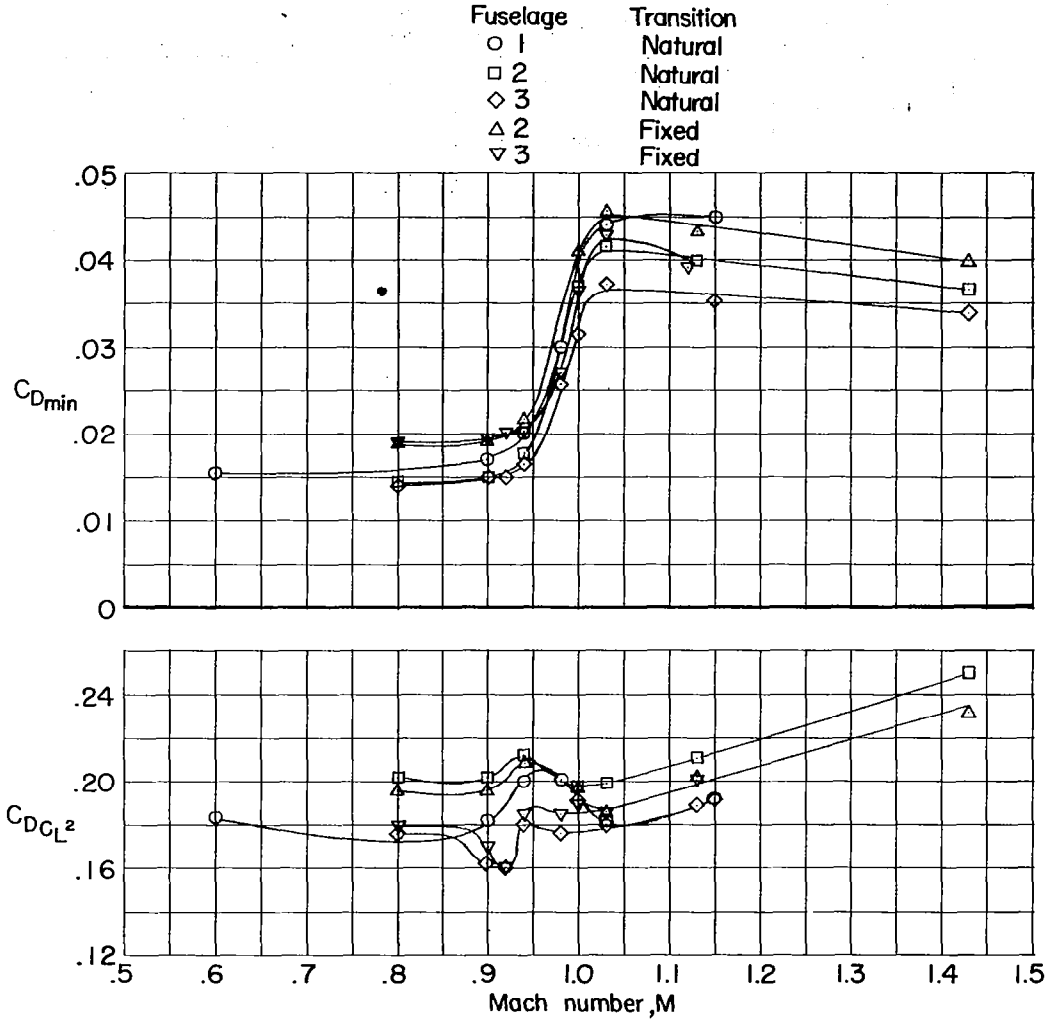

Figure 37.- Continued.

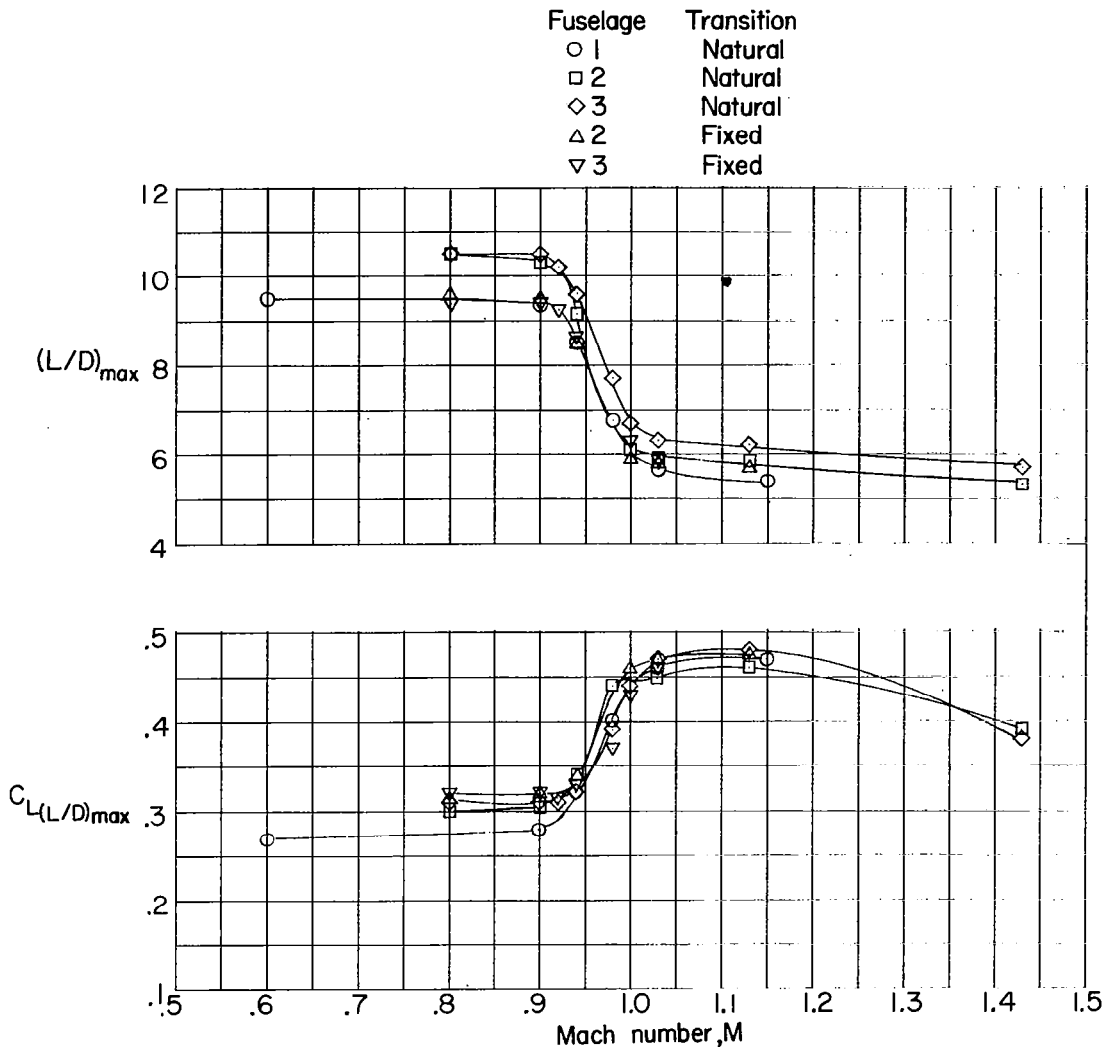

Figure 37.- Concluded.

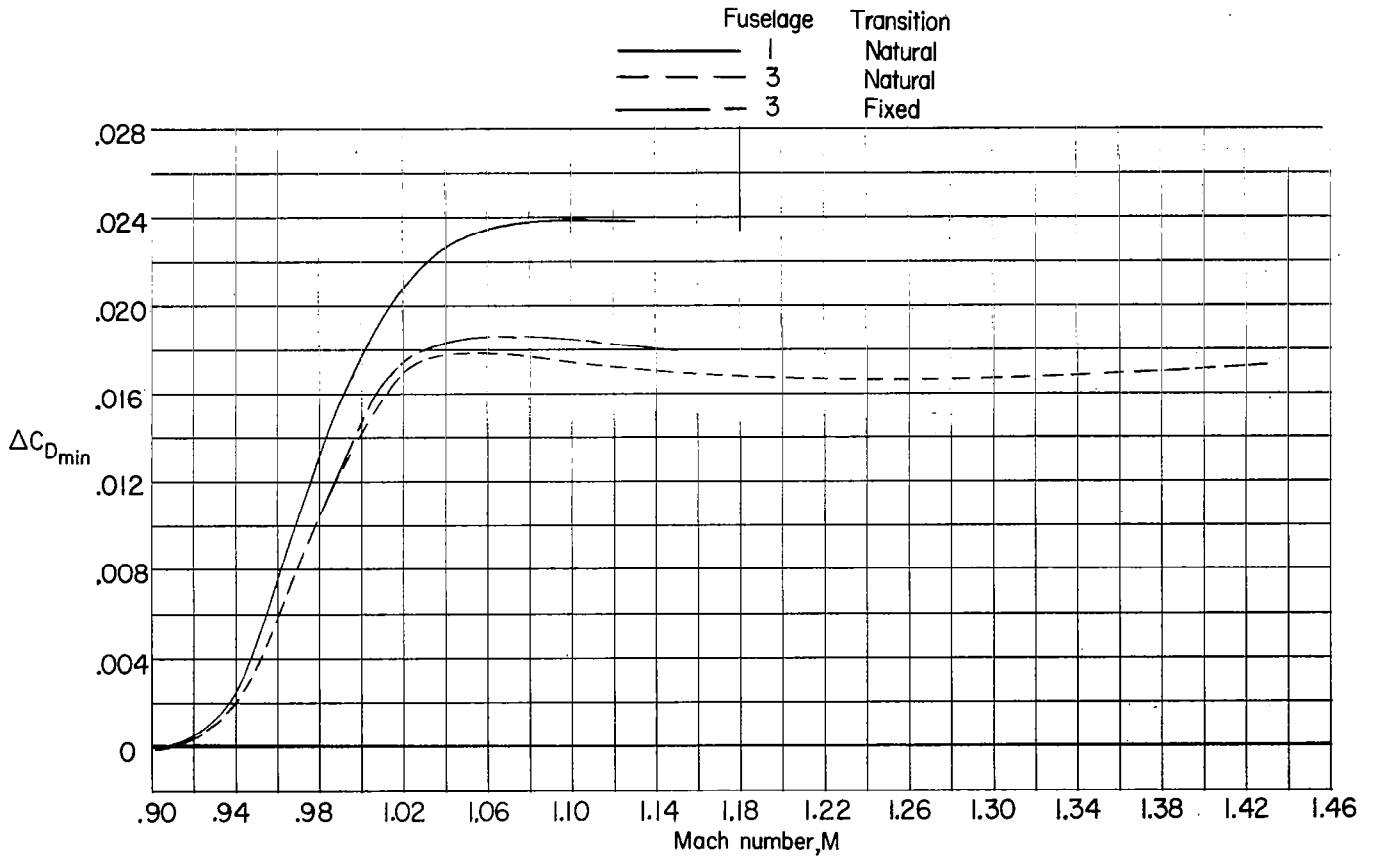

Figure 38.- Effects of fuselage modification and fixed transition on wave-drag variation with Mach number; wing 1, tails off.

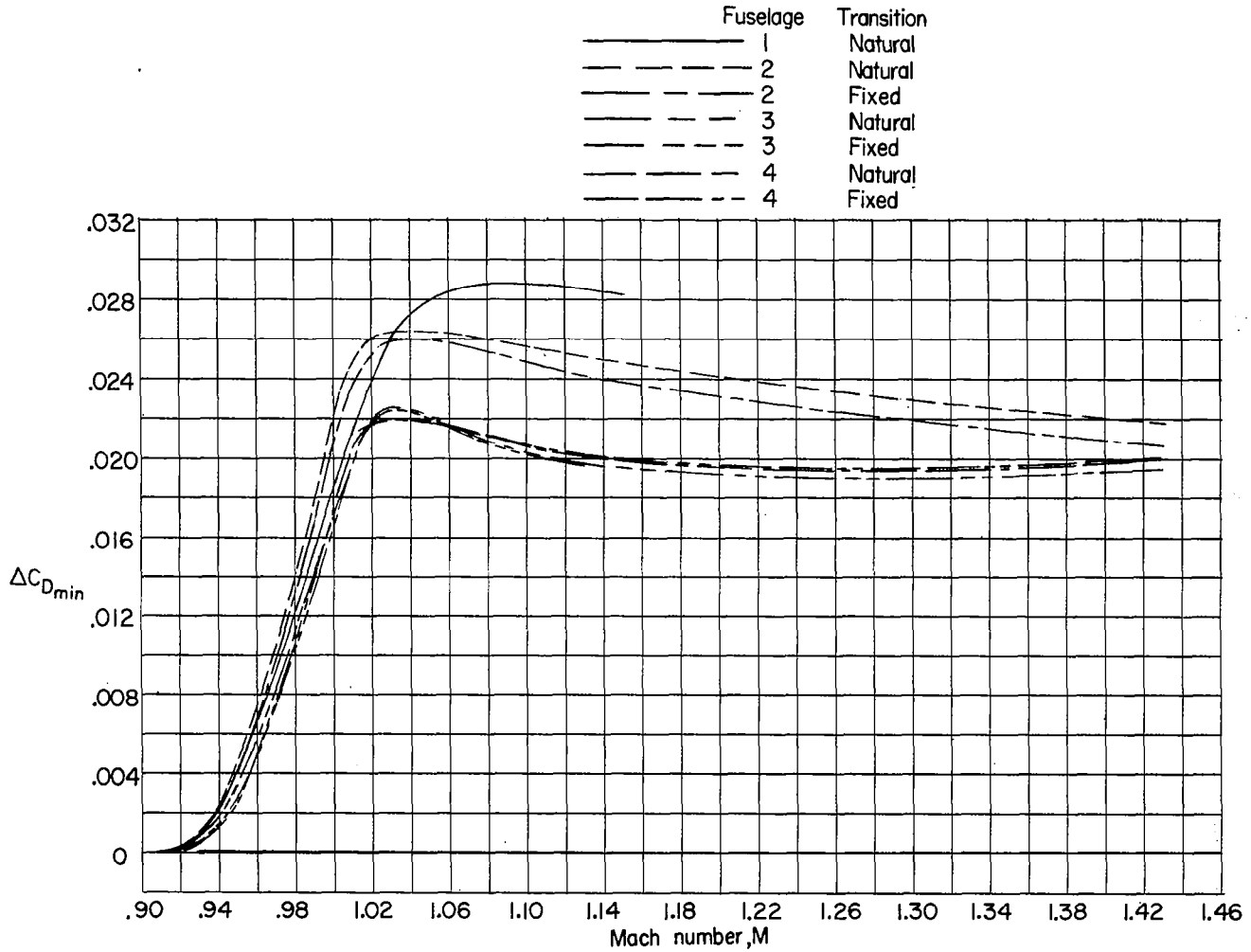

Figure 39.- Effects of fuselage modification and fixed transition on wave-drag variation with Mach number; complete model, wing 1, tail 2, $i_t = 0^o$.

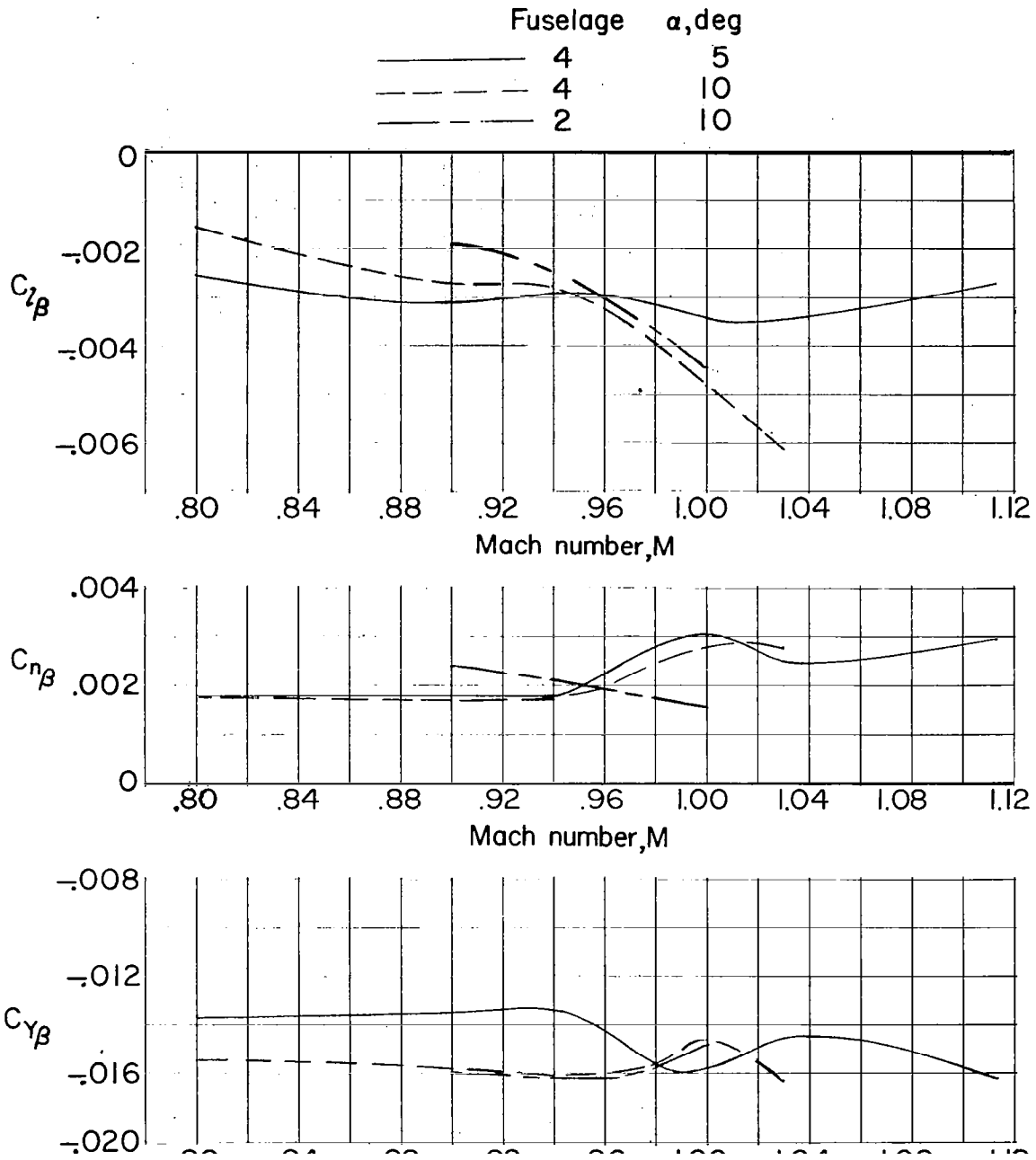
Fuselage α,deg
4 5
4 10
2 10
0
-.002
-.004
-.006
C_{l_β}
.80 .84 .88 .92 .96 1.00 1.04 1.08 1.12
Mach number,M
.004
.002
0
C_{n_β}
.80 .84 .88 .92 .96 1.00 1.04 1.08 1.12
Mach number,M
-.008
-.012
-.016
-.020
C_{Y_β}

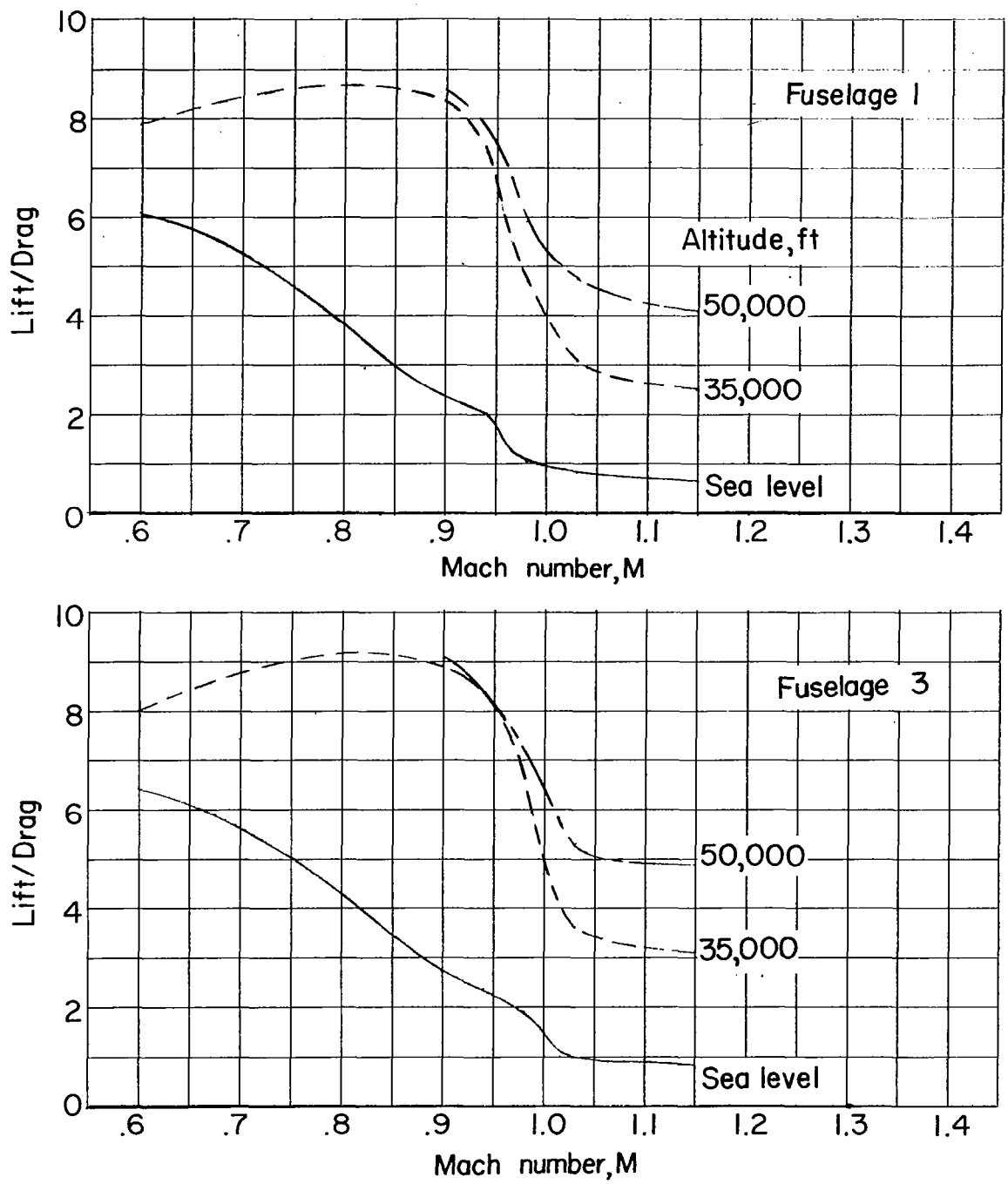

Figure 41.- Variation with Mach number of the trimmed lift-drag ratio at several altitudes; assumed wing loading of 55.5 lb/sq ft, wing 1, tail 2.

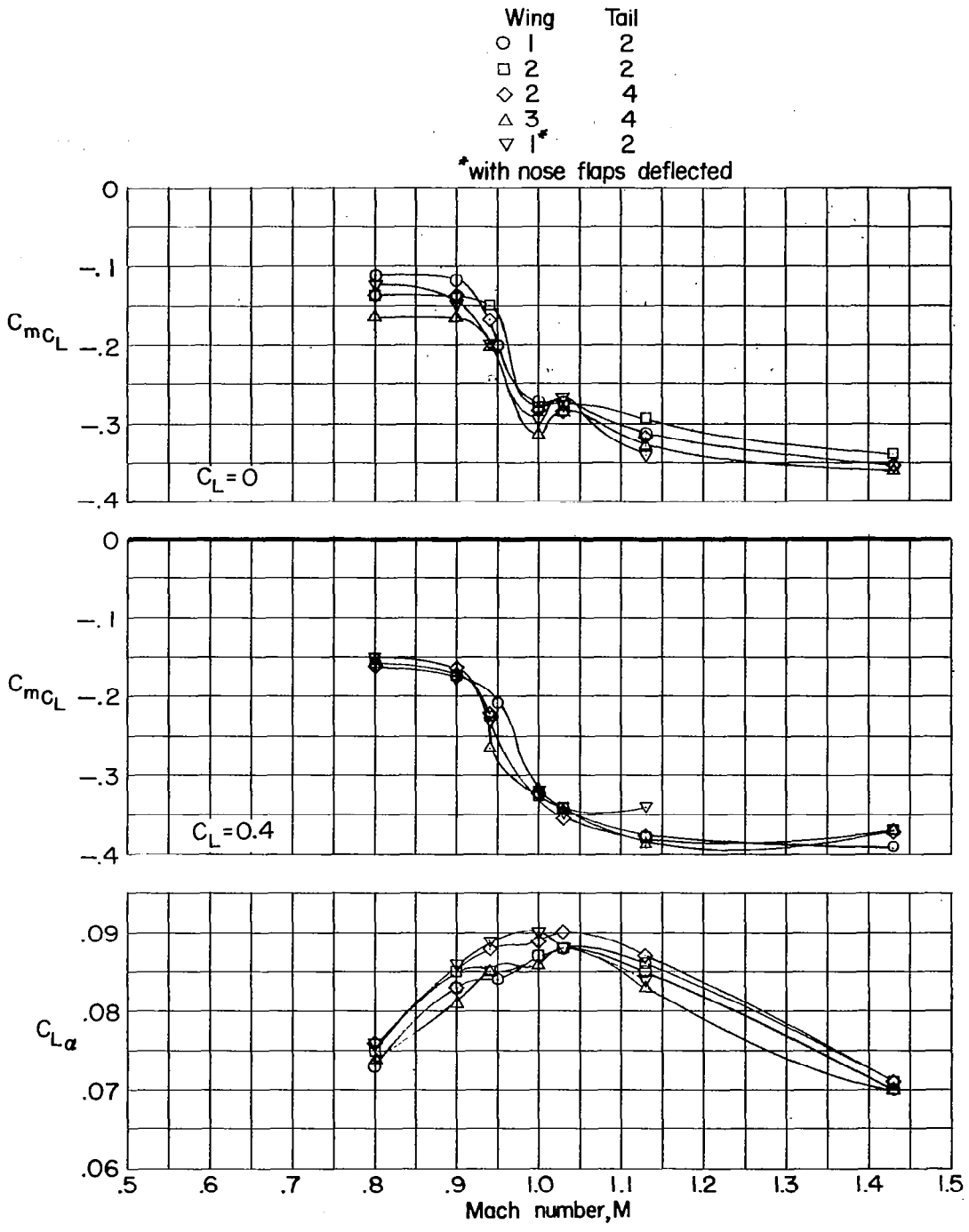

Figure 42.- Variation of longitudinal aerodynamic parameters with Mach number for several wing modifications, fuselage 4, $i_t = 0^\circ$.

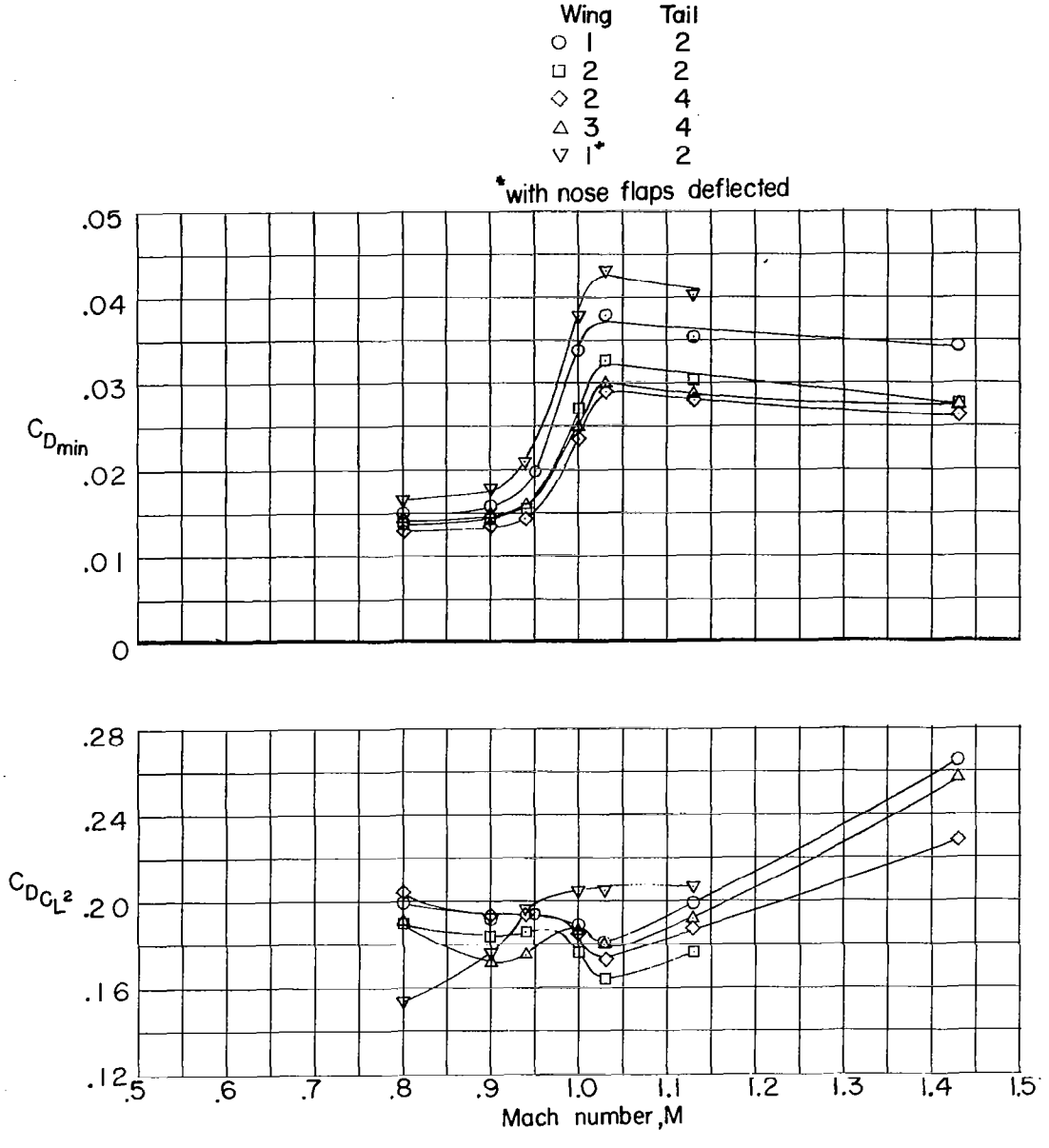

Figure 42.- Continued.

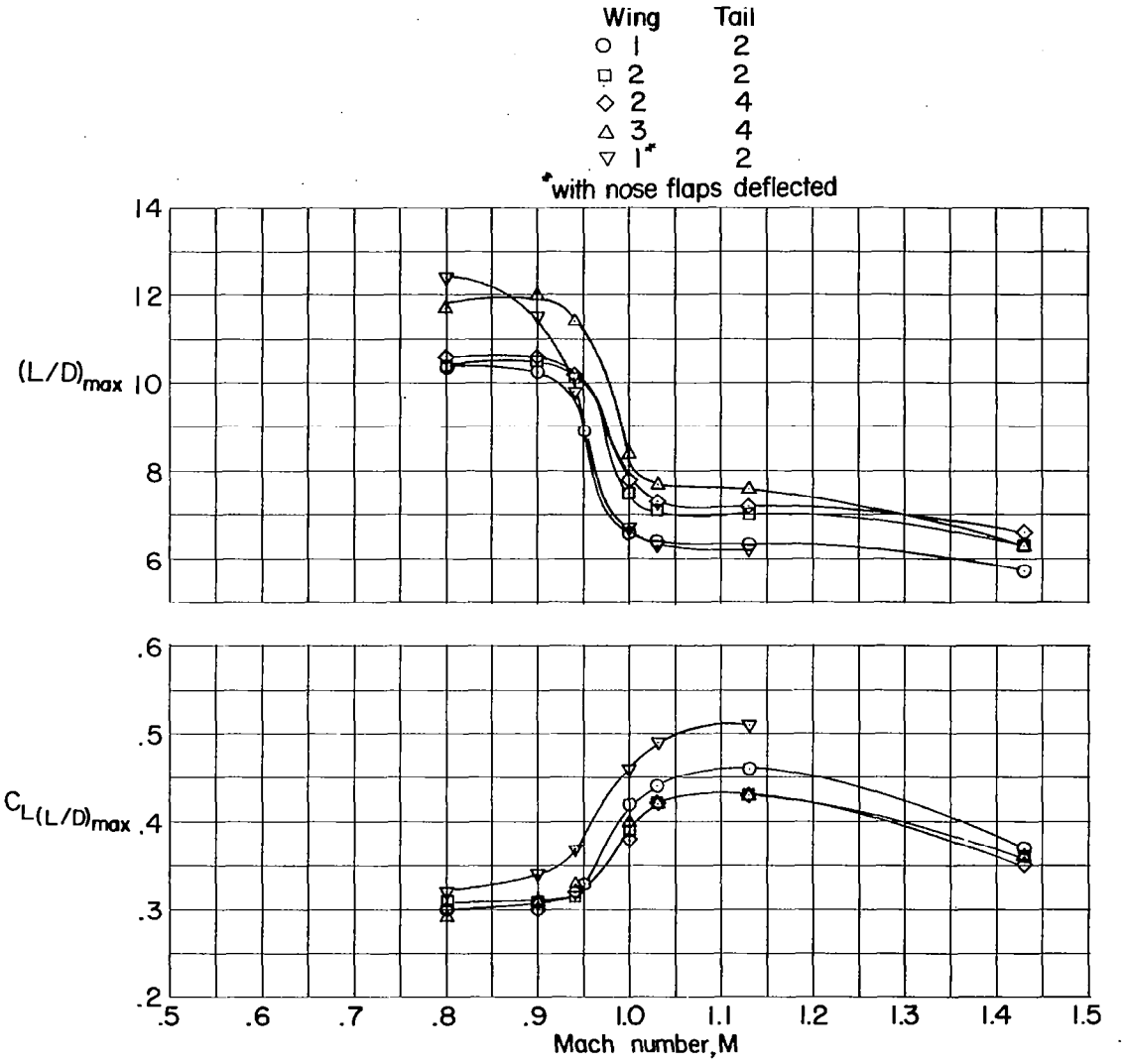

Figure 42.- Concluded.

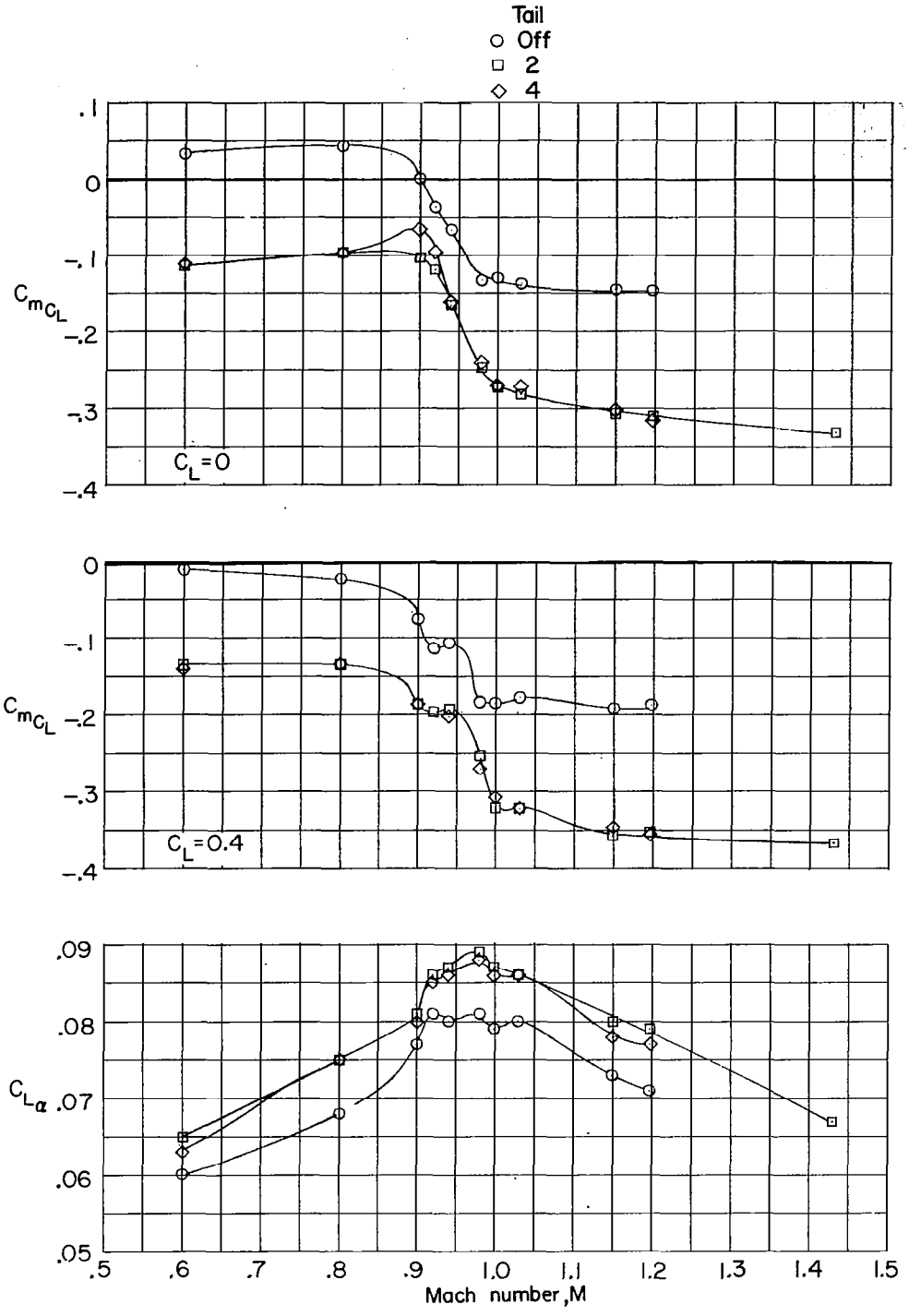

Figure 43.- Effects of tails and tail thickness on variation of longitudinal parameters with Mach number; fuselage 2, wing 1, $i_t = 0^o$.

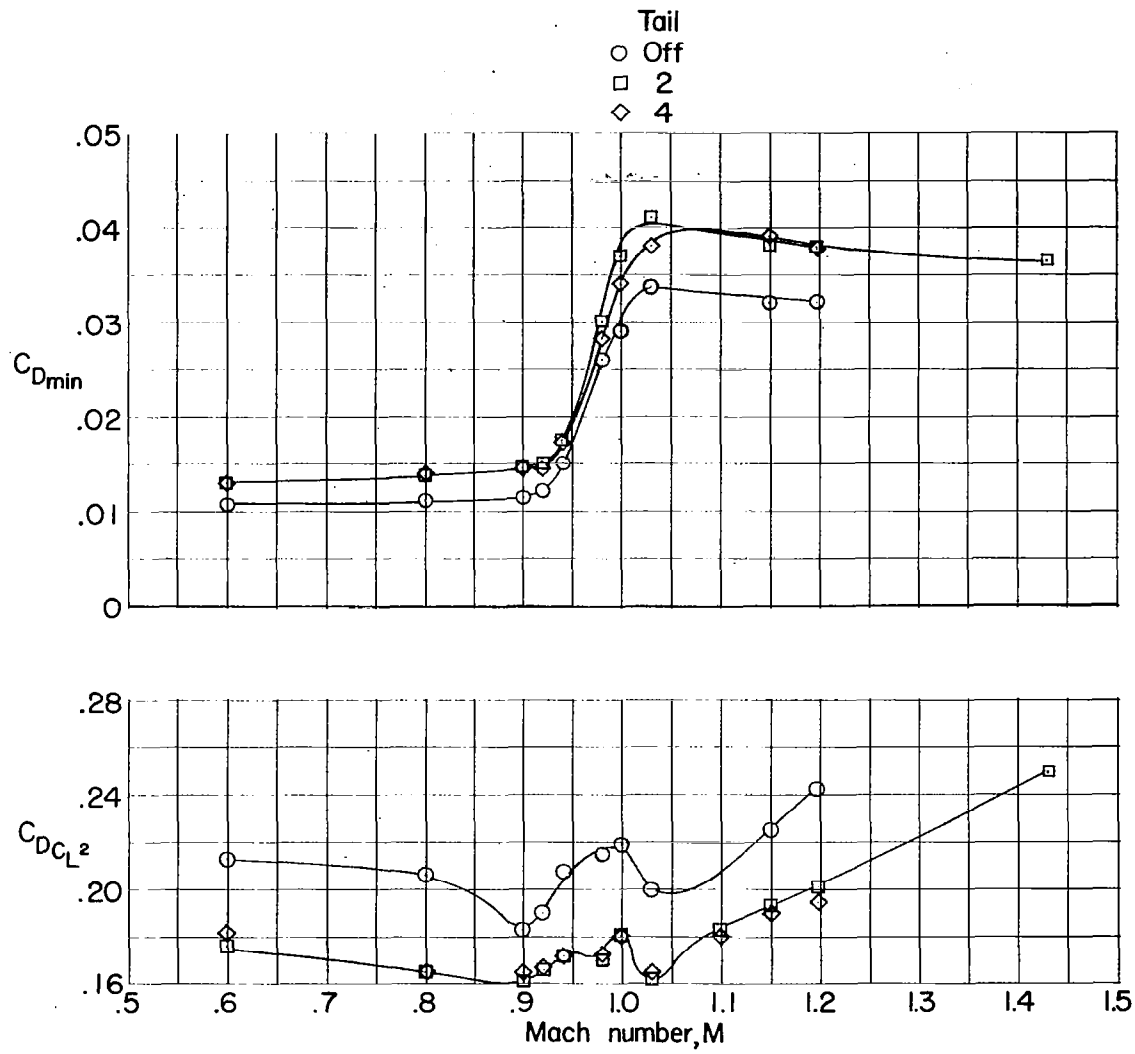

Figure 43.- Continued.

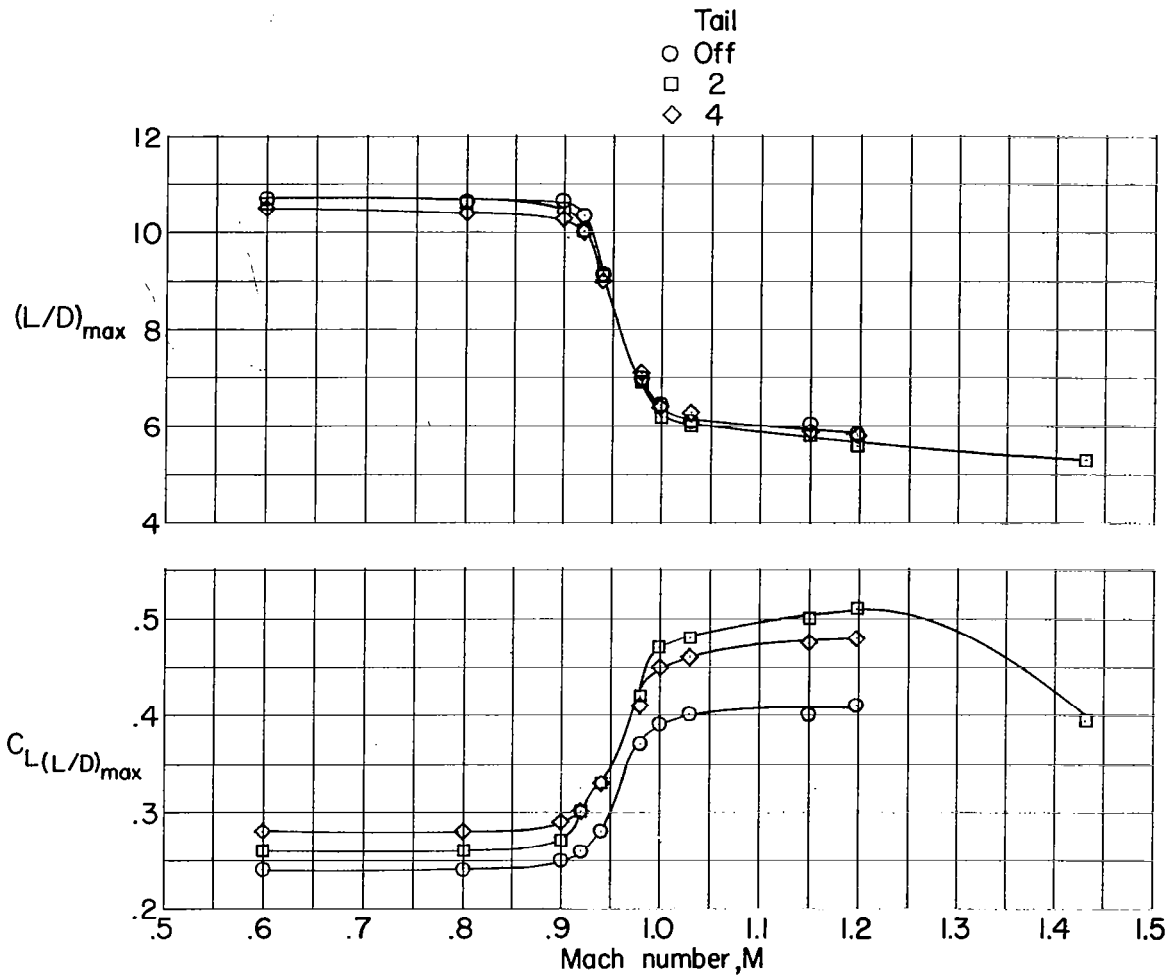

Figure 43.- Concluded.

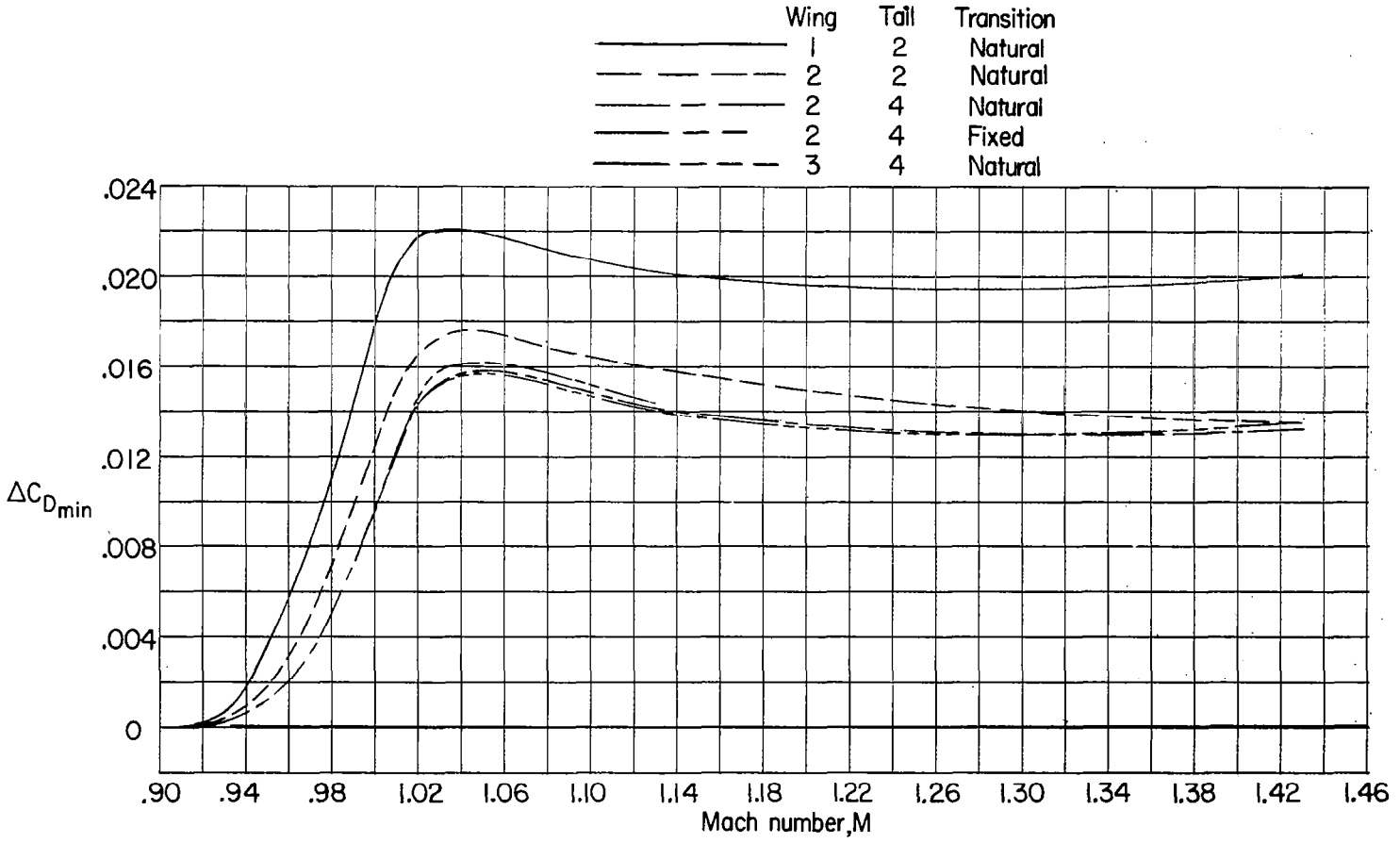

Figure 44.- Effects of wing and tail modifications on variation of wave drag with Mach number; fuselage 4, $i_t = 0^\circ$.

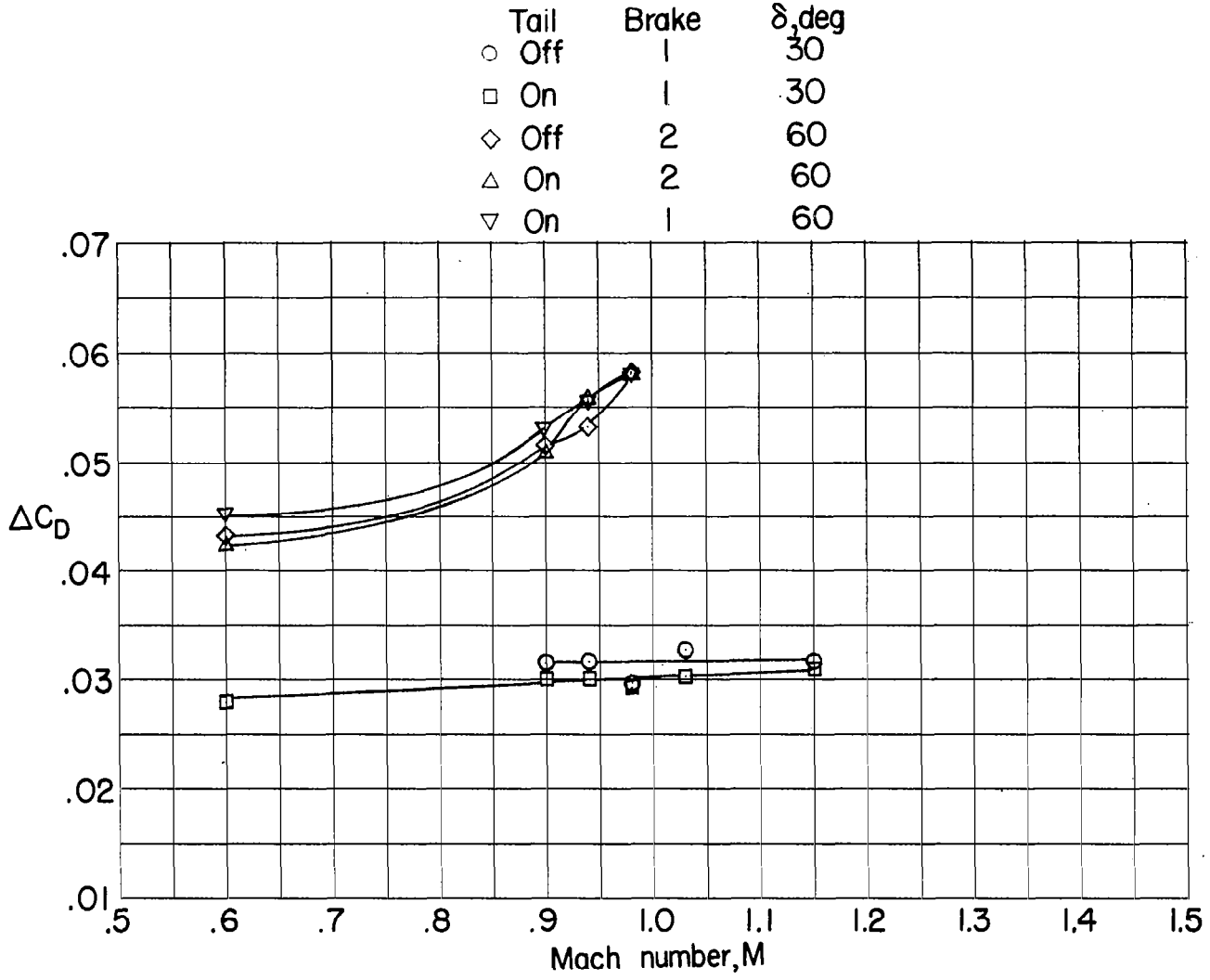

Figure 45.- Variation of the drag increment due to speed-brake deflection with Mach number at $C_L = 0.0$; fuselage 1, wing 1, tail 2, $i_t = 0^o$.

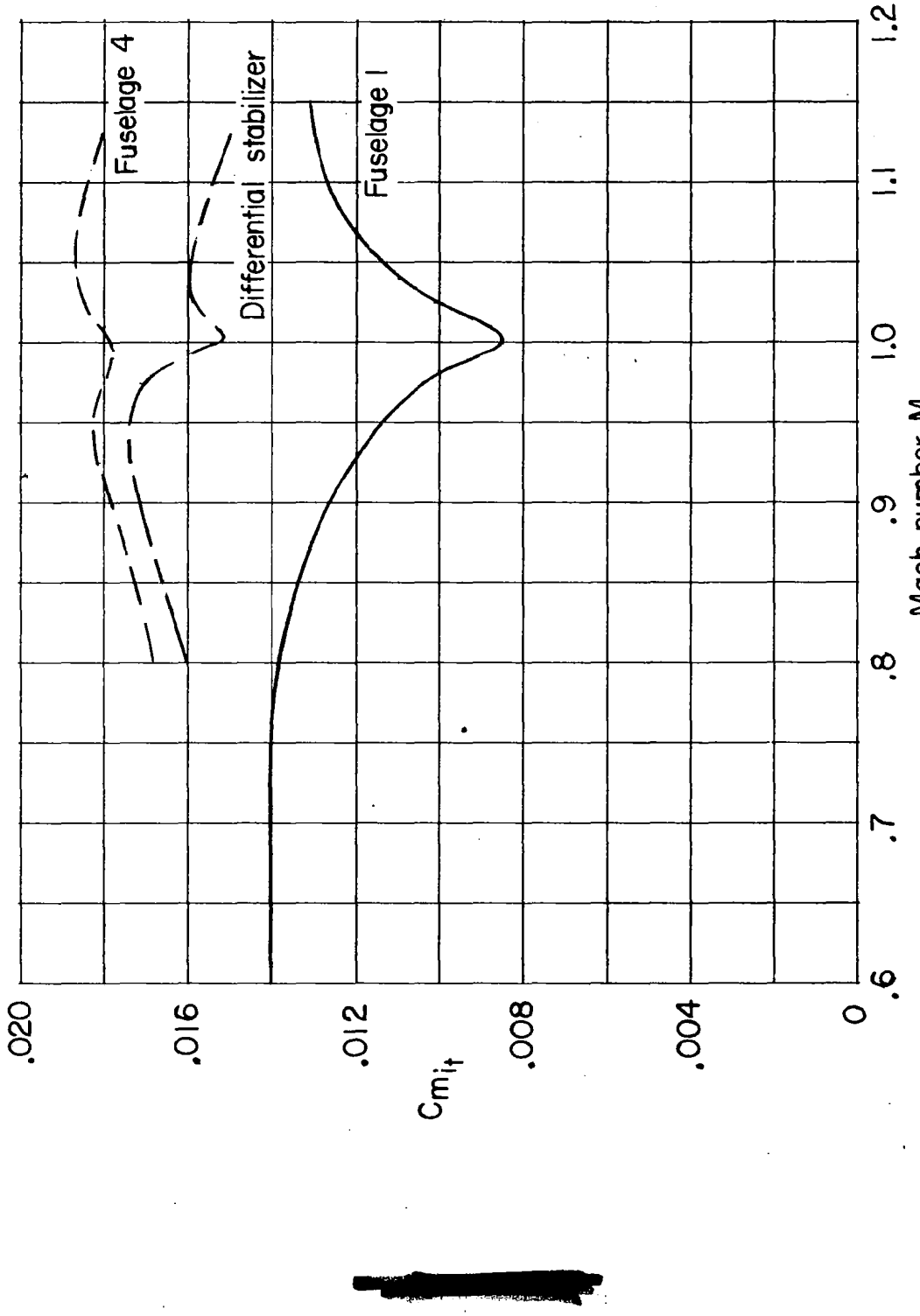

Figure 46.- Variation of stabilizer effectiveness with Mach number at $C_L < 0.2$.

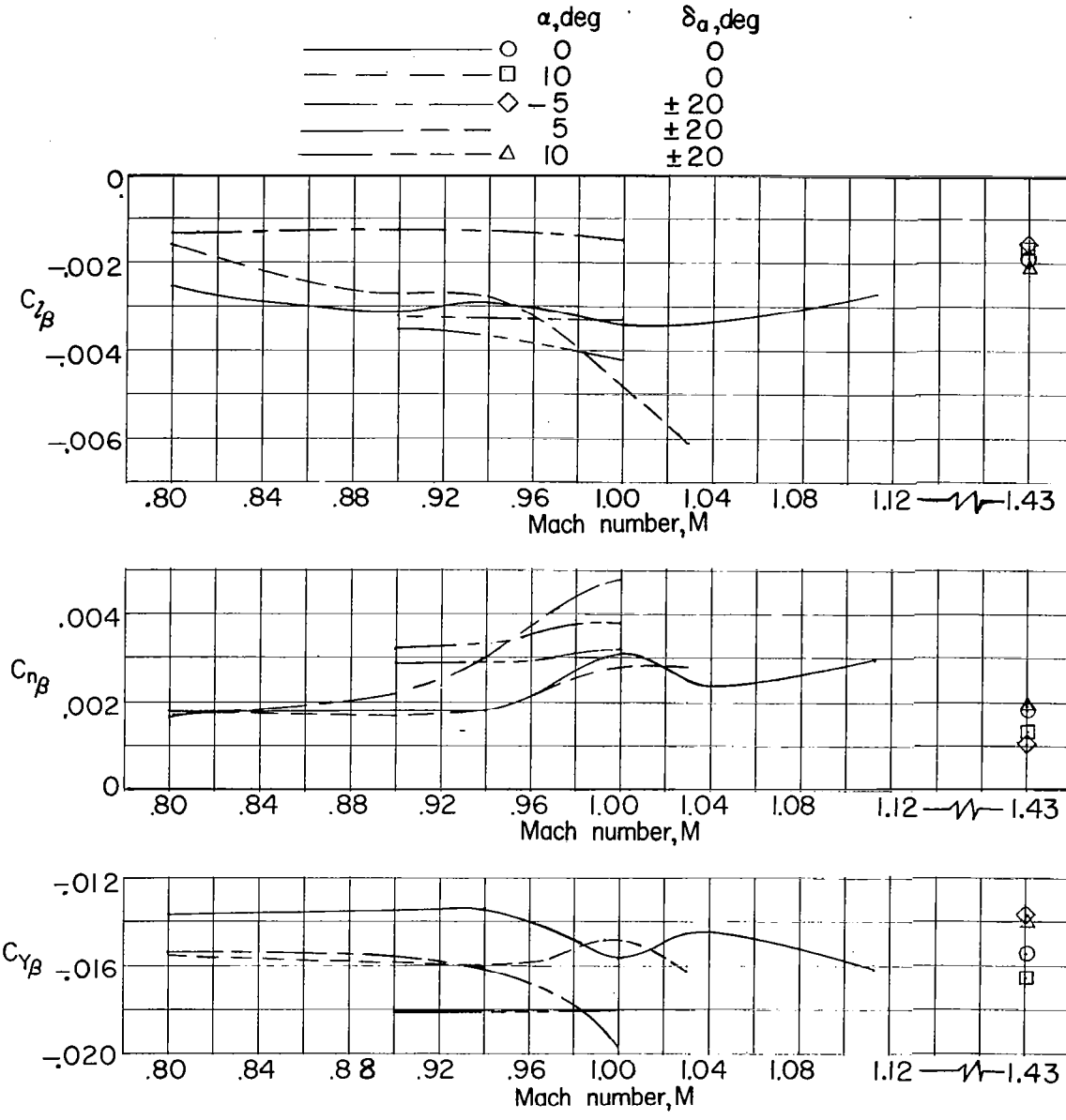

Figure 47.- Effect of ailerons on variation of lateral-stability derivatives with Mach number; fuselage 4, wing 1, tail 2, $i_t = 0^\circ$.

NASA - Langley Field, Va. L-477

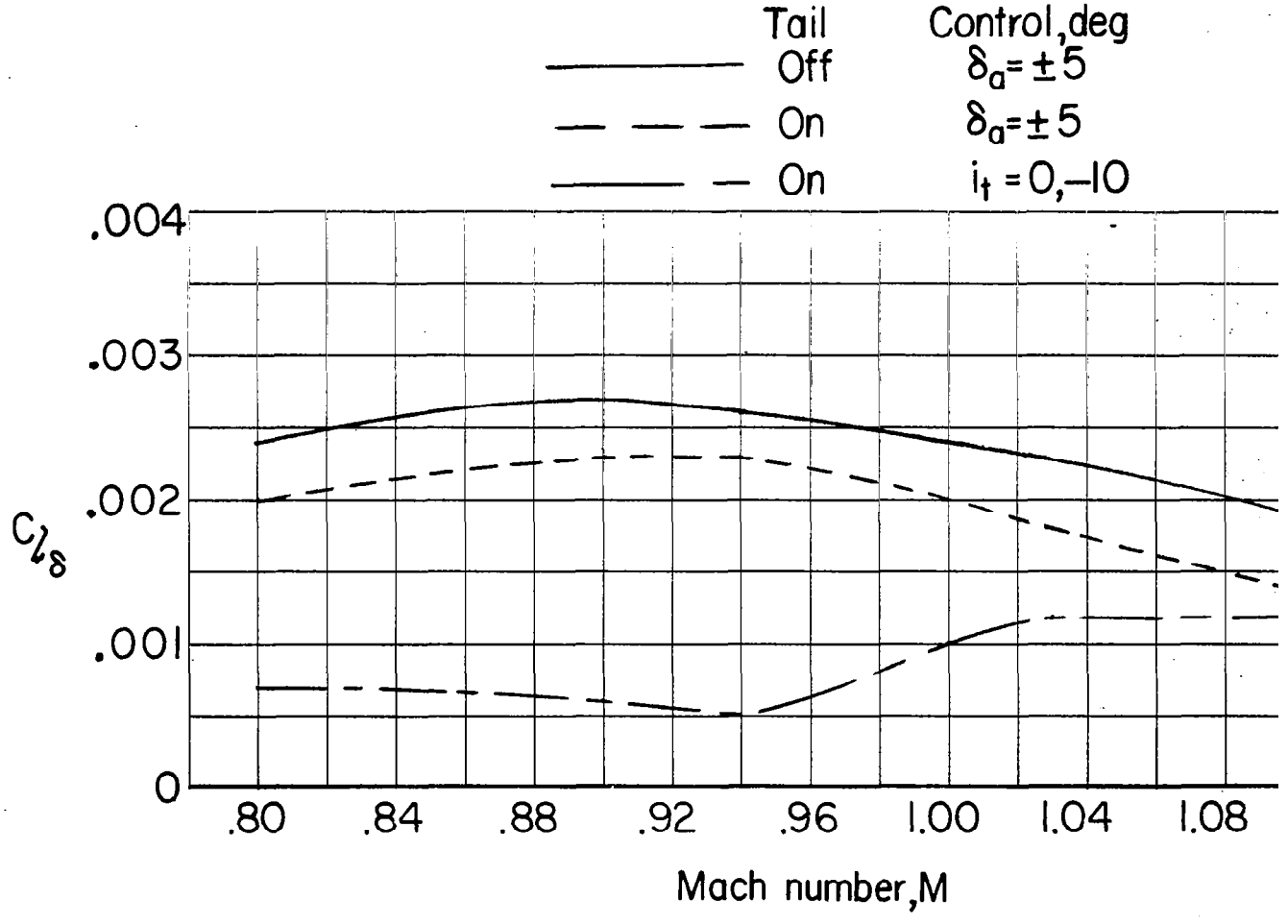

Figure 48.- Comparison of rolling effectiveness of ailerons and a differential stabilizer; fuselage 3.